

Article

In Vitro Antioxidant and In Vivo Antigenotoxic Features of a Series of 61 Essential Oils and Quantitative Composition–Activity Relationships Modeled through Machine Learning Algorithms

Milan Mladenović^{1,*},[†] , Roberta Astolfi^{2,†}, Nevena Tomašević¹, Sanja Matić³ , Mijat Božović⁴ ,
Filippo Sapienza² and Rino Ragno^{2,*} 

¹ Kragujevac Center for Computational Biochemistry, Department of Chemistry, Faculty of Science, University of Kragujevac, Radoja Domanovića 12, P.O. Box 60, 34000 Kragujevac, Serbia; nevena.tomasevic@pmf.kg.ac.rs

² Rome Center for Molecular Design, Department of Drug Chemistry and Technology, Faculty of Pharmacy and Medicine, Rome Sapienza University, P. le A. Moro 5, 00185 Rome, Italy; roberta.astolfi@uniroma1.it (R.A.); filippo.sapienza@uniroma1.it (F.S.)

³ Department of Science, Institute for Information Technologies Kragujevac, University of Kragujevac, Jovana Cvijića bb, 34000 Kragujevac, Serbia; sanjamatic@kg.ac.rs

⁴ Faculty of Science and Mathematics, University of Montenegro, Džordža Vašingtona bb, 81000 Podgorica, Montenegro; mijatboz@ucg.ac.me

* Correspondence: milan.mladenovic@pmf.kg.ac.rs (M.M.); rino.ragno@uniroma1.it (R.R.);

Tel.: +381-638932160 (M.M.); +39-49913937 (R.R.); Fax: +381-34335040 (M.M.); +39-49913627 (R.R.)

[†] These authors contributed equally to this work.

Abstract: The antioxidant activity of essential oils (EOs) is an important and frequently studied property, yet it is not sufficiently understood in terms of the contribution of EOs mixtures' constituents and biological properties. In this study, a series of 61 commercial EOs were first evaluated as antioxidants in vitro, following as closely as possible the cellular pathways of reactive oxygen species (ROS) generation. Hence, EOs were assessed for the ability either to chelate metal ions, thus interfering with ROS generation within the respiratory chain, or to neutralize 2,2-diphenyl-1-picrylhydrazyl (DPPH[•]) and lipid peroxide radicals (LOO[•]), thereby halting lipid peroxidation, as well as to neutralize 2,2'-azino-bis(3-ethylbenzothiazoline-6-sulfonic acid cation radicals (ABTS^{•+}) and hydroxyl radicals (OH[•]), thereby preventing the ROS species from damaging DNA nucleotides. Showing noteworthy potencies to neutralize all of the radicals at the ng/mL level, the active EOs were also characterized as protectors of DNA double strands from damage induced by peroxy radicals (ROO[•]), emerging from 2,2'-azobis-2-methyl-propanimidamide (AAPH) as a source, and OH[•], indicating some genome protectivity and antigenotoxicity effectiveness in vitro. The chemical compositions of the EOs associated with the obtained activities were then analyzed by means of machine learning (ML) classification algorithms to generate quantitative composition–activity relationships (QCARs) models (models published in the AI4EssOil database available online). The QCARs models enabled us to highlight the key features (EOSs' chemical compounds) for exerting the redox potencies and to define the partial dependencies of the features, viz. percentages in the mixture required to exert a given potency. The ML-based models explained either the positive or negative contribution of the most important chemical components: limonene, linalool, carvacrol, eucalyptol, α -pinene, thymol, caryophyllene, *p*-cymene, eugenol, and chrysanthone. Finally, the most potent EOs in vitro, Ylang-ylang (*Cananga odorata* (Lam.)) and Ceylon cinnamon peel (*Cinnamomum verum* J. Presl), were promptly administered in vivo to evaluate the rescue ability against redox damage caused by CCl₄, thereby verifying their antioxidant and antigenotoxic properties either in the liver or in the kidney.

Keywords: essential oils; antioxidant and antigenotoxic features in vitro and in vivo; machine learning



Citation: Mladenović, M.; Astolfi, R.; Tomašević, N.; Matić, S.; Božović, M.; Sapienza, F.; Ragno, R. In Vitro Antioxidant and In Vivo Antigenotoxic Features of a Series of 61 Essential Oils and Quantitative Composition–Activity Relationships Modeled through Machine Learning Algorithms. *Antioxidants* **2023**, *12*, 1815. <https://doi.org/10.3390/antiox12101815>

Academic Editors: Simona Gabriela Bungau and Delia Mirela Tit

Received: 24 August 2023

Revised: 25 September 2023

Accepted: 26 September 2023

Published: 29 September 2023



Copyright: © 2023 by the authors. Licensee MDPI, Basel, Switzerland. This article is an open access article distributed under the terms and conditions of the Creative Commons Attribution (CC BY) license (<https://creativecommons.org/licenses/by/4.0/>).

1. Introduction

Essential oils (EOs) are liquid mixtures of volatile compounds extracted from aromatic plants, usually by hydro-distillation and steam distillation [1], but also through a suitable mechanical process without heating [2]. Their medicinal potential is traditionally associated with antimicrobial activity or antiviral properties [3]. Although there is a scarce understanding of their mechanism of action, considerable attention has been raised regarding the antioxidant activity of EOs due to the presence of aliphatic compounds (hydrocarbons and their oxygenated derivatives), terpenes (hydrocarbons and oxygenated derivatives), phenols and phenol derivatives, *O*- and *O,S*-heterocycles, as well as *N*- and *N,S*-heterocycles, that contribute to free radical scavenging activity [1,4]. As oxidative stress reducers, EOs might contribute to preventing the pathogenesis of aging and degenerative diseases, such as atherosclerosis, cardiovascular diseases, diabetes, and cancer [5]. Similarly, equally important redox-potent EOs could preserve processed food enriched with fats and oils and prevent spoilage and quality deterioration, thus representing a replacement for common synthetic antioxidants (such as butylated hydroxyanisole (BHA) or butylhydroxytoluene (BHT)) that are suspected to be potentially harmful to human health [6].

Reactive oxygen species (ROS), including superoxide anion radical [$O_2^{\bullet-}$], hydroperoxyl radical [HOO^{\bullet}], and hydroxyl radical [OH^{\bullet}], reactive lipid species (viz. lipid peroxyl radical [LOO^{\bullet}]), reactive nitrogen species (RNS), such as nitric oxide radical [NO^{\bullet}], and non-free radicals, like hydrogen peroxide (H_2O_2) and peroxyxynitrite (ONOO), are *in vivo* oxidative stress inducers by interacting with cellular biomolecules (proteins, lipids, DNA, and carbohydrates) [7]. Therefore, *in vitro* and *in vivo* methods are used to screen EOs as antioxidants [8]. EOs can be considered preventive antioxidants as they can retard the initial formation of radical species within the Fenton-type [9] and Haber–Weiss reactions [10] by chelating the redox active metal ions (e.g., Fe^{2+}) [1]. In addition, EOs could be investigated as either chain-breaking antioxidants or termination-enhancing antioxidants for their ability to slow (or block) autoxidation by competing with propagation reactions (i.e., reacting with peroxyl radicals faster than the oxidizable substrate to form species that do not propagate the oxidation chain) [1]. To stop the propagation of peroxyl radicals, EOs could either scavenge them or neutralize them by hydrogen donation [1].

In this report, a series of 61 commercial EOs were extensively evaluated as potential antioxidants agents through the determination of their total antioxidant capacity (TAC) [11], their ability to chelate transition metal ions (M^{n+}) by means of the ferric reducing antioxidant power or FRAP assay [12], and their neutralizing affinities toward either 2,2-di(4-*tert*-octylphenyl)-1-picrylhydrazyl π -radical (DPPH $^{\bullet}$) [13], LOO^{\bullet} [14], 2,2'-azinobis-(3-ethylbenzothiazoline-6-sulfonic acid) cation radical (ABTS $^{\bullet+}$) [15], and OH^{\bullet} [16,17]. In addition, EOs have also been evaluated for their ability to protect against DNA damage induced by either peroxyl radicals (ROO^{\bullet}) or OH^{\bullet} [18–20], to the best of the authors' knowledge at the first time. Moreover, the results obtained in this study aided to update and upgrade the previously reported biological profiles of targeted EOs (Table 1 and Supplementary Materials Tables S1 and S3–S5) [21–96].

Table 1. Antioxidant activity of examined EOs and referent compounds against specific radicals.

EOs IDs	M ⁿ⁺ a	DPPH• b	LOO• c	ABTS•+ d	OH• e	ROO• f	OH• g
Official Latin names of biological source/sources			EC ₅₀ ^h (µg/mL)			ROO-RBD ₅₀ ⁱ (µg/mL)	OH-RBD ₅₀ ^j (µg/mL)
Chamomile Morocco <i>Cladanthus mixtus</i> (L.) Chevall.	>1	>1	>1	>1	>1	137.71 ± 0.53 _k	143.71 ± 0.37
Clary sage <i>Salvia sclarea</i> L.	>1	>1	>1	>1	>1	176.43 ± 0.32	168.31 ± 0.95
Sage oil <i>Salvia officinalis</i> L.	>1	>1	>1	>1	>1	142.56 ± 0.46	144.13 ± 0.32
Red thyme <i>Thymus praecox</i> Opiz “coccineus”	>1	0.230 ± 0.23	0.007 ± 0.006	0.003 ± 0.003	0.010 ± 0.06	NA	NA ^l
Tea tree <i>Melaleuca alternifolia</i> (Maiden & Betche) Cheel	>1	>1	>1	>1	>1	23.33 ± 0.13	46.14 ± 0.46
Melissa <i>Melissa officinalis</i> L.	>1	>1	>1	>1	>1	172.46 ± 0.57	129.13 ± 0.34
Mountain pine <i>Pinus mugo</i> Turra	>1	>1	>1	>1	>1	NA	110.92 ± 0.42
Geranium Bourbon Pelargonium x <i>asperum</i> Ehrh. ex Willd.	>1	>1	>1	>1	>1	NA	105.16 ± 0.11
Oregano <i>Origanum vulgare</i> L.	>1	0.110 ± 0.46	0.005 ± 0.005	0.004 ± 0.003	0.024 ± 0.011	184.90 ± 0.23	155.00 ± 0.54
Ylang-ylang <i>Cananga odorata</i> (Lam.) Hook. f. & Thomson	0.84 ± 0.47	0.630 ± 0.45	0.32 ± 0.26	0.76 ± 0.12	0.35 ± 0.14	64.12 ± 0.43	134.11 ± 0.67
Coriander <i>Coriandrum sativum</i> L.	>1	>1	>1	>1	>1	NA	143.54 ± 0.36
Lavender <i>Lavandula angustifolia</i> Mill.	>1	>1	>1	>1	>1	44.10 ± 0.54	209.76 ± 0.33
Myrtle <i>Myrtus communis</i> L.	>1	>1	>1	>1	>1	113.05 ± 0.54	NA
Garlic <i>Allium sativum</i> L.	>1	>1	>1	>1	>1	195.62 ± 0.31	NA
Cardamom <i>Elettaria cardamomum</i> (L.) Maton	>1	>1	>1	>1	>1	NA	202.89 ± 0.65
Mandarin <i>Citrus reticulata</i> Blanco	>1	>1	>1	>1	>1	197.55 ± 0.54	NA
Hyssop <i>Hyssopus officinalis</i> L.	>1	>1	>1	>1	>1	141.42 ± 0.56	31.07 ± 0.64

Table 1. Cont.

EOs IDs	M ⁿ⁺ a	DPPH• b	LOO• c	ABTS•+ d	OH• e	ROO• f	OH• g
Grapefruit <i>Citrus paradisi</i> Macfad.	1.58 ± 0.76	>1	>1	>1	>1	126.74 ± 0.21	103.10 ± 0.47
Lemongrass <i>Cymbopogon</i> <i>citratus</i> (DC.) Stapf	>1	0.720 ± 0.37	0.45 ± 0.18	0.65 ± 0.38	0.58 ± 0.27	52.85 ± 0.43	80.93 ± 0.41
Siberian pine <i>Abies sibirica</i> Ledeb.	>1	>1	>1	>1	>1	108.20 ± 0.11	132.61 ± 0.48
Camphor <i>Cinnamomum</i> <i>camphora</i> (L.) J. Presl	>1	>1	>1	>1	>1	NA	133.43 ± 0.73
Cade <i>Juniperus</i> <i>oxycedrus</i> L.	>1	0.007 ± 0.006	0.007 ± 0.003	0.017 ± 0.01	0.023 ± 0.014	NA	197.70 ± 0.51
Cedar leaves <i>Thuja occidentalis</i> L.	>1	0.550 ± 0.21	0.60 ± 0.34	0.35 ± 0.14	0.27 ± 0.12	96.44 ± 0.34	150.16 ± 0.38
Ginger <i>Zingiber officinale</i> Roscoe	>1	>1	>1	>1	>1	8.29 ± 0.54	56.34 ± 0.24
Cumin <i>Cuminum</i> <i>cyminum</i> L.	>1	>1	>1	>1	>1	168.58 ± 0.13	173.92 ± 0.43
Patchouli <i>Pogostemon</i> <i>cablin</i> Benth.	>1	>1	>1	>1	>1	63.56 ± 0.43	136.71 ± 0.47
Orange bitter <i>Citrus</i> <i>aurantium</i> L.	>1	>1	>1	>1	>1	NA	25.70 ± 0.32
Eucalyptus <i>Eucalyptus</i> <i>globulus</i> Labill.	0.78 ± 0.42	>1	>1	>1	>1	NA	NA
Pine Silvestre Natural <i>Pinus sylvestris</i> L.	>1	>1	>1	>1	>1	NA	213.0 ± 0.24
Bergamot <i>Citrus limon</i> (L.) Osbeck (syn. <i>Citrus</i> × <i>bergamia</i> Risso & Poit.)	1.72 ± 0.84	>1	>1	>1	>1	NA	58.70 ± 0.54
Juniper <i>Juniperus</i> <i>communis</i> L.	>1	>1	>1	>1	>1	NA	198.26 ± 0.67
Birch <i>Betula lenta</i> L.	>1	0.014 ± 0.012	0.014 ± 0.007	0.08 ± 0.04	0.12 ± 0.11	205.29 ± 0.41	NA
Fennel <i>Foeniculum</i> <i>vulgare</i> Mill.	0.75 ± 0.26	>1	>1	>1	>1	NA	NA
Cedar fruit <i>Citrus medica</i> L.	0.63 ± 0.37	>1	>1	>1	>1	54.50 ± 0.42	95.01 ± 0.54
Lemon <i>Citrus limon</i> (L.) Osbeck	1.28 ± 0.79	>1	>1	>1	>1	NA	136.18 ± 0.32
Roman chamomile <i>Chamaemelum</i> <i>nobile</i> (L.) All.	1.34 ± 0.49	>1	>1	>1	>1	NA	65.90 ± 0.21

Table 1. Cont.

EOs IDs	M ⁿ⁺ a	DPPH• b	LOO• c	ABTS•+ d	OH• e	ROO• f	OH• g
Savory <i>Satureja hortensis</i> L.	1.46 ± 0.49	0.110 ± 0.03	0.18 ± 0.09	0.065 ± 0.012	0.032 ± 0.007	NA	NA
Rosemary <i>Rosmarinus officinalis</i> L.	1.39 ± 0.67	0.375 ± 0.25	0.23 ± 0.11	0.26 ± 0.11	0.42 ± 0.24	NA	NA
Ceylon cinnamon peel <i>Cinnamomum verum</i> J. Presl	0.95 ± 0.78	0.023 ± 0.11	0.032 ± 0.006	0.125 ± 0.45	0.078 ± 0.06	60.99 ± 0.51	78.36 ± 0.43
<i>Eucalyptus globulus</i>	1.26 ± 0.56	>1	>1	>1	>1	NA	54.84 ± 0.11
Orange sweet <i>Citrus sinensis</i> (L.) Osbeck	>1	>1	>1	>1	>1	NA	NA
Niaouly <i>Melaleuca quinquenervia</i> (Cav.) S.T.Blake	>1	>1	>1	>1	>1	138.65 ± 0.46	195.34 ± 0.45
Artemisia <i>Artemisia vulgaris</i> L.	>1	>1	>1	>1	>1	197.40 ± 0.31	30.40 ± 0.46
Cajeput <i>Melaleuca cajuputi</i> Powell	>1	>1	>1	>1	>1	86.55 ± 0.41	NA
Black pepper <i>Piper nigrum</i> L.	>1	>1	>1	>1	>1	NA	NA
White thyme <i>Thymus vulgaris</i> L.	>1	0.120 ± 0.06	0.18 ± 0.12	0.089 ± 0.022	0.046 ± 0.031	204.18 ± 0.63	88.03 ± 0.23
Marjoram <i>Origanum marjorana</i> L.	>1	>1	>1	>1	>1	324.83 ± 0.41	60.02 ± 0.64
Clove <i>Syzygium aromaticum</i> (L.) Merr. & L. M. Perry	>1	0.008 ± 0.003	0.024 ± 0.007	0.0173 ± 0.009	0.098 ± 0.034	163.54 ± 0.46	88.36 ± 0.54
Cypress <i>Cupressus sempervirens</i> L.	>1	>1	>1	>1	>1	NA	99.03 ± 0.63
Nutmeg natural <i>Myristica fragrans</i> Houtt.	>1	0.840 ± 0.34	0.54 ± 0.27	0.66 ± 0.28	0.72 ± 0.24	NA	NA
Peppermint <i>Mentha piperita</i> L.	>1	>1	>1	>1	>1	NA	NA
Lemon verbena <i>Aloysia citriodora</i> Palau	>1	>1	>1	>1	>1	159.59 ± 0.54	95.99 ± 0.24
Basil <i>Ocimum basilicum</i> L.	>1	>1	>1	>1	>1	194.21 ± 0.31	NA
Palmarosa <i>Cymbopogon martini</i> (Roxb.) W.Watson	>1	>1	>1	>1	>1	NA	NA
Laurel <i>Laurus nobilis</i> L.	>1	0.680 ± 0.12	0.75 ± 0.36	>1	>1	NA	78.70 ± 0.54

Table 1. Cont.

EOs IDs	M ⁿ⁺ ^a	DPPH• ^b	LOO• ^c	ABTS•+ ^d	OH• ^e	ROO• ^f	OH• ^g
Natural anise pure <i>Pimpinella anisum</i> L.	>1	>1	>1	>1	>1	NA	83.71 ± 0.15
<i>Incense</i> <i>Boswellia</i> spp.	>1	>1	>1	>1	>1	NA	83.96 ± 0.78
<i>Mentha</i> <i>suaveolens</i> (Sicily) <i>Mentha</i> <i>suaveolens</i> Ehrh.	>1	>1	>1	0.89 ± 0.24	0.56 ± 0.12	NA	145.21 ± 0.34
<i>Coridothymus</i> <i>capitatus</i> (Sicily) <i>Thymbra capitata</i> (L.) Cav. (syn. <i>Thymus capitatus</i> (L.) Hoffmanns. & Link)	>1	0.256 ± 0.18	0.232 ± 0.14	0.09 ± 0.06	0.22 ± 0.17	215.90 ± 0.45	24.26 ± 0.41
<i>Thymus vulgaris</i> (Sicily) <i>Thymus vulgaris</i> L.	>1	0.990 ± 0.35	0.69 ± 0.36	0.84 ± 0.15	0.56 ± 0.50	232.47 ± 0.51	200.03 ± 0.53
<i>Origanum hirtum</i> (Sicily) <i>Origanum vulgare</i> subsp. <i>hirtum</i> (Link) Ietsw.	>1	0.570 ± 0.27	0.70 ± 0.28	0.39 ± 0.17	0.12 ± 0.08	NA	NA
AA ^m	NA	5.180 ± 0.46	>100	15.47 ± 0.36	>100	NA	NA
BHT ⁿ	NA	13.25 ± 0.41	3.12 ± 0.98	10.16 ± 1.41	30.14 ± 0.24	NA	NA
EDTA ^o	3.18 ± 0.59	NA	NA	NA	NA	NA	NA
Q ^p	NA	NA	NA	NA	NA	NA	NA

^a Metal-ion-chelating capacity; ^b Neutralization of DPPH radical; ^c Interruption of lipid peroxidation; ^d Neutralization of ABTS cation radical; ^e Neutralization of hydroxyl radical; ^f Protection of DNA against the damage induced by the alkoxy radical; ^g Protection of DNA against the damage induced by the hydroxyl radical; ^h Effective concentration that neutralizes the 50% of free radical; ⁱ Concentration that stimulates 50% of relative electrophoretic bands density (RBD) increase (viz. protection) of DNA damaged by alkoxy radical; ^j Concentration that stimulates 50% of relative electrophoretic bands density (RBD) increase (viz. protection) of DNA damaged by hydroxyl radical; ^k The measurement is presented with standard deviation from three independent experiments; ^l Not available; ^m Ascorbic acid; ⁿ Butylated hydroxytoluene; ^o Ethylenediaminetetraacetic acid; ^p Quercetin.

The in vitro antioxidant properties of the 61 EOs were analyzed by means of machine learning (ML) classification algorithms (Table 2) to correlate their chemical compositions (Supplementary Materials Table S2) with the obtained potencies, as a main objective of the enclosed study. Hence, a list of quantitative composition–activity relationships (QCARs) models was generated to shed light on the chemical components mainly responsible for the redox properties and to relate their contributions in terms of the positive or negative modulation of metal ion chelation/free radical neutralization. Previous applications of ML to EOs have enabled the correlation of their chemical composition to antimicrobial [96–99], antiviral [100], and anticancer properties [101,102].

In addition, EOs showing high potency in exerting antioxidant activity in vitro were selected for in vivo investigation using adult Wistar rats pre-exposed to carbon tetrachloride (CCl₄) [103], in terms of their hepatoprotective/antioxidant effects and anti-genotoxic potentials.

To the best of the authors' knowledge, this is the very first wide investigation in vitro and in vivo of EOs as antioxidants integrated with the application of ML algorithms to explain the antioxidant properties of EOs and their composition associated with in vivo data.

Table 2. Parameters and statistical coefficients of the best ML models.

Model	ML1	ML2	ML3	ML4	ML5	ML6	ML7
Free Radical Threshold	M ⁿ⁺	DPPH [•]	LOO [•]	ABTS ^{+•}	OH [•]	ROO-RBD _{50s}	OH-RBD ₅₀
Algorithm	GB	SVM	SVM	KNN	RF	GB	KNN
N level	3	2	0	0	1	1	3
Scaling	1	0	0	0	0	1	1
PCA	0.9	0.0	0.99	0.6	0.8	0.7	0.8
nMCC _{Pred}	0.81	0.90	0.98	0.93	0.95	0.73	0.68
nMCC _{CV}	0.60	0.90	0.91	0.80	0.82	0.68	0.58

2. Materials and Methods

2.1. Essential Oils

The 61 EOs were acquired from Farmalabor srl (Assago, Italy). Their chemical compositions were analyzed by gas chromatography–mass spectrometry (GC-MS) as previously reported [97] (Table 3 and Supplementary Material Table S2). Briefly, each component was identified by comparing the obtained mass spectra with those reported in the Nist 02 and Wiley mass spectra libraries. Linear retention indices (LRIs) of each compound were also calculated using a mixture of aliphatic hydrocarbons. Knowing the chemical composition of the 61 EOs and their associated properties (Supplementary Material Table S2) [97] made them eligible as a dataset to develop QCARs models by means of ML algorithms [96–102]; therefore, they were also used herein to generate a list of ML models for antioxidant activities.

Table 3. The Ylang-ylang and Ceylon cinnamon peel Eos' chemical compositions.

Ylang-Ylang EO Component (%)	Ceylon Cinnamon Peel EO Component (%)
eucalyptol (0.24)	eugenol (34.63)
eugenol (0.58)	linalool (3.19)
linalool (10.36)	α-pinene (0.25)
methyl benzoate (2.06)	acetylcoumarin (1.29)
<i>p</i> -methylanisole (3.28)	α-phellandrene (0.34)
α-copaene (1.24)	<i>o</i> -cymene (0.69)
farnesyl acetate	β-phellandrene (0.51)
τ-cadinol (1.69)	α-terpineol (0.31)
δ-cadinene (3.84)	α-copaene (0.48)
farnesol (2.61)	limonene (0.20)
geraniol (1.50)	tetradecanal (0.46)
nerol acetate (12.21)	<i>trans</i> -3-phenyl-2-propenal (49.11)
δ-cadinene (3.84)	β-isosafrole (0.89)
farnesol (2.61)	2-methoxycinnamaldehyde (0.20)
geraniol (1.50)	caryophyllene oxide (0.21)
nerol acetate (12.21)	caryophyllene (4.01)
caryophyllene (15.47)	humulene (0.63)
(<i>E</i>)-β-farnesene (13.92)	cinnamyl ester acetic acid (2.61)
humulene (4.29)	
cinnamyl ester acetic acid (0.96)	
germacrene D (18.23)	
<i>trans</i> -calamenene (0.30)	
γ-cadinene (2.77)	
β-elemene (0.48)	
β-ylangene (0.47)	

For experimental purposes, the EOs were dissolved in dimethyl–sulfoxide (DMSO) at 50 mg/mL to obtain complete solubilization and further diluted in the medium for in vitro and in vivo experiments, always resulting in a DMSO concentration that does not affect experimental protocols.

2.2. Chemicals and Reagents

Sulfuric acid (CAS No. 7664-93-9), sodium phosphate dibasic (CAS No. 7558-79-4), sodium phosphate monobasic (CAS No. 13472-35-0), ammonium molybdate (CAS No. 12054-85-2), ferrous sulfate (CAS No. 7782-63-0), ferrozine (3-(2-Pyridyl)-5,6-diphenyl-1,2,4-triazine-4',4''-disulfonic acid sodium salt, CAS No. 69898-45-9), linoleic acid (CAS No. 60-33-3), Tween-40 (CAS No. 9005-66-7), ammonium thiocyanate (CAS No. 1762-95-4), DPPH (2,2-Diphenyl-1-picrylhydrazyl, CAS No. 1898-66-4), ABTS (2,2'-azino-bis(3-ethylbenzothiazoline-6-sulphonic acid), CAS No. 30931-67-0), potassium persulfate (CAS No. 7727-21-1), iron(III)chloride hexahydrate (CAS No. 10025-77-1), ascorbic acid (CAS No. 50-81-7), EDTA (Ethylenediaminetetraacetic acid, CAS No. 60-00-4), 2-deoxy-ribose (CAS No. 533-67-5), hydrogen peroxide (CAS No. 7722-84-1), TBA (2-thiobarbituric acid, CAS No. 504-17-6), TCA (trichloroacetic acid, CAS No. 76-03-9), DTNB (CAS No. 69-78-3), hydrochloric acid (CAS No. 7647-01-0), sodium carbonate (CAS No. 497-19-8), sodium bicarbonate (CAS No. 144-55-8), sodium dodecyl sulfate (CAS No. 151-21-3), acetic acid (CAS No. 64-19-7), sodium hydroxide (CAS No. 1310-73-2), and epinephrine (CAS No. 51-43-4) were purchased from Sigma-Aldrich Corp (St. Louis, MO, USA). Deoxyribonucleic acid from salmon sperm (CAS No. 100403-24-5) was purchased from Sigma Aldrich (St. Louis, MI, USA), while 2,2'-azo-bis(2-methylpropionamide) dihydrochloride (AAPH) was obtained from Acros, Organics (New Jersey, USA). Low-melting-point agarose (CAS No. 9012-36-6), normal-melting-point agarose (CAS No. 9012-36-6), and ethidium bromide (CAS No. 11497653) were obtained from Alfatrade Enterprise D.O.O. (Serva Electrophoresis GmbH, Heidelberg, Germany). Assay kits for the determination of aspartate transaminase (AST, Ref. MX41264), alanine transaminase (ALT, Ref. MX41274), alkaline phosphatase (ALP), γ -glutamyltransferase (γ -GT, Ref. MX41288), and the total protein concentration (Ref. 1001290) were purchased from Spinreact (Girona, Spain). The Xanthine Oxidase Assay Kit (ab102522) and Nitric Oxide Assay Kit (ab 65328) were purchased from Abcam, while the cytochrome c reductase NADPH assay kit (CY0100-1KT) and Glutathione Peroxidase Assay Kit (MAK437) were purchased from Sigma-Aldrich Corp (St. Louis, MO, USA).

2.3. Antioxidant Activity

2.3.1. Total Antioxidant Capacity

The TAC of the EOs was evaluated using the phosphomolibdenum method [11]. An aliquot of 100 μ L of each EO was mixed with 1 mL of reagent solution (0.6 M sulfuric acid, 28 mM sodium phosphate, and 4 mM ammonium molybdate). The mixture was incubated at 95 $^{\circ}$ C for 90 min, and after cooling to room temperature (25 $^{\circ}$ C), the absorbance was measured at 695 nm. All measurements were performed using a Dynamica HALO DB-20 UV-Vis spectrophotometer. The results were calculated using a calibration curve for ascorbic acid and expressed as the mg of ascorbic acid equivalents per g of EO (mg AAE/g EOs).

2.3.2. Metal Chelating Ability (Ferric-Reducing Antioxidant Power (FRAP) Assay)

To evaluate the ability of EOs to chelate transition metals and avoid the generation of free radicals, a ferrous ion chelation assay was used [12]. The reaction mixture contained 1 mL of 0.125 mM FeSO₄ solution and 1 mL of 0.3125 mM ferrozine water solution, as well as 2 mL of serial dilutions of EOs or reference compound dissolved in methanol. The mixtures were kept for 10 min at room temperature (25 $^{\circ}$ C), and the absorbance was measured at 562 nm. The ability of EOs to chelate metal ions was expressed as the percentage of inhibition and calculated according to Formula (1):

$$\%inhibition = \frac{A_c - A_t}{A_c} * 100 \quad (1)$$

where A_t is the absorbance of the sample and A_c is the absorbance of the control sample. The concentration of the tested EOs that reduces 50% of the initial metal ion/free radical

concentration, i.e., the EC₅₀ value, was calculated using the dose–response sigmoidal curve, as implemented in OriginPro v8.1 (OriginLab Corporation, Northampton, MA, USA).

2.3.3. DPPH-Radical-Neutralizing Activity Assay (DPPH Assay)

The determination of the potency of EOs to neutralize the DPPH radical was performed according to the described method [13]. An aliquot of 2 mL of each EO (serial dilutions in methanol 2–0.0078 µg/mL) or the reference compound was mixed with 1 mL of 80 µg/mL DPPH solution in methanol. The control sample contained no EOs or reference compounds and was prepared using 1 mL of DPPH solution and 1 mL of methanol. After 30 min, the absorbance was measured at 517 nm. All measurements were performed in triplicate, and the average absorbance was calculated for each concentration. The ability of the EO to neutralize DPPH was expressed as the percentage of inhibition according to Formula (1), and the EC₅₀ value was calculated similarly for the FRAP assay.

2.3.4. Inhibition of Lipid Peroxidation

The potential of EOs to inhibit lipid peroxidation was estimated by the thiocyanate method [14]. Samples were prepared by adding 0.5 mL of each EO (serial dilutions in methanol 2–0.0078 µg/mL), 2.5 mL linoleic acid emulsion (prepared by mixing 0.2804 g linoleic acid), and 0.2804 g Tween-40 in 50 mL 40 mM sodium phosphate buffer, pH 7.0. The reaction mixtures were incubated at 37 °C for 72 h. To 0.1 mL of this solution, 4.7 mL of 75% ethanol, 0.1 mL of 30% ammonium thiocyanate solution, and 0.1 mL of 20 mM FeSO₄ solution were added. After stirring for 3 min, the absorbance was measured at 500 nm against methanol (blank). The inhibition percentage of linoleic acid peroxidation was calculated using Formula (1), and the EC₅₀ value was calculated similarly to the FRAP assay.

2.3.5. ABTS-Radical-Cation-Neutralizing Activity (ABTS Assay)

The ability of EOs to neutralize the 2,2'-azino-bis(3-ethylbenzothiazoline-6-sulfonic acid (ABTS) radical cation [15] was measured as follows: 0.2 mL of each EO (serial dilutions in methanol 2–0.0078 µg/mL) or reference compound and 1.8 mL of the ABTS radical cation working reagent (prepared 16 h earlier by mixing equal amounts of 7 mM ABTS and 2.45 mM K₂S₂O₈ and adjusted to an absorbance of 0.7 at 734 nm before addition to the tubes). In parallel, a control sample was prepared with only methanol. The reaction mixtures were kept in the dark for 30 min, and then the absorbance was measured at 734 nm. The percentage of neutralization of the ABTS radical cation was calculated using Formula (1), and the EC₅₀ value was calculated similarly to the FRAP assay.

2.3.6. Hydroxyl-Radical-Neutralizing Activity (Hydroxyl Radical Antioxidant Capacity (HORAC)) Assay

The determination of the hydroxyl-radical-neutralizing activity of EOs was measured according to the method described in [16]. Reaction mixtures were prepared as follows: 0.2 mL of serial dilutions of each EO dissolved in methanol were mixed with 0.2 mL of 10 mM FeCl₃ solution, 0.1 mL of 1 mM ascorbic acid solution, 0.1 mL of 1 mM EDTA solution, 0.2 mL of 10 mM 2-deoxy-ribose solution, and 0.1 mL of 10 mM H₂O₂ solution. The tubes were then incubated at 37 °C for 1 h, 1 mL of 0.5% TBA in 10% TCA water solution was added, and the resulting mixture was incubated at 80 °C for 30 min. After cooling to room temperature (25 °C), the absorbance was measured at 535 nm. The percentage of inhibition was calculated using Formula (1), and the EC₅₀ value was calculated similarly to the FRAP assay.

2.4. Antigenotoxic Activity In Vitro

The Protective Activity of Essential Oils against Peroxyl- and Hydroxyl-Radicals-Induced DNA Damage

The protective effect of the EOs (25, 50, 100, 200, and 400 µg/mL) against either peroxyl-radical-induced (generated by 2,2'-azobis-2-methyl-propanimidamide (AAPH)) or hydroxyl-radical-induced DNA damage was evaluated in vitro using salmon sperm DNA [18,20]. In both assays, quercetin (100 µg/mL) was used as a reference [19]. DNA bands on agarose gels were visualized under UV light (UV Transilluminator, Vilber Lourmat, France) at 365 nm, photographed, and analyzed using ImageJ software (version 1.48 for Windows, Softonic International, Barcelona, Spain).

2.5. Machine Learning

All analyses were performed using the Python programming language (version 3.7) [104,105] by executing in-house code in the Jupyter Notebook platform [96,97,106]. The chemical composition of each EO and the antioxidant activity data were imported and transformed into a dataframe and pre-processed to the final datasets to obtain the classification models. Scikit-learn (sklearn) [107] and the Pandas [108,109] libraries were used to implement ML algorithm protocols. Initial QCAR models were elaborated through 5 different classification algorithms (SVM, RF, GB, DT, and KNN). The dataset was divided into training and test sets using a ration (80:20) using the stratify splitting method implemented in sklearn.

During model development, an unsupervised dimensionality reduction/transformation was also performed with principal component analysis (PCA) [110] to extract 60%, 70%, 80%, 90%, and 99% of the explained variance (Table S6, Supplementary Material). Moreover, components represented by an occurrence as low as 1, 2, 3, and 4 times were therefore eliminated from the training set (n-level). Data were also processed using the MinMaxScaler function (scaling), which allows the original values to be scaled to ranges between 0 and 1.

Different cut-off values (thresholds) related to the antioxidant EC₅₀ were used to develop ad hoc models with the optimal active/inactive ratio defined by the threshold value itself (Supplementary Material Table S7). The PCA, n-level, scaling, and threshold represented the dataset pretreatment parameters.

Differently from previously reported studies, the models were optimized in predictive ability; therefore, cross-validation was only performed on the final models to characterize their robustness. The optimal pretreatment parameters and ML hyperparameters (Supplementary Material Tables S8 and S9) were selected through the predictive Matthews correlation coefficient (MCC_{pred}) obtained by comparing the experimental classes (active or inactive) with the predicted one.

Due to the high number of considered pretreatment parameters and hyperparameter combinations, the ML modeling strategy was conducted as follows:

1. Coarse ML models generation was run with 100 and 1000 random combination runs from all possible considered combinations (Tables S6–S8, Supplementary Material) [111], so we selected the suboptimal ML algorithms and associated pretreatment parameters (n-level, scaling, threshold, and PCA). For details, see Supplementary Material;
2. Refined models were investigated with 10,000 and 100,000 random combination runs from all possible considered combinations (Supplementary Material Tables S6, S7 and S9), while avoiding those non-selected in the previous point. The selection of the final models was based on the MCC_{pred} values. For details, see Supplementary Material (Tables S10–S65);
3. The final model was finally defined by retaining the optimal parameters selected at point 2 and using the full dataset. The accuracy (ACC), F1 score, and MCC were used to evaluate the binary classification models numerically and graphically. The importance of each chemical component present in the EOs was independently evaluated through the “feature importance” (FI) and partial dependence (PD) [112] methods, as implemented in the Skater Python library [113]. In addition, Spearman’s correlation

coefficient was used to weight the correlation between the percentage presence of a component in the EOs and its partial dependence, thus obtaining the weighted FI values (WFI). Models were evaluated by leave-some-out CV by means of five groups using the stratified K-fold method while monitoring the average value of MCC_{CV} obtained from 50 random CV iterations [98,114].

2.6. Animals and Study Design

Forty male albino Wistar rats weighing 220 ± 20 g used in this study were obtained from the Animal House of the Military Medical Academy, Belgrade, Serbia, and acclimated for 3 days before the experiment. They were maintained under a 12 h light–dark cycle, and food and water were provided ad libitum. All animal procedures were approved by the Ethical Committee of the Faculty of Science, University of Kragujevac (Ethical approval number 1-03/2023), which acts according to the relevant Serbian guidelines, including the Guidelines for the Care and Use of Laboratory Animals and the Law on Animal Welfare (“Official Gazette of the Republic of Serbia,” No. 810 41/09) and the Euro-pean Directive for the Welfare of Laboratory Animals Directive 2010/63/EU.

In the current study, the rats were randomly divided into 8 groups of 5 rats each. Group I (negative control) was injected intraperitoneally with 1 mL/kg body weight of commercial olive oil (Monini Olio Extra Vergine di Oliva). Group II (positive control) received a single intraperitoneal dose of CCl_4 , 1 mL/kg body weight, 1:1 mixture in olive oil [115]. The remaining groups of animals (groups III to VIII) were co-treated (1, 200, and 400 mg/kg body weight) with EOs selected among the more potent against each of the in vitro redox species and CCl_4 (1 mL/kg body weight). The rats were sacrificed after 24 h under light ether anesthesia, and the kidney and liver organs were removed and cleaned.

2.7. Measurement of Antioxidant Markers

Isolated kidney and liver organs were used for the measurement of redox and toxicity markers and the determination of DNA-protective activity. Rat liver and kidney samples were homogenized in phosphate buffer (5 mM, pH 7.4) to obtain a 10% (*w/v*) homogenate and then centrifuged at 4000 rpm for 15 min at 4 °C. The supernatants were used to estimate the catalytic activity of superoxide dismutase (SOD) [116], the level of TBARS [117], the catalytic activity of catalase (CAT) [118], and the concentration of reduced glutathione (GSH) [119] through the colorimetric method. Total protein concentrations were determined according to the Lowry method [120]. All colorimetric measurements were performed using a Dynamica HALO DB-20 UV-VIS spectrophotometer.

2.7.1. Measurement of Serum Toxicity Markers

Blood samples were collected from each animal for serum preparation according to the Quick method [121]. Serum for the determination of biochemical parameters, aspartate transaminase (AST) [122], alanine aminotransaminase (ALT) [123], alkaline phosphatase (ALP) [124], and γ -glutamyltransferase (γ -GT) [125] was prepared through the Quick method [121], immediately immersed in liquid nitrogen, and stored at -80 °C until use. The catalytic activities of AST and ALT at 340 nm and of ALP and γ -GT at 405 nm were determined through the UV-VIS kinetic methods according to the recommendations of the Expert Panel of the International Federation of Clinical Chemistry (IFCC) [59–62]. Total protein concentrations were determined through the Lowry method using bovine serum albumin as the standard [63]. All kinetic and colorimetric measurements were performed using a Dynamica HALO DB-20 UV-VIS spectrophotometer.

2.7.2. Xanthine Oxidase Catalytic Activity

Xanthine oxidase activity in kidney homogenates was estimated using a spectrophotometric xanthine oxidase assay kit from Abcam (ab102522) [126]. Briefly, 50 μ L of kidney homogenate (H_2O_2 standard or xanthine oxidase positive control diluted in dH_2O) and 50 μ L of sample reaction mix (containing assay buffer, xanthine oxidase substrate

mix, developer solution V, and OxiRed probe) were added to each well and mixed well. Measurement was performed immediately at 570 nm and again after incubation of the reaction at 25 °C for 10–20 min. The calculation was performed using the H₂O₂ standard curve and expressed as U/L.

2.7.3. NADPH Oxidase Catalytic Activity

Renal NADPH oxidase activity was measured using a cytochrome c reductase NADPH assay kit (Sigma, USA) [127]. This assay measures the reduction of cytochrome c by NADPH–cytochrome c reductase in the presence of NADPH. The absorbance spectrum of cytochrome c changes with its oxidation/reduction state. The reduction of cytochrome c is monitored by the increase in the absorbance of cytochrome c at 550 nm. The results are expressed as U/mg protein. One unit of enzyme activity reduces 1 μmol of oxidized cytochrome c per minute in the presence of 100 μmol of NADPH at pH 7.8 and 25 °C.

2.7.4. Nitric Oxide Catalytic Activity

Nitric oxide (measured as nitrates/nitrites concentration) was determined using the Abcam colorimetric nitric oxide assay kit (ab 65328) [128]. To each well, 85 μL of kidney homogenates (previously deproteinized) or nitrate standard solutions diluted in assay buffer, 5 μL of nitrate reductase enzyme, and 5 μL of enzyme cofactor were added. The blank sample contained assay buffer only. The covered plate was incubated for 60 min at room temperature (25 °C). Next, 5 μL of Enhancer was added to the standard and sample wells only, and the incubation continued for an additional 10 min. Finally, 50 μL of Griess Reagent I and 50 μL of Griess Reagent II were added to the standard and sample wells, and the OD was measured at 540 nm. The concentration of nitrates/nitrites was determined from the standard curve.

2.7.5. Glutathione Peroxidase Activity

Renal glutathione peroxidase (GPx) activities of EO were determined through the method based on the oxidation of GSH (Sigma-Aldrich Chemical Co., USA) by hydrogen peroxide (H₂O₂) (El-Nasr Pharmaceutical Co., Oubour, Qalyubia, Egypt) in the presence of GPx [48]. The decrease in absorbance was measured at 340 nm as NADPH (Sigma-Aldrich Chemical Co., USA) and it was converted to NADP⁺, reflecting the amount of oxidized glutathione formed and, consequently, the activity of GPx. Enzyme activity was expressed as U/mg protein, where one unit is defined as the amount of enzyme oxidizing 1 μmol NADPH per minute at 25 °C.

2.8. Assessment of *In Vivo* Antigenotoxic Activity

The DNA-protective potential of EO was detected using the alkaline comet assay [129]. Images were visualized and captured using a 40x objective of a Nikon (Ti-Eclipse) fluorescence microscope attached to a CCD camera. One hundred randomly selected cells (fifty cells per two replicate slides) per treatment were analyzed using a visual scoring method [130]. Comets were classified into five types defined as T0, T1, T2, T3, and T4 (no or very low damage, low, medium, and long DNA migration, and the highest level of degradation, respectively). Total comet scores and the percentage of reduction (%R) in the total comet scores were calculated as described elsewhere [131].

2.9. Statistical Analysis

The results are expressed as mean ±SEM, and the statistical evaluation of data was performed through one-way analysis of variance (ANOVA) using the SPSS statistical software package, version 13.0, running on Microsoft Windows version 10. The significance level was set at $p < 0.05$.

3. Results

3.1. Determination of In Vitro Antioxidant Activity

3.1.1. Total Antioxidant Capacity

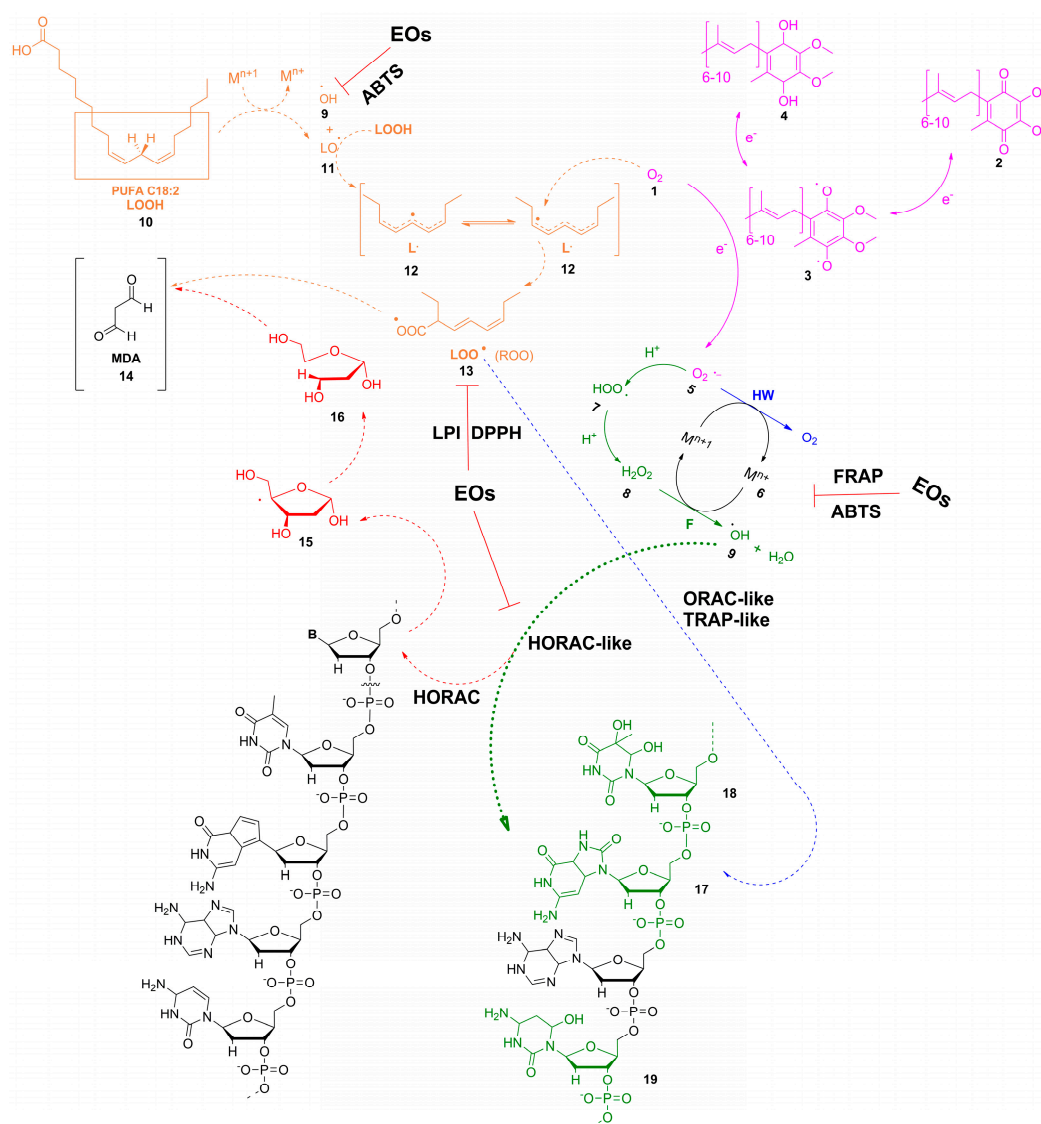
TAC (Supplementary Materials Table S3), for the majority of the EOs herein not previously reported (NPR, Supplementary Materials Table S1), refers to the general ability of a given EO to oxidize free radicals, and it was evaluated here in vitro using the phosphomolybdenum method. However, because the TAC results do not explain the metal-chelating/free-radical-neutralizing potency of either ROS or RNS but instead only compare the potency of an antioxidant with an ascorbic acid (AA) by AA equivalents (AAE; the higher the number of $\mu\text{g AAE/mg}$, the greater should be the antioxidant potency), the test may lead to false positive values.

Therefore, EOs ranging from 0.002 (*Origanum hirtum* EO) to 1.231 $\mu\text{g AAE/mg}$ (Black pepper EO) were considered suitable for future in vitro studies. Notably, Black pepper EO had no potency against $\text{M}^{\text{n}+}$, DPPH \bullet , LOO \bullet , ABTS \bullet^+ , or OH \bullet , whereas *Origanum hirtum* EO showed remarkable potency for all radical species except for $\text{M}^{\text{n}+}$ (Table 1). Consequently, TAC data poorly correlated with the antioxidant potentials of the tested EOs. For example, among all EOs with a TAC higher than 0.250 $\mu\text{g AAE/mg}$, only Birch EO with a TAC value of 0.522 $\mu\text{g AAE/mg}$ exerted potency against all redox species except $\text{M}^{\text{n}+}$. EOs with lower TAC, such as Cedar leaf EO, showed a similar profile. On the other hand, remarkable potency against $\text{M}^{\text{n}+}$, DPPH \bullet , LOO \bullet , ABTS \bullet^+ , and OH \bullet (Table 1) was observed for EOs with low TAC values (0.119 to 0.006 $\mu\text{g AAE/mg}$), such as Savory, Rosemary, Ylang-ylang (YY EO), and Ceylon cinnamon peel (CCP EO). In contrast, EOs showing TAC ranging from 0.131 μg to 0.003 $\mu\text{g AAE/mg}$ had only the ability to chelate $\text{M}^{\text{n}+}$ (Supplementary Materials Table S3).

3.1.2. Metal-Ions-Chelating Activity

Regarding Eos' chelating abilities of metal ions, the Fe^{2+} ion ($\text{M}^{\text{n}+}$) is involved in the redox signaling of molecular oxygen O_2 (Scheme 1, pink pathway, 1), a major precursor of ROS in biological systems. O_2 , being an electron acceptor of coenzyme Q in the mitochondrial electron transport chains (Scheme 1, pink pathway, 2–4), generates $\text{O}_2^{\bullet-}$, the first oxidative stress inducer (Scheme 1, pink pathway, 5) [7,132]. $\text{O}_2^{\bullet-}$ is a short-living species undetectable by in vitro assays [7]; nevertheless, it reacts with other radicals to form other reactive species [133] that can be routinely determined either in vitro or in vivo [9,10], making the variety of in vitro or in vivo methods somewhat correlated (Scheme 1).

$\text{O}_2^{\bullet-}$ has a low membrane permeability; therefore, it reacts mainly in the physiological compartment where it is generated and then passes through ion channels, initiating two crucial reactions for the triggering of oxidative stress: the Fenton-type (Scheme 1, green pathway, F) [9] and the Haber–Weiss reaction (Scheme 1, blue pathway, HW) [10]. Both reactions are catalyzed by transition metal ions ($\text{M}^{\text{n}+}$, usually Fe^{2+} and Fe^{3+} , but also Cu^{2+} , Ni^{2+} , Co^{2+} , and V^{2+}) [12]. Thus, the Fenton reaction catalyzed by Fe^{2+} ions (Scheme 1, green pathway, 6) yields hydroperoxide radical (HOO \bullet) (Scheme 1, green path, 7), H_2O_2 (Scheme 1, green path, 8) and OH \bullet (Scheme 1, green path, 9) [9,133], whereas the Haber–Weiss reaction, catalyzed by Fe^{3+} ions, yields new amounts of O_2 (Scheme 1, blue path 10) [133]. Subsequently, either O_2 or HOO \bullet is involved in the lipid autooxidation/peroxidation of polyunsaturated fatty acid (Scheme 1, orange pathway, 11) [134,135], on the level of propagation, while targeting the carbon-centered lipid radicals (alkyl radicals, L \bullet , Scheme 1, orange path, 12) to yield LOO \bullet (Scheme 1, orange pathway, 13), and, finally, malondialdehyde (MDA) (Scheme 1, orange pathway, 14) [135]. Metal ion chelation in vivo could slow down peroxidation, prevent the decomposition of lipid hydroperoxides into other components capable of abstracting hydrogen, and stop the reaction chain of lipid peroxidation [134].



Scheme 1. The inter-correlation of methods used for monitoring/neutralizing in vitro and in vivo, emphasizing the emergence of ROS by means of the EOs herein. The in vivo emergence of redox-inducing species (pink path, thick arrows): O_2 , (1), coenzyme Q quinone form (2), coenzyme Q radical form (3), coenzyme Q hydroquinone form (4), $O_2^{\bullet-}$ (5); The in vitro assays: FRAP and ABTS assays (green path, thick arrows): Fe^{2+} ion (6), hydroperoxide radical (HOO^{\bullet} , 7), H_2O_2 (8), OH^{\bullet} (9); FRAP and ABTS assays (blue path, normal arrow): Fe^{3+} ion (10); DPPH and LPI assays (orange path, dashed arrows): polyunsaturated fatty acid (10), lipid oxy-radical, L^{\bullet} (11), lipid radical, L^{\bullet} (12), lipid peroxy-radical, LOO^{\bullet} (13), malondialdehyde (14); HORAC assay (red path, dashed arrows): 2'-deoxyribose radical (15), riboxyradical (16); ORAC- or TRAP-like electrophoretic assay (blue path, dashed arrow): 8-oxoG (17); HORAC-like electrophoretic assay (green path, dashed arrows): 8-oxoG (17), thymineglycol (18), 6-hydroxy-5,6-dihydrocytosine (19).

Because M^{n+} metal ions play an important role at the very beginning of redox signaling or later in the redox signaling cascade (Scheme 1, green path, thick arrows), the chelating ability of the present EOs was measured by FRAP assay. As already indicated, 12 out of 61 EOs (~20% of the TAC-active EOs) (namely, YY, Grapefruit, Eucalyptus, Bergamot, Fennel, Cedar fruit, Lemon, Roman chamomile, Savory, Rosemary, CCP, and *Eucalyptus globulus* EOs) showed chelating properties in the range of $EC_{50} = 0.63\text{--}1.72 \mu\text{g/mL}$. Nevertheless, no significant linear regression correlation was obtained between TAC and M^{n+} potencies. Interestingly, the YY, CCP, Rosemary, and Savory EOs were active in all an-

tioxidant assays and characterized by medium to high EC₅₀ values of 0.84, 0.95, 1.39, and 1.46 µg/mL, respectively (compared to NPR, 25–68,380 µg/mL, 195 µg/mL, and NPR, Supplementary Materials Table S3).

3.1.3. DPPH•-Radical-Neutralizing Activity

The mechanism of DPPH• neutralization is comparable to that against LOO• (see next) during the rate-limiting propagation step of lipid peroxidation (Scheme 1, orange pathway, dashed arrows, 13) [7,135,136]; therefore, the results of the DPPH assay could be used to predict lipid peroxidation inhibition potency [137]. Only 17 EOs (Red thyme, Oregano, YY, Lemongrass, Cade, Cedar leaves, Birch, Savory, Rosemary, CCP, White thyme, Clove, Laurel, *Coridothymus capitatus*, *Thymus vulgaris*, and *Origanum hirtum*) exhibited good affinity to neutralize DPPH radicals [13] over the EC₅₀ concentration range of 0.007 µg/mL (Cade EO) to 0.99 µg/mL (*Thymus vulgaris* EO). CCP, Savory, Rosemary, and YY EO were characterized with an EC₅₀s of 0.023, 0.110, 0.375, and 0.630 µg/mL, respectively (Table 1 and Supplementary Materials Table S3).

As for metal-ions-chelating activity, no significant linear correlation was observed between TAC and DPPH assays values. Nevertheless, the present EOs probably reduced the divalent N-atom of DPPH• to the hydrazine DPPH•H by donating either their alcoholic or methylene protons [1] through the “hydrogen atom transfer” (HAT) mechanism or phenolic protons through the “proton-coupled electron transfer” (PCET) mechanism [137].

3.1.4. Lipid Peroxidation Inhibition Activity

EOs were evaluated for their ability to stop lipid peroxidation processes within the membrane [135,136] by means of in vitro [14] and in vivo [103] lipid peroxidation inhibition (LPI) assays (see next). Here, each EO neutralized LOO• in vitro within a linoleic acid/water emulsion system [14] and was compared against the BHT, used as a reference.

At first glance, all EOs active in the DPPH assay showed remarkable potency for LOO•, and none of the DPPH•-inactives exerted any affinity for LOO•. The total EC₅₀ concentration range of active EOs against LOO• ranged from 0.005 (Oregano EO) to 0.75 µg/mL (Laurel EO). In addition, the results of the DPPH and LPI assays significantly correlated with an r^2 value of 0.79 ($[EC_{50}] LOO\bullet = 1.0511 \times [EC_{50}] DPPH\bullet + 0.0599$), indicating some predictivity ability for LPI from a DPPH assay. Among the 17 EOs found active in the DPPH• assay above, Red thyme, Oregano, YY, Lemongrass, Rosemary, Natural nutmeg, *Thymus vulgaris*, *Coridothymus capitatus*, and White thyme were more potent against LOO• and Cade and Birch EO were equally potent against both radicals, whereas Cedar leaf, CCP, Clove, and *Origanum hirtum* EO were more potent against DPPH• with respect to LOO•. Interestingly, CCP, Savory, Rosemary, and YY EOs, potent against any given metal ion/radical species, showed EC₅₀s against LOO• of 0.032, 0.180, 0.230, and 0.230 µg/mL, respectively (Supplementary Materials Table S3).

By exerting potency through the lipid peroxidation assay, the above-listed EOs can be classified either as chain-breaking antioxidants (when containing hydroxyl groups), interrupting lipid peroxidation at the rate-limiting propagation step and neutralizing the LOO•, or as termination-enhancing antioxidants (when containing nonphenolic terpenoids, i.e., methylene C-H as proton donors) [1], resulting in an overall increase in the rate of oxidative chain termination [1] and for the most potent EOs confirmed in vivo (see text below) [103].

3.1.5. ABTS-Cation-Radical-Neutralizing Activity

Either Fenton-type reactions [9] or lipid peroxidation initiation reactions [34,35] produce an excess of OH• (Scheme 1, green and orange paths, dashed arrows, 9). While the effect of these EOs on Fenton-type OH• biosynthesis was later determined by modulating the catalase-driven decomposition of H₂O₂ in vivo (Scheme 1, dark green path, bold arrows) [7,103], it was first assessed indirectly in vitro using the ABTS assay [15] (ABTS^{•+}/DPPH• and ABTS^{•+}/LOO• interrelationships are reported in the Supplementary

Material). Thus, in the ABTS/H₂O₂/peroxidase (catalase) in vitro system, ABTS acts as a reducing agent, substituting the enzyme's compound I (i.e., porphyrin radical cation, Por⁺⁺-Fe^{IV}=O) for compound II (i.e., hydroxoferryl derivative), for which the ABTS^{•+} is formed, and returning to the initial form of the enzyme [38,138], thus supporting H₂O₂ decomposition. The rationale for using the ABTS assay was due to the question: "If the EOs are capable of neutralizing the ABTS^{•+} in vitro, could they support catalase in vivo in terms of facilitating the decomposition of oxidative-stress-generated H₂O₂?"

ABTS^{•+} neutralization was evaluated after the radical was formed by ABTS oxidation with K₂S₂O₈ [15], where each EO provided the reducing equivalent to the N atom, likely via the sequential proton loss electron transfer (SPLET) mechanism [40,139]. Thus, the overall EC₅₀ concentration range of active EOs against ABTS^{•+} was from the most potent 0.003 (Red thyme EO) to the least potent 0.89 µg/mL (*Mentha suaveolens* EO) (Table 1 and Supplementary Materials Table S3). All EOs that were potent against DPPH[•] also neutralized ABTS^{•+}, except for Laurel, which had an EC₅₀ against ABTS^{•+} greater than 1 µg/mL. On the other hand, *Mentha suaveolens* EO, which was virtually inactive against DPPH[•] (EC₅₀ > 1 µg/mL), was highly active against ABTS^{•+}, with an EC₅₀ value of 0.890 µg/mL. Again, as already observed above for other assays, Rosemary, CCP, Savory, and YY EOs continued to exert a good level of potency also against ABTS^{•+} with an EC₅₀s of 0.065, 0.125, 0.260, and 0.760 µg/mL, respectively.

3.1.6. Hydroxyl-Radical-Neutralizing Activity

Based on the results of the ABTS assay, EOs were further tested for their ability to neutralize the hydroxyl radicals in vitro (Table 1) by means of the HORAC assay, in terms of preventing the OH[•] from attacking the C'4 position of 2'-deoxy-D-ribose (Scheme 1, red pathway, dashed arrows, 15) and causing its conversion to the ribosyl radical (Scheme 1, red pathway, dashed arrows, 16) and malondialdehyde (MDA) (Scheme 1, red pathway, dashed arrows, 14) [16,17]. The neutralization of OH[•] by each EO was compared to BHT. Thus, all EOs found potent OH[•] scavengers by the ABTS^{•+} assay and did indeed show a good affinity for OH[•], and none of the ABTS^{•+}-inactives exerted an affinity for OH[•]. However, a non-perfect correlation was found ($r^2 = 0.7601$) for the equation $[EC_{50}]_{OH^{\bullet}} = 0.6389 \times [EC_{50}]_{ABTS^{\bullet+}} + 0.0501$, implying that the ABTS assay should be taken with caution as a predictor of potency against OH[•].

The EC₅₀ concentration of active EOs against OH[•] ranged from 0.01 (Red thyme EO) to 0.72 µg/mL (Nutmeg natural EO). In summary, eight EOs (Oregano, Clove, Red thyme, *Coridothymus capitatus*, Rosemary, Birch, Cade, and Nutmeg natural) were about 10% to 600% more sensitive to ABTS^{•+}, whereas *Origanum hirtum*, YY, Savory, White thyme, CCP, *Thymus vulgaris*, Cedar leaf, and Lemongrass EOs were from 1.12- to 3.25-folds more sensitive to OH[•]. Moreover, Savory-, CCP-, YY-, and Rosemary-derived EOs were also active against OH[•], with EC₅₀s of 0.032, 0.078, 0.35, and 0.42 µg/mL, respectively (Supplementary Materials Table S3).

3.2. Antigenotoxic Activity In Vitro

Being able to prevent the 2'-deoxy-D-ribose degradation, EOs were further evaluated in vitro for their ability to prevent OH[•]-induced damage to a DNA double-strand [18–20] by interfering with salmon sperm DNA, while the selected EOs were also indirectly evaluated for their potency to neutralize OH[•] in vivo [104].

The damage within the DNA double-strand was induced by the 2-hydroperoxy-2-methylpropanimidamide radical (ROO[•]), released from AAPH by the homolytic cleavage of the two nitrogen–carbon bonds to form two isobutyrimidamide radicals (R[•]) and subsequent oxidation with O₂ [20,21]. The antioxidant potential of each EO has been evaluated using the electrophoresis-based version of the ORAC or TRAP assays [137]. The ROO[•] (and its homolog LOO[•]) is associated with the modification of DNA, such as 8-oxoG (Scheme 1, blue pathway, dashed arrows, 17), which could lead to inflammation and degenerative pathologies, including cardiovascular and neurological diseases, as well as the development

of some cancers [140]. On the other hand, OH^\bullet , here formed in vitro in the Fenton-type oxidation of H_2O_2 catalyzed by FeSO_4 , also attacked the salmon DNA double-strand [8,18], and probably generated the aberrant adducts, such as 8-oxo-dG (Scheme 1, green pathway, dashed arrows, 17), thymine glycol (Scheme 1, green pathway, dashed arrows, 18), and 6-hydroxy-5,6-dihydrocytosine (Scheme 1, green pathway, dashed arrows, 19) [141,142].

To suppress the listed DNA lesions, EOs were evaluated using relative electrophoretic band densities (RBD) of DNA (Figures 1 and 2, and Supplementary Material Figures S1–S59) knowing that RBD values approaching 1 indicate better protection (Supplementary Material Tables S4 and S5). Each EO was administered at double-diluted concentrations ranging from 400 to 25 $\mu\text{g}/\text{mL}$ and compared to quercetin (Q, 100 $\mu\text{g}/\text{mL}$) as a reference compound [18,20]. The highest starting concentration tested against $\text{M}^{\text{n}+}$, DPPH^\bullet , LOO^\bullet , $\text{ABTS}^{\bullet+}$, and OH^\bullet radicals was acceptable considering that only high concentrations of an antioxidant can efficiently compete with LOO^\bullet and OH^\bullet at the cellular site of radical formation [8]; (2) was used as a metric to predict which EO concentration could be tested in vivo [103]. An analysis of RBD values alone (see Supplementary Materials) did not provide significant conclusions regarding the efficacy of EOs but only indicated their affinity for either ROO^\bullet or OH^\bullet . Therefore, $\text{ROO}^\bullet\text{RBD}_{50}$ or $\text{OH}^\bullet\text{RBD}_{50}$ values, i.e., concentrations that stimulate a 50% increase in relative electrophoretic band density [RBD] (i.e., protection), were calculated (Table 1) to differentiate the potencies of all EOs.

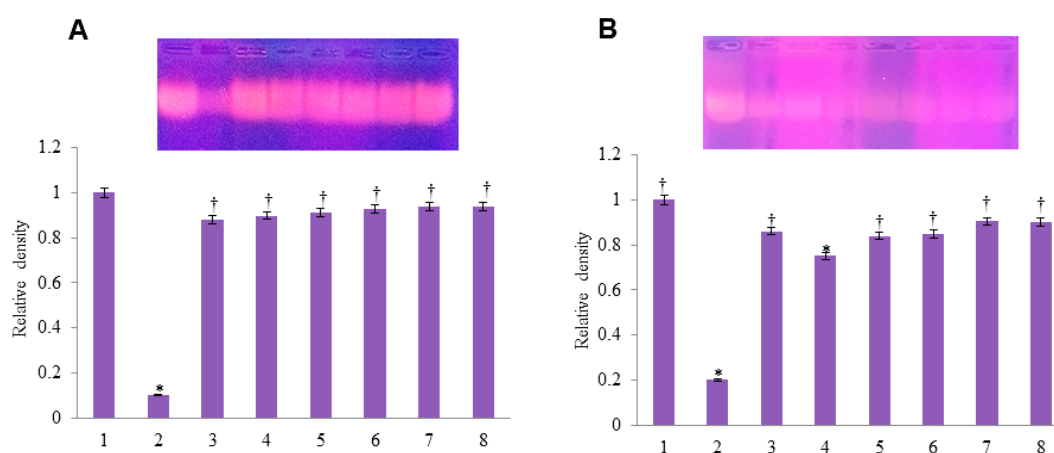


Figure 1. Protective effect of CCP EO against peroxyl- (A) and hydroxyl- (B) radicals-induced DNA damage. DNA from salmon sperm (lane 1, negative control), DNA damage control (lane 2, positive control), quercetin (lane 3, 100 $\mu\text{g}/\text{mL}$, standard), essential oils in concentrations of 25, 50, 100, 200, and 400 $\mu\text{g}/\text{mL}$ (lanes 4, 5, 6, 7, and 8). * $p < 0.05$ when compared with the negative control group; † $p < 0.05$ when compared with the positive control group.

3.2.1. EOs with Increasing Dose-Dependent Potency to Protect DNA from ROO^\bullet and OH^\bullet

Among the tested EOs, 33 of them (Chamomile Morocco, Tea tree, Melissa, Mountain pine, Geranium Bourbon, Oregano, Lavender, Myrtle, Hyssop, Lemongrass, Siberian pine, Camphor, Ginger, Cumin, Patchouli, Orange bitter, Eucalyptus, Bergamot, Fennel, Savory, Rosemary, CCP, *Eucalyptus globulus*, Artemisia, White thyme, Marjoram, Cypress, Peppermint, Palmarosa, Natural anise, Frankincense, *Mentha suaveolens*, and *Coridothymus capitatus*) protected salmon DNA from damage induced by either ROO^\bullet or OH^\bullet in a dose-dependent manner, with the level of protection increasing with increasing concentrations (Tables S4 and S5, detailed analysis of data is reported in the Supplementary Materials). By determining the $\text{ROO}^\bullet\text{RBD}_{50}$ and $\text{OH}^\bullet\text{RBD}_{50}$ values, it appeared that only CCP EO either neutralized $\text{M}^{\text{n}+}$, DPPH^\bullet , LOO^\bullet , $\text{ABTS}^{\bullet+}$, and OH^\bullet or protected the DNA from either ROO^\bullet or OH^\bullet (Figure 1), with $\text{ROO}^\bullet\text{RBD}_{50}$ and $\text{OH}^\bullet\text{RBD}_{50}$ values as low as 60.99 and 78.36 $\mu\text{g}/\text{mL}$, respectively (Table 1); therefore, the EO was selected for in vivo administration. Savory and Rosemary EOs, initially selected for in vivo assays, were discarded due to undetermined $\text{ROO}^\bullet\text{RBD}_{50}$ or $\text{OH}^\bullet\text{RBD}_{50}$ values (Table 1).

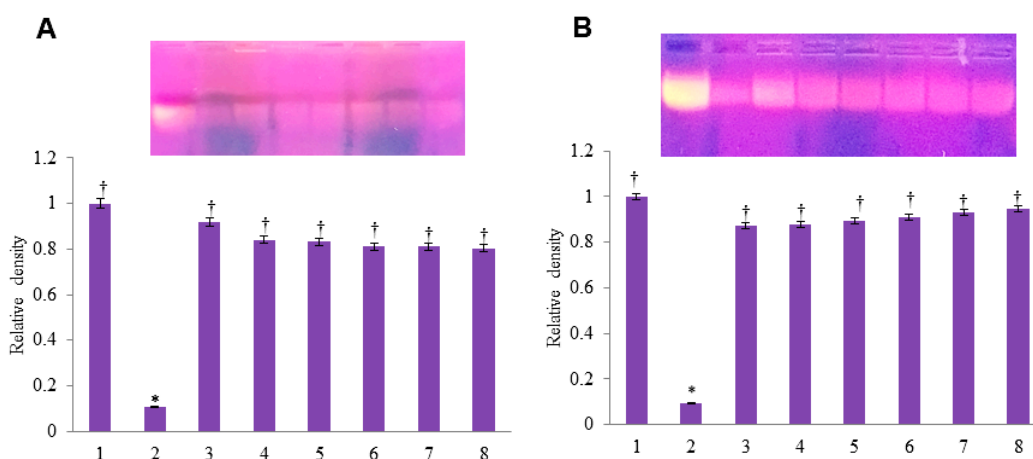


Figure 2. Protective effect of YY EO against peroxyl- (A) and hydroxyl- (B) radicals-induced DNA damage. DNA from salmon sperm (lane 1, negative control), DNA damage control (lane 2, positive control), quercetin (lane 3, 100 $\mu\text{g}/\text{mL}$, standard), essential oils in concentrations of 25, 50, 100, 200, and 400 $\mu\text{g}/\text{mL}$ (lanes 4, 5, 6, 7, and 8). * $p < 0.05$ when compared with the negative control group; † $p < 0.05$ when compared with the positive control group.

3.2.2. EOs with Decreasing Dose-Dependent Potency to Protect from ROO^\bullet and OH^\bullet

Clary sage, Red thyme, Coriander, Grapefruit, Roman chamomile, Black pepper, and Clove EOs dose-dependently reduced DNA damage induced by radicals, but with no efficacy against ROO^\bullet or OH^\bullet (Supplementary Materials Tables S4 and S5). However, despite showing remarkable $\text{ROO}^\bullet\text{RBD}_{50\text{s}}$ and $\text{OH}^\bullet\text{RBD}_{50\text{s}}$ (Table 1), none of the EOs within this subgroup showed satisfactory efficacy against $\text{M}^{\text{n}+}$, DPPH^\bullet , LOO^\bullet , $\text{ABTS}^{\bullet+}$, or OH^\bullet and were not further evaluated.

3.2.3. EOs with Increasing and Decreasing Dose-Dependent Potency to Protect DNA from ROO^\bullet and OH^\bullet , Respectively

Sage, Garlic, Cade, Cedar leaves, Pine Silvestre natural, Juniper, Birch, Orange sweet, Cajeput, Nutmeg natural, Verbena, Basil, Laurel, *Thymus vulgaris*, and *Origanum hirtum* EOs, at increased concentrations, protected DNA with more power from the damage induced by ROO^\bullet , while, at the same time, gradually losing their efficacy against OH^\bullet (Supplementary Materials Tables S4 and S5). Again, despite showing remarkable $\text{ROO}^\bullet\text{RBD}_{50\text{s}}$ and $\text{OH}^\bullet\text{RBD}_{50\text{s}}$ (Table 1), none of the listed EOs had efficacy against $\text{M}^{\text{n}+}$, DPPH^\bullet , LOO^\bullet , $\text{ABTS}^{\bullet+}$, or OH^\bullet and were not further evaluated.

3.2.4. EOs with Decreasing and Increasing Dose-Dependent Potency to Protect DNA from ROO^\bullet and OH^\bullet , Respectively

YY, Cardamom, Mandarin, Cedar fruit, Lemon, and Niaouly EOs exhibited a decreasing ability to protect DNA from ROO^\bullet -induced damage with increasing concentration but showed increasing efficacy against OH^\bullet . The most interesting EO was YY EO with $\text{ROO}^\bullet\text{RBD}_{50}$ of 64.12 $\mu\text{g}/\text{mL}$ and $\text{OH}^\bullet\text{RBD}_{50}$ of 134.11 $\mu\text{g}/\text{mL}$ (Table 1, Figure 2), and CCP EO with exceptional affinity to neutralize $\text{M}^{\text{n}+}$, DPPH^\bullet , LOO^\bullet , $\text{ABTS}^{\bullet+}$, and OH^\bullet . These data were induced to select YY and CCP EOs for the subsequent in vivo evaluation.

3.3. Machine-Learning-Based QCAR Models

As mentioned above, the correlations of the in vitro antioxidant potencies of EOs with their chemical compositions were analyzed by means of ML algorithms to generate QCAR models (Table 2 and Supplementary Material Model development section). The predictivity and robustness of each derived model were evaluated using the MCC_{Pred} and MCC_{cv} values. For comparison purposes with other metrics (i.e., accuracy), Normalized MCC (nMCC) was considered, defined as $\text{nMCC} = \text{MCC} + 1/2$, and linearly projecting the

original range into the 0-1 interval. A model was generated for each of the evaluated in vitro assays (Table 2). In general, for all of the in vitro antioxidant activities, the procedure led to obtaining a model endowed with acceptable to good $nMCC_{Pred}$ and $nMCC_{CV}$ values in the ranges of 0.68–0.98 and 0.58–0.91, respectively, indicating the models to be endowed with good levels of both predictivity and robustness. The models can be freely used for the prediction of any untested EOs antioxidant potencies, as a part of the AI4EssOil Project (<https://www.ai4essoil.com/front/>, accessed on 20 September 2023).

Among the models, ML3 obtained for the lipid peroxidation arrest and generated by the SVM was that with the highest $nMCC_{Pred}$ and $nMCC_{CV}$ values (Table 2). The same ML algorithm “recognized” that DPPH• radical neutralization could be used to predict potency against LOO•, giving a model with excellent prediction accuracy (Table 2, model ML2). These data are in good agreement with the above reported considerations. Good models were obtained when describing the potencies against ABTS•+ (Table 2, model ML4) and OH• (Table 2, model ML5), but using KNN and RF algorithms, respectively. The ML model describing metal ion chelation (Table 1, model ML1) was of slightly lower predictive power, while the least quality models were those describing DNA double-strand protection (Table 1, models ML6 and ML7). Analysis of feature importance revealed that all models shared limonene (cyclic monoterpene, hydrocarbon), linalool (acyclic monoterpene, alcohol), carvacrol (cyclic monoterpene, phenol), eucalyptol (bicyclic monoterpene, hydrocarbon), α -pinene (bicyclic monoterpene, hydrocarbon), thymol (cyclic monoterpene, phenol), caryophyllene (bicyclic sesquiterpene, hydrocarbon), *p*-cymene (cyclic monoterpene, hydrocarbon), eugenol (cyclic monoterpene, hydrocarbon/phenol), and chrysanthone (tricyclic sesquiterpene, hydrocarbon/phenol) as the most important chemical components, which were characterized by the WFI (Figure 3) and PD plots (Figures 4 and 5, and Supplementary Materials Figures S60–S67). In general, the results of all models were in good agreement with the previously reported chemical/biological properties.

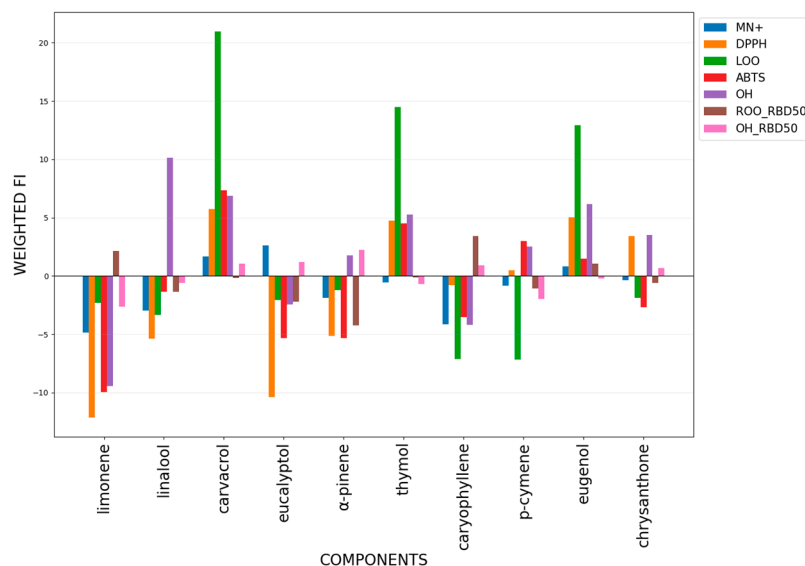


Figure 3. The WFI trends of the 10 components, which are most important and present in the 61 essential oils.

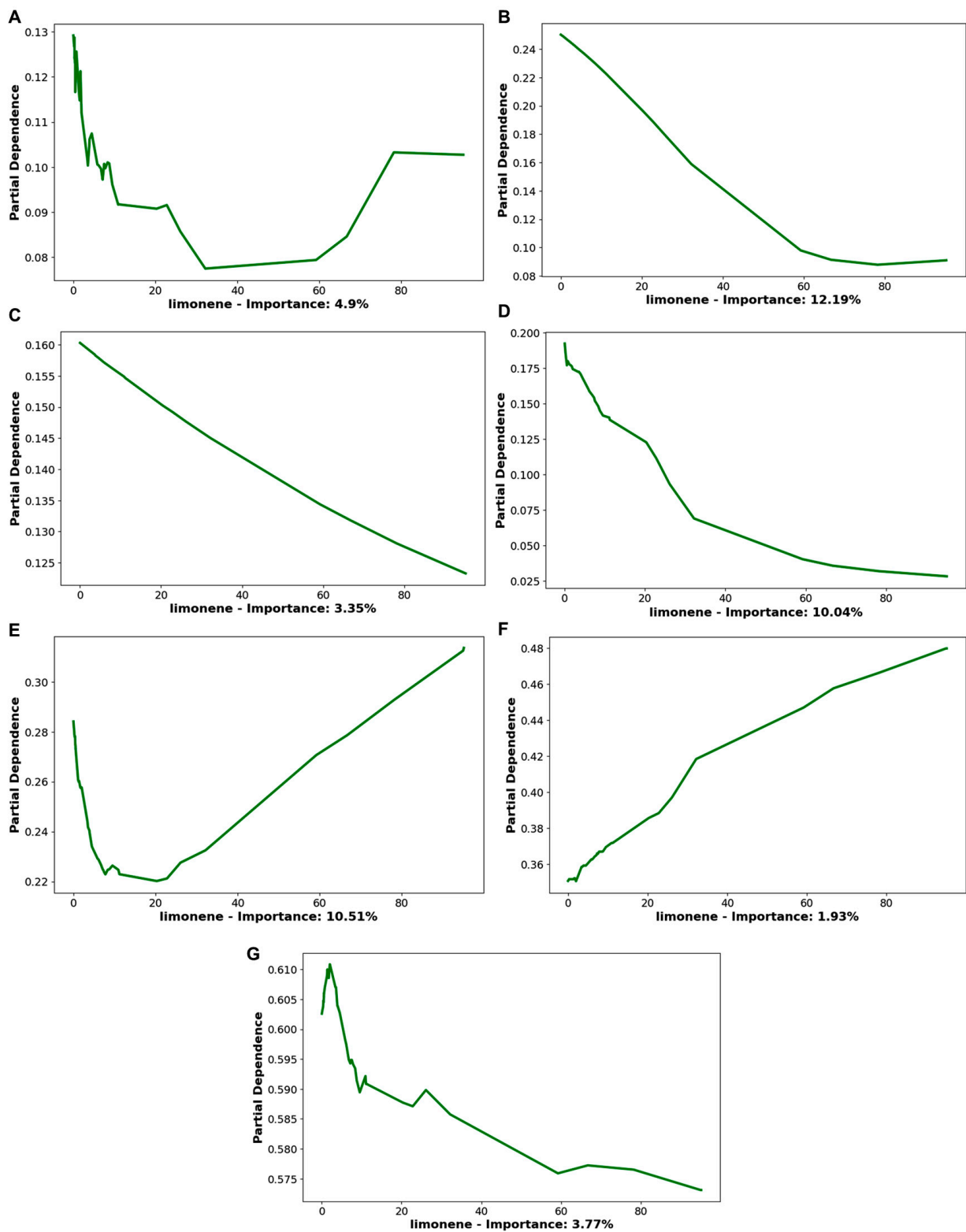


Figure 4. Partial dependence plots of limonene in the model of M^{n+} (A), $DPPH^{\bullet}$ (B), LOO^{\bullet} (C), $ABTS^{\bullet+}$ (D), OH^{\bullet} (E), $ROO-RBD_{50}$ (F), $HO-RBD_{50}$ (G).

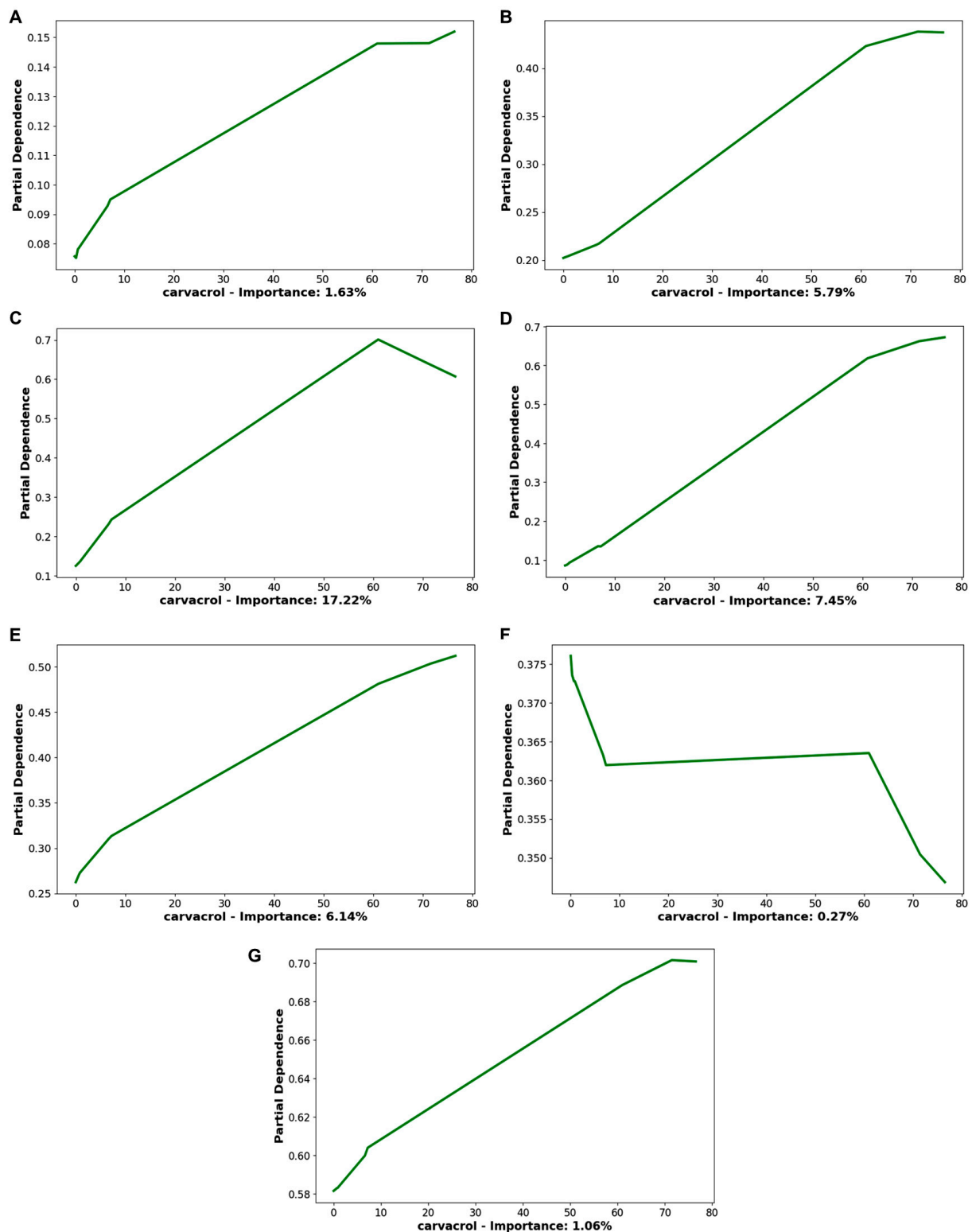


Figure 5. Partial dependence plots of carvacrol in the model of M^{H} (A), DPPH^{\bullet} (B), LOO^{\bullet} (C), ABTS^{H} (D), OH^{\bullet} (E), ROO-RBD_{50} (F), HO-RBD_{50} (G).

3.3.1. The Contribution of Limonene to the Antioxidant Activity

The presence of limonene was recognized by the ML models as negative and somehow opposite to the antioxidant activity in all models except for the one obtained to describe the neutralization of the ROO^{\bullet} radical (Figure 3). Moreover, by analyzing the partial

dependence plots of limonene for each free radical, it can be confirmed that the curve is downward in five out of seven radicals, i.e., against M^{n+} (Figure 4A), DPPH \bullet (Figure 4B), LOO \bullet (Figure 4C), ABTS \bullet^{+} (Figure 4D), and HO \bullet RBD₅₀ (Figure 4G), which agreed with the WFI trends. Notably, limonene was the most abundant component (32.20%, Supplementary Materials Table S2) in Cedar fruit EO, the most potent metal chelator EO, which is likely to decrease the potency (Table 1). On the other hand, the component was missing in Cade EO, the most potent EO against DPPH \bullet (Table 1), and was present in low amounts in the Oregano (0.54%) and Red thyme (0.29%) EOs; thus, it was not high enough to disturb the high potencies of the EOs during lipid peroxidation and against ABTS \bullet^{+} , respectively (Table 1). Moreover, limonene was also missing in YY EO, which was very active for OH \bullet , while protecting salmon DNA (Table 1 and Supplementary Materials Table S2). Nevertheless, in the PD plots, limonene shows also a double aspect; in the case of the OH \bullet radical (Figure 4E), it can be seen that when the limonene percentage is more than 20%, its influence is positively related to the EC₅₀, in agreement with the observation that the potency of Red thyme EO (Table 1) could be even higher. In contrast, in the case of ROO \bullet , the curve for limonene was fully ascending and, therefore, a positive partial dependence curve (Figure 4F). Considering that limonene is a nonphenolic terpenoid with a cyclohexadiene structure, it could exert some activity against ROO \bullet similar to that of γ -terpinene in terms of donating its methylene C-H while neutralizing the radical [1]. The low amount of limonene found in CCP EO (0.20%) likely did not contribute to decreasing its high potency against ROO \bullet . In addition, all EOs active against ROO \bullet and having limonene as one of the most abundant components should also be associated with cytotoxic antioxidant activity [1]. For the above observation, the prediction of ML6 regarding the biological activity of limonene was quite consistent.

3.3.2. The Contribution of Linalool to the Antioxidant Activity

Compared to limonene, similar results were obtained from the inspection of the WFIs for linalool, where the compound exerted a negative impact on EOs' antioxidant activities in all ML models but the one obtained against the OH \bullet radical (Figure 3). The PD plots, except for the OH \bullet -related (Supplementary Materials Figure S60E) confirmed a descending curve and thus an associated negative importance for this component to the antioxidant activity as its concentration increases. In that sense, the highest potency of Red thyme EO against the OH \bullet radical (Table 1) could be associated with the limited presence of linalool (5.16%, Supplementary Materials Table S2). Some affinity of linalool to neutralize the OH \bullet could be associated with its ability to donate either alcoholic or methylene protons through the HAT mechanism [1,143]. However, a difficult-to-interpret graph was obtained from the model for describing the EOs' protective activities on a DNA double-strand against the OH \bullet radical (i.e., based on the HO \bullet RBD₅₀ values) where an alternating line trend can be seen when the concentration of this component is between 0 and 20%. The descending curve was in part a reflection of 10.36% of linalool in the composition of YY EO (Supplementary Materials Table S2). Moreover, it was interesting that linalool was indicated to contribute negatively to the neutralization of DPPH \bullet (Figure S60B), despite the reported potency of this component against that radical [1,143], as well as against the ABTS \bullet^{+} (Supplementary Materials Figure S60D), confirming its hydroxyl portion has not been a reaction center in either HAT [138] or SPLET fashion [139]. While linalool has been absent in the chemical composition of Cade EO (Table 1, Supplementary Materials Table S2), thus not diminishing its highest potency against DPPH \bullet (Supplementary Materials Figure S60C), its presence in Red thyme EO's chemical composition in 5.16% (Supplementary Materials Table S2) likely contributed to lower potency against ABTS \bullet^{+} (Table 1). Additionally, having just a minor positive impact on lipid peroxidation inhibition, if occurring in more than 40% (Supplementary Materials Figure S60C) (in agreement with the low quantity of 2.43%, Supplementary Materials Table S2, within Oregano EO, Table 1), and no positive impact against ROO \bullet (Supplementary Materials Figure S60F) (following low quantity of 3.19%, Supplementary Materials Table S2, in the chemical composition of CCP EO, Table 1)

whatsoever, linalool has not been able to act as an antioxidant in a termination-enhancing antioxidant activity fashion [1] (somehow in disagreement with the reported affinity of linalool to act against ROO^\bullet [143]).

3.3.3. The Contribution of Carvacrol to EOs' Antioxidant Activity

The presence of carvacrol was classified as positive in all models except for the model obtained on ROO^\bullet (RBD_{50}) (Figure 3). A very interesting feature of carvacrol is its ability to influence metal ions chelation in a concentration-dependent way (Figure 5A), despite the fact that carvacrol, as a monohydroxylated, might not be able to form the complex with Fe^{2+} [144–146] as its phenolic portion alone could not be strong enough to hold the interaction. Nevertheless, Horvathova et al. confirmed some chelating potential [147], and carvacrol was not contained in the Cedar fruit EO (Table 1 and Supplementary Materials Table S2), the most potent EO in the metal chelation. On the other hand, carvacrol contributed to the neutralization against either DPPH^\bullet (Figure 5B) or OH^\bullet (Figure 5E), likely due to its phenolic proton by PCET mechanism [137]. Still, it was not found in the chemical composition of Cade EO (Supplementary Materials Table S2), the most potent against DPPH^\bullet (Table 1), but it was found in Red thyme EO at 7.20% (Table 1 and Supplementary Materials Table S2), the most potent OH^\bullet scavenger EO sample. However, while protecting the DNA double-strand from OH^\bullet , carvacrol was not listed in the 20 most important and influential components by model ML5 (Table 2 and Figure 5G). In fact, it was missing in YY EO (Table 1 and Supplementary Materials Table S2). On the other hand, the neutralization potential of carvacrol-containing EO toward $\text{ABTS}^{\bullet+}$ (Figure 5D) is likely associated with the SPLET mechanism [139], an effect associated with Red thyme EO. Moreover, by inspecting the partial dependence trend (Figure 5C), the presence of this component is particularly important and positive against LOO^\bullet . Indeed, the most potent EO against the LOO^\bullet , Oregano EO (Table 1), contained carvacrol at a percentage as high as 76.54% (Supplementary Materials Table S2), which was not surprising, as the phenolic group of carvacrol guaranteed the activity of containing EOs against the LOO^\bullet in a chain-breaking antioxidants fashion [1,147,148]. However, regarding the affinity against the ROO^\bullet (Figure 5F), this component was not listed among the 20 most important and influential components regarding antioxidant activity against that free radical (Figure 5F), proving carvacrol's inability to stop the ROO^\bullet by means of termination-enhancing antioxidant activity [1].

3.3.4. The Contribution of Thymol to the Antioxidant Activity

Both thymol and eugenol were associated with positive WFI in most models, thus representing two important positive components for antioxidant activity (Figure 3). However, thymol, like carvacrol, and as a structural isomer, does not appear among the ML model's recognized 20 most important components for the chelation of metal ions (Supplementary Materials Figure S61A), which was somehow in disagreement with the report in which thymol should better stabilize the Fe^{2+} than carvacrol [147,148]. Thymol was likewise not among the 20 most important components related to the neutralization of ROO^\bullet (Supplementary Materials Figure S61F), likely due to the lack of termination-enhancing antioxidant activity features [1]. On the contrary, thymol was proposed as positively modulating the LOO^\bullet radical neutralization (Supplementary Materials Figure S61C), likely owing to chain-breaking antioxidant features [1,146]. However, it was not contained in the Oregano EO, the most active EO against LOO^\bullet radical neutralization (Table 1 and Table S2, Supporting Information). Regarding other radicals' activities, thymol (Supplementary Materials Figure S61B,D,E,G) was calculated with a similar profile to that of carvacrol, although not contained (Supplementary Materials Table S2) in Cade and YY EOs (Table 1) but found in even 66.31% (Supplementary Materials Table S2) in Red thyme EO (Table 1).

3.3.5. The Contribution of Eugenol to the Antioxidant Activity

Considering the eugenol, ML7 is the only model in which its presence seems to have a slightly negative WFI (Supplementary Materials Figure S62G). In fact, in YY EO, only 0.58% of eugenol was found (Table 1 and Supplementary Materials Table S2), and it was not listed among the 20 most important compounds. Its chelating features (Supplementary Materials Figure S62A) could be attributed partially to both phenolic and methoxy portions [146]. Although eugenol was not contained in the Cedar fruit EO (Table 1 and Supplementary Materials Table S2), its ability to neutralize DPPH• (Supplementary Materials Figure S62B), OH• (Supplementary Materials Figure S62E), or ABTS•+ (Supplementary Materials Figure S62D) radicals is due to its phenolic proton via PCET [137] or SPLET [139] mechanisms, while against LOO• (Supplementary Materials Figure S62C), eugenol contained in EO might act in a chain-breaking antioxidants fashion [1,148,149]. In CCP EO (Table 1), eugenol was contained at 34.63% (Supplementary Materials Table S2) and, likely differently from carvacrol and thymol, it managed to neutralize the ROO• (Supplementary Materials Figure S62F) via the allylic double bond's termination-enhancing antioxidant activity [1].

3.3.6. The Contribution of Chrysanthone to the Antioxidant Activity

Chrysanthone was classified as a positive component for the EOs' antioxidant activities against the DPPH• (Supplementary Materials Figure S63C) and the OH• (Supplementary Materials Figures S63E and S63G) by models ML2 and ML5, respectively (Table 2). Its activity was likely due to the phenolic protons through a PCET mechanism [137]. In contrast, a negative trend was associated with metal ions chelation and neutralization of ABTS•+, LOO•, and ROO• (Supplementary Materials Figure S63). Interestingly, chrysanthone was correctly not listed in the composition of the most potent EOs against the listed radicals (Table 1 and Supplementary Materials Table S2).

3.3.7. The Contribution of Eucalyptol to the Antioxidant Activity

Overall, contradictory results between radicals were obtained for some components, such as eucalyptol, α -pinene, caryophyllene, and *p*-cymene, (Figure 3). These may be due either to different antioxidant activity against various free radicals from the same component or imperfect model accuracy. In particular, eucalyptol was classified as strongly influencing metal ions chelation (Supplementary Materials Figure S64A), but it was not contained in the most active Cedar fruit EO (Table 1 and Supplementary Materials Table S2). Eucalyptol was also found with a definite positive trend for the OH• neutralization, leading to damaging either 2'-deoxyribose (Supplementary Materials Figure S64E) or DNA (Supplementary Materials Figure S64G), although it was contained at a very low percentage (0.25%) in the Red thyme EO (Table 1 and Supplementary Materials Table S2), in agreement with previous findings [149]. As for the remaining redox species (Supplementary Materials Figure S64B–D,F), the negative slopes of partial dependence plots curves confirmed the lack of potency for eucalyptol in agreement with its absence in Cade, Oregano, CCP, and YY EOs (Table 1 and Supplementary Materials Table S2).

3.3.8. The Contribution of α -Pinene to the Antioxidant Activity

As for α -pinene, the component exerted a positive modulation on antioxidant activity only against OH• radicals (Figure 3), being a constituent of Red thyme EO at 0.38% (Supplementary Materials Table S2). As proposed by the ML5 and ML7 models, to fully contribute to the protection of either 2'-deoxy-D-ribose or a DNA double-strand, at least 7.72% and 8% of α -pinene would be required in the EO mixture (Supplementary Materials Figure S65E,G), respectively. The component's contribution was likely due to its ability to undergo photooxidation in the presence of OH•, thus neutralizing the radical [150]. Surprisingly, α -pinene was calculated to have a negative trend contribution targeting both LOO• (Supplementary Materials Figure S65C) and ROO• (Supplementary Materials Figure S65G), as confirmed by 0.37% and 0.25% of α -pinene in Oregano EO and CCP EO, respectively (Table 1 and

Supplementary Materials Table S2). As for the descendent partial dependence curve, while targeting DPPH• (Supplementary Materials Figure S65C), it corresponds to the previously reported very low potency of α -pinene against distinct radicals [151] and in agreement with its lack of presence in Cade EO (Table 1 and Supplementary Materials Table S2).

3.3.9. The Contribution of Caryophyllene to the Antioxidant Activity

Regarding caryophyllene, remarkably, it was the only abundant compound (Supplementary Materials Table S2) in all of the above-listed potent EOs (Table 1). Still, its contribution was recognized as positive only for ROO• and OH• (Supplementary Materials Figure S66F,G). Thus, its role in preventing DNA damage can be associated with its 4.01% and 15.47% in CCP and YY EO, respectively (Supplementary Material Table S2). Its positive trend in the activity against ROO• (Supplementary Material Figure S66F) could be associated with the termination-enhancing antioxidant mechanism, donating the methylene proton of the endocyclic double bond [1]; its interaction with the OH• (Supplementary Materials Figure S66G) was expected [152] due to the known ability to make a covalent bond while reacting with alkoxy radicals [153]. As for the metal ions chelating ability (Supplementary Material Figure S66A), caryophyllene could have a positive impact if present between 5% and 15%. It also had no impact on the neutralization of DPPH•, LOO•, ABTS•+, or ABTS•+ (Table S2, Supplementary Material Figure S66B–E), as it was poorly present in Cade EO, Oregano EO, and Red thyme EO (Supplementary Material Table S2).

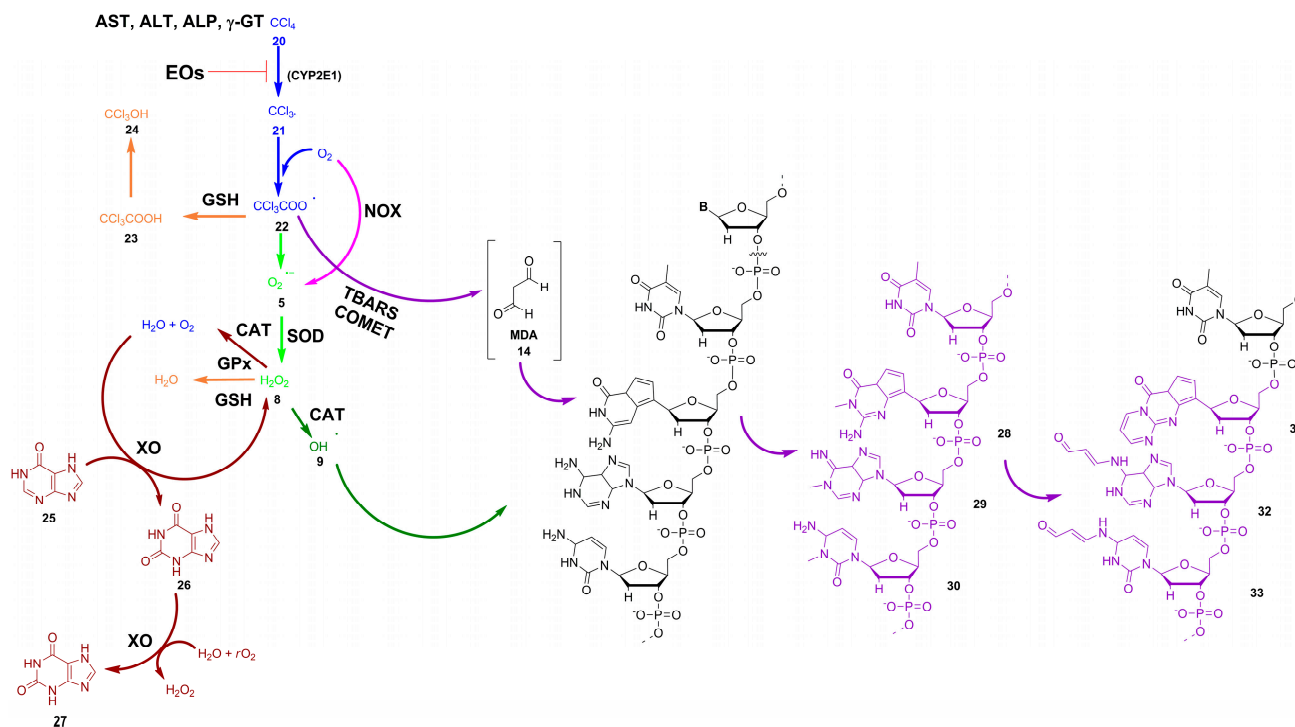
3.3.10. The Contribution of *p*-Cymene to the Antioxidant Activity

The EOs' potency contribution of *p*-cymene was positive while neutralizing DPPH•, ABTS•+, and OH• (Figure 3). The low affinity of *p*-cymene toward DPPH• (Supplementary Material Figure S67B) could be associated with the fact that hydrocarbons are very rarely H-donors to DPPH• [136]. This component was not found in the Cade EO (Table 1 and Supplementary Material Table S2). It was also surprisingly negatively contributing to the neutralization of LOO• (Supplementary Material Figure S67C), given that its occurrence in the Oregano EO was 6.80% (Table 1 and Supplementary Material Table S2). Yet, *p*-cymene, as expected [154], was predicted to be of high importance for ABTS•+, which could be associated with its presence at 10.46% in the chemical composition of Red thyme EO (Supplementary Material Table S2 and Figure S67D). On the other hand, despite not being expected to occur [154], the hydroxyl radical addition onto *p*-cymene was surprising and could be considered an inevitable limitation of the model ML6 (Supplementary Material Figure S67E). The negative trend of *p*-cymene in model ML7 suggested its failure to counteract OH•, which could be associated with its incapability of reaching the DNA environment (Supplementary Material Figure S67G). The strong negative trend visible in the partial dependence plot is consistent with the lack of metal-chelating features for *p*-cymene (Supplementary Material Figure S67A) required to chelate the Fe²⁺ [146]. Moreover, the negative influence against ROO• (Supplementary Material Figure S67F) of *p*-cymene was likewise expected due to the absence of chain-breaking features [1,146], in agreement with its absence in the CCP EO (Table 1 and, Supplementary Materials Table S2).

3.4. Antioxidant Activity of Targeted EOs In Vivo

YY and CCP EOs, the EOs exerting high potencies against each redox species in *in vitro* assays, (Tables 1 and 3), were promptly evaluated against the cellular damage caused by intraperitoneal (*i.p.*) administration of 1 mL/kg body weight (bwt) of CCl₄ [155] to adult Wistar rats [103] (Scheme 2, blue pathway, 23). To counteract the hazardous behavior of CCl₄, EOs were *i.p.* administered in a separate protocol simultaneously with CCl₄ [156] in three different concentrations (1, 200, and 400 mg/kg bwt) in agreement with the *in vitro* results discussed above. Upon administration, CCl₄ is likely to be oxidized by rat CYP2E1 for the production of trichloromethyl radical (*r*CCl₃•, Scheme 2, blue pathway, 24), an intermediate metabolite that is further oxidized to trichloromethylperoxy radical (*r*CCl₃OO•, Scheme 2, blue pathway, 25) [155,157,158]. The *r*CCl₃OO• could initiate the

peroxidation of polyunsaturated fatty acids in the membrane of either hepatocytes or kidneys (Tables 1–4: group II), leading to *r*MDA formation (Scheme 2, blue pathway, 14), whereas its excess may generate cellular $rO_2^{\bullet-}$ (Scheme 2, blue pathway, 5) and H_2O_2 (Scheme 2, blue pathway, 5) [155,157,158].



Scheme 2. The inter-correlation of methods used for monitoring/neutralizing in vitro and in vivo, emphasizing the emergence of ROS, by means of the EOs herein. The in vivo assays: (blue pathway, bold arrows) CCl_4 (20), trichloromethyl (CCl_3^{\bullet} , 21), trichloromethylperoxy radical (CCl_3OO^{\bullet} , 22); TBARS assay (purple path, bold arrows): malondialdehyde (14); SOD assay (light green pathway, bold arrows): H_2O_2 (8); CAT assay (dark green pathway, bold arrows): OH^{\bullet} (9); GSH assay (orange pathway, bold arrows): CCl_3OOH (23), CCl_3OH (24); XO assay (brown path, bold arrows): hypoxanthine (25), xanthine (26), uric acid (27); comet assay: (purple and dark green paths, bold arrows) M_1G (28), M_1A (29), M_1C (30), N^2 -oxopropenyl-dG (31), N^2 -oxopropenyl-dA (32), N^2 -oxopropenyl-dC (33).

Table 4. Total protein content, catalytic activities of enzymes, and concentrations of antioxidant markers in rat liver exposed to different doses of YY and CCP EO co-administered with CCl_4 .

Group	<i>r</i> TP (g/L)	<i>r</i> TBARS (nmol/mg)	<i>r</i> SOD (U/mg)	<i>r</i> CAT (U/mg)	<i>r</i> GSH (mg/g)
I	5.56 ± 0.14 ^{a†}	2.48 ± 0.02 [†]	5.27 ± 0.95 [†]	120.87 ± 0.15 [†]	32.24 ± 0.12 [†]
II	6.97 ± 0.12 *	4.40 ± 0.14 *	2.76 ± 0.36 *	70.10 ± 0.3 *	14.62 ± 0.16 *
III	18.94 ± 0.17 ^{*†}	1.84 ± 0.08 ^{*†}	4.95 ± 0.74 ^{*†}	78.93 ± 0.08 ^{*†}	15.76 ± 0.20 ^{*†}
IV	15.82 ± 0.23 ^{*†}	0.84 ± 0.09 ^{*†}	5.07 ± 0.63 ^{*†}	113.24 ± 0.10 ^{*†}	16.96 ± 0.12 ^{*†}
V	12.90 ± 0.34 ^{*†}	0.66 ± 0.08 ^{*†}	5.15 ± 0.69 ^{*†}	118.15 ± 0.15 ^{*†}	20.26 ± 0.13 ^{*†}
VI	8.07 ± 0.24 ^{*†}	2.01 ± 0.02 ^{*†}	4.83 ± 0.44 ^{*†}	73.47 ± 0.23 ^{*†}	17.15 ± 0.14 ^{*†}
VII	14.56 ± 0.17 ^{*†}	0.94 ± 0.03 ^{*†}	5.11 ± 0.78 ^{*†}	111.76 ± 0.22 ^{*†}	21.62 ± 0.02 ^{*†}
VIII	14.14 ± 0.41 ^{*†}	0.22 ± 0.06 ^{*†}	5.24 ± 0.85 [†]	118.87 ± 0.11 ^{*†}	29.32 ± 0.18 ^{*†}

^a Values represent mean ± SEM from three independent experiments; n = 5 rats per group; I—Negative control, 1 mL/kg bwt olive oil, i.p.; II—Positive control, 1 mL/kg bwt of CCl_4 , 1:1 mixture in olive oil, i.p.; III—1 mg/kg bwt of YY EO + 1 mL/kg bwt of CCl_4 , i.p.; IV—200 mg/kg bwt of YY EO + 1 mL/kg bwt of CCl_4 , i.p.; V—400 mg/kg bwt of YY EO + 1 mL/kg bwt of CCl_4 , i.p.; VI—1 mg/kg bwt of CCP EO + 1 mL/kg bwt of CCl_4 , i.p.; VII—200 mg/kg bwt of CCP EO + 1 mL/kg bwt of CCl_4 , i.p.; VIII—400 mg/kg bwt of CCP EO + 1 mL/kg bwt of CCl_4 , i.p.; * $p < 0.05$ when compared with the negative control group; [†] $p < 0.05$ when compared with the positive control group.

Therefore, the efficacies of EOs as lipid peroxidation inhibitors and consequent redox-stress-reducing mediators in vivo within either the liver or kidneys were assessed by monitoring the concentrations of the thiobarbituric-acid-reactive substance (*r*TBARS) [118] and reduced glutathione (*r*GSH) [119], as well as through the catalytic activities of superoxide dismutase (*r*SOD) [116] and catalase (*r*CAT) [118] (Scheme 2, blue pathway, Tables 1 and 3, respectively). The *r*TBARS [117], *r*GSH [119], and *r*CAT [118] values were expressed through the total protein content (*r*TP) [120]. On the other hand, the radical-induced damage of the hepatocyte membrane was elucidated through the liver toxicity markers, i.e., catalytic activities of aspartate transaminase (*r*AST) [159,160] and alanine transaminase (*r*ALT) [123], while damage to the bile was assessed through the catalytic activity of alkaline phosphatase (*r*ALP) [124] and γ -glutamyltransferase (*r* γ -GT) [125] (Table 2). Finally, the early indicators of oxidative-stress-associated chronic kidney disease (CDK) [127] after CCl₄-induced intoxication and its prevention by EOs were investigated by monitoring the catalytic activities of renal toxicity markers, such as xanthine oxidase (*r*XO) [126] and NADPH oxidase (*r*NOX) [127], as well as the protectors of the kidneys, nitric oxidase (*r*NO) [128] and glutathione peroxidase (*r*GPx) [48].

3.4.1. Liver Redox Status

In general, within all of the observed results, dose-dependent effects were observed upon administration of either YY EO or CCP EO.

The *r*TBARS Concentrations

On the liver hepatocytes membrane, *r*CCl₃OO• radical can induce the formation of malondialdehyde (*r*MDA), a toxic metabolite major side-product of lipid peroxidation (Scheme 2, blue pathway, 14) [134]. Therefore, the hepatoprotective properties of YY and CCP EOs were determined upon the complexation of *r*MDA with thiobarbituric acid, leading to the formation of *r*TBARS (Scheme 2), whose increased concentration is related to membrane damage [157]. While counterbalancing the CCl₄ administration consequence and metabolites, an interesting dose-dependent trend of increased hepatoprotective effects with the rise of EOs' concentration and any hepatic or renal toxicity was noted. Therefore, to avoid any redundancy, only the results in the concentration of 400 mg/kg bwt are discussed herein, whereas the effects of EOs in the lower quantities are reported in the Supplementary Materials. Administration of CCl₄ resulted in a 1.77-fold increase in *r*TBARS concentration in liver homogenates compared to the negative control (compare *r*TBARS of group II with I in Table 4). On the other hand, either YY or CCP EO dose-dependently decreased *r*TBARS concentration, where the CCP EO was more potent than the YY EO (compare V and VIII with I in Table 3), and the *r*TBARS was only 26.61% and 8.87% of that for the negative control and 15.00% and 5.00% of that caused by CCl₄ (compare V and VIII with II in Table 3). In agreement with the in vitro data and ML models, it can be speculated that the slightly higher affinity of CCP vs. YY EO to counteract the *r*CCl₃OO• in vivo could be attributed to the percentages profile of eugenol (34.63% in CCP EO vs. 0.58% in YY EO, Table 3), limonene (0.20% in CCP EO vs. 0.00% in YY EO, Table 3), and caryophyllene (4.01% in CCP EO vs. 15.47% in YY EO, Table 3), components all recognized as positively important by the ML3 model for the LOO•.

The *r*SOD Catalytic Activities

The CCP and YY EOs were also of notable efficacy in modulating the catalytic activity of *r*SOD for the *r*CCl₃OO• to *r*CCl₃• and *r*O₂•⁻ conversion (Scheme 2, light green pathway, bold arrows, 24 and blue pathway, 5) [155]. Moreover, the produced *r*O₂•⁻ likely acts as a secondary source of lipid peroxidation, and *r*SOD catalyzes the dismutation of *r*O₂•⁻ into oxygen (O₂) and hydrogen peroxide (H₂O₂) (Scheme 2, blue pathway, 8); as a consequence, any decrease in *r*SOD catalytic activity is associated with undergoing oxidative stress [116]. This scenario was confirmed by a 1.91-fold decrease in *r*SOD catalytic activity compared to the negative control (compare group II with I in Table 4) because of the produced *r*CCl₃OO•

breakdown. Either CCP EO or YY EO were very efficient (compare groups V and VII with I in Table 4) in recovering up to 97.72% and 99.43% of the *r*SOD catalytic activity, respectively.

The *r*CAT Catalytic Activities

The in-vivo-generated *r*H₂O₂ is promptly decomposed to *r*OH• (Scheme 2, dark green pathway, bold arrows, 9) and this could lead to 8-oxo-dG, thymineglycol, and 6-hydroxy-5,6-dihydrocytosine (Scheme 2, dark green path, bold arrows 17, 18 and 19) [140]. Considering that the decrease in the catalytic activity of *r*CAT induces oxidative stress in tissue [118], either CCP EO or YY EO were found efficient in positively modulating the catalytic activity of *r*CAT, so that an excess of *r*H₂O₂ is promptly decomposed to water and molecular oxygen (Scheme 2, blue pathway). Thus, CCl₄ caused a moderate decrease (58%) in the catalytic activity of *r*CAT (compare group II with I in Table 4), which was associated with kidney necrosis [156]. The maximal protection from *r*H₂O₂ was obtained with the higher concentration of either EO, leading to complete recovery of the native *r*CAT activity (compare groups V and VIII with I in Table 4).

The *r*GSH Concentrations

CCP and YY EOs were also assessed through the monitoring of *r*GSH concentration (Scheme 2, dark orange path, bold arrows), as its decrease indicates oxidative stress [155]. Hence, *r*GSH may provide two-level protection, either by reducing the *r*CCl₃OO• to form *r*CCl₃OOH (Scheme 2, orange pathway, bold arrows, 23) and *r*CCl₃OH (Scheme 2, orange pathway, bold arrows, 24) [155] or by converting the excess of *r*H₂O₂ to *r*H₂O (Scheme 2, orange pathway, bold arrows) [160]. Therefore, after the administration of CCl₄ in liver homogenates, a lower *r*GSH concentration (2.21-fold) was observed than in the negative control (compare group II with I in Table 4). The administration of either YY or CCP EO at the concentration of 400 mg/kg bwt resulted in expressive hepatoprotective features against CCl₄ (compare groups V and VIII with I in Table 4), as 400 mg/kg bwt of the two essential oils rescued about 32% and 83% of the lost *r*GSH concentration for the two EOs, respectively. In the presence of CCl₄, the YY or CCP EO restored about 63% and 91% of the basal *r*GSH, respectively.

3.4.2. The Hepatocytes Toxicity Status

The *r*AST and *r*ALT Catalytic Activities

The disruption of hepatocytes' membrane upon the CCl₄-induced damage was further monitored through the catalytic activities of *r*AST and *r*ALT, whereas the condition of the bile duct was determined by means of the catalytic activities of *r*ALP and *r*γ-GT (Table 5). The increments of *r*AST and *r*ALT catalytic activities (compare group II with I in Table 5) by 7.64- and 5.71-fold, respectively, were indicative of the hepatocyte's membrane damage by CCl₄ administration, revealing the early symptoms of hepatocellular toxicity and cirrhosis [159], whereas the increase of *r*ALP and *r*γ-GT catalytic activities (compare group II with I in Table 5) by 2.06- and 4.94-fold, respectively, indicated bile problems [161]. Complementary with the data for *r*TBARS and *r*SOD (Table 4), both YY and CCP EO downgraded the catalytic activities of liver and bile toxicity markers with the rise of concentration.

The *r*AST and *r*ALT catalytic activities associated to YY and CCP EOs, indicated that both EOs at the highest EO concentrations greatly prevented the CCl₄-induced hepatotoxicity (compare groups V and VII with I in Table 5). In particular, YY and CCP EOs slowed down the *r*AST CCl₄ enhanced activity from about 7.64- to 1.79- and 2.22-fold, respectively. More remarkably, the YY and CCP EOs almost completely restored the *r*ALT activity, being 5% and 27% faster when co-administered with CCl₄ [161]. While increasing the dosage, it seemed that YY EO was overall better tolerated by hepatocytes than CCP EO.

Table 5. Catalytic activities of serum biochemical markers within the rats exposed to different doses of YY and CCP EO and CCl₄.

Group	rAST (U/L)	rALT (U/L)	rALP (U/L)	rγ-GT (U/L)
I	7.88 ± 0.14 ^{a†}	36.66 ± 0.02 [†]	142.45 ± 0.15 [†]	3.35 ± 0.32 [†]
II	60.18 ± 0.12 [*]	209.31 ± 0.14 [*]	292.82 ± 0.31 [*]	16.54 ± 0.35 [*]
III	38.60 ± 0.17 ^{*†}	91.33 ± 0.08 ^{*†}	246.10 ± 0.08 ^{*†}	10.24 ± 0.37 ^{*†}
IV	24.37 ± 0.23 ^{*†}	41.65 ± 0.09 ^{*†}	210.66 ± 0.10 ^{*†}	6.45 ± 0.43 ^{*†}
V	14.07 ± 0.34 ^{*†}	38.35 ± 0.08 ^{*†}	172.18 ± 0.15 ^{*†}	4.43 ± 0.21 ^{*†}
VI	20.60 ± 0.24 ^{*†}	80.62 ± 0.02 ^{*†}	279.78 ± 0.23 ^{*†}	9.43 ± 0.34 ^{*†}
VII	19.87 ± 0.17 ^{*†}	51.80 ± 0.03 ^{*†}	259.88 ± 0.22 ^{*†}	6.12 ± 0.36 ^{*†}
VIII	17.50 ± 0.41 ^{*†}	46.66 ± 0.06 ^{*†}	179.26 ± 0.11 ^{*†}	4.06 ± 0.21 ^{*†}

^a Values represent mean ± SEM from three independent experiments; n = 5 rats per group; I—Negative control, 1 mL/kg bwt olive oil, i.p.; II—Positive control, 1 mL/kg bwt of CCl₄, 1:1 mixture in olive oil, i.p.; III—1 mg/kg bwt of YY EO + 1 mL/kg bwt of CCl₄, i.p.; IV—200 mg/kg bwt of YY EO + 1 mL/kg bwt of CCl₄, i.p.; V—400 mg/kg bwt of YY EO + 1 mL/kg bwt of CCl₄, i.p.; VI—1 mg/kg bwt of CCP EO + 1 mL/kg bwt of CCl₄, i.p.; VII—200 mg/kg bwt of CCP EO + 1 mL/kg bwt of CCl₄, i.p.; VIII—400 mg/kg bwt of CCP EO + 1 mL/kg bwt of CCl₄, i.p.; * *p* < 0.05 when compared with the negative control group; [†] *p* < 0.05 when compared with the positive control group.

The rALP and γ-GT Catalytic Activities

Similar dose-response protective features of either YY or CCP EO were verified in bile, where the highest concentration displayed similar potencies (compare group V and VIII with I in Table 5), reducing the CCl₄-induced rALP catalytic activity increase of more 200% to about 121% and 125%, respectively. In contrast, for γ-GT, CCP EO maintained the catalytic activity of the enzyme more effectively than YY EO (compare groups V and VIII with I in Table 5), rescuing almost 95% of the γ-GT activity enhancement induced by CCl₄.

3.4.3. Kidneys' Redox Status

The rTBARS Concentrations

Through the analysis of kidney homogenates, it was determined that rMDA had also been generated within the cell membranes of the kidneys' nephrons, for which it was measured as a 4.05-fold increase in the rTBARS concentration in samples saturated with CCl₄ compared to the negative control (compare group II with I in Table 6), indicating a higher rate of toxicity than that in the liver [157]. Either YY or CCP EO at the highest tested concentration showed full potential for the kidneys' recovery (compare groups V and VII with I in Table 6), holding the CCl₄ rTBARS's augmented value of about 71% and 63%, respectively. Data contained in Tables 4 and 6 generally indicate that EOs were more selective for the liver system than for the kidneys, considering the lipid peroxidation stopping, which was also confirmed by the kidneys' rSOD catalytic activities.

The rSOD Catalytic Activities

EOs were of notable efficiency while restoring the catalytic activity of rSOD, which was about 61% of the basal value after the application of CCl₄ (compare groups II and I in Table 6), confirming the high-intensity lipid peroxidation of the nephrons' cell membrane. At the highest dosage, CCP EO overpowered YY EO, raising the rGSH concentration 1.88-fold (vs. 1.76-fold of YY EO) and 114-fold (vs. 1.07-fold of YY EO) above the CCl₄ and negative control groups (compare groups V and VIII with II and I in Table 6).

Table 6. Total protein content, catalytic activities of enzymes, and concentrations of antioxidant markers in rat kidneys exposed to different doses of YY EO, CCP EO, and CCl₄.

Group	<i>r</i> TP (g/L)	<i>r</i> TBARS (nmol/mg)	<i>r</i> SOD (U/mg)	<i>r</i> CAT (U/mg)	<i>r</i> GSH (mg/g)
I	3.91 ± 0.14 ^{a†}	0.43 ± 0.02 [†]	5.11 ± 0.32 [†]	170.78 ± 0.15 [†]	39.58 ± 0.12 [†]
II	5.78 ± 0.12 [*]	1.74 ± 0.14 [*]	3.12 ± 0.43 [*]	52.54 ± 0.3 [*]	19.67 ± 0.16 [*]
III	3.96 ± 0.17 [†]	3.85 ± 0.08 ^{*†}	4.26 ± 0.23 ^{*†}	147.05 ± 0.08 ^{*†}	24.64 ± 0.20 ^{*†}
IV	2.59 ± 0.23 ^{*†}	3.72 ± 0.09 ^{*†}	4.44 ± 0.25 ^{*†}	166.27 ± 0.10 ^{*†}	31.78 ± 0.12 ^{*†}
V	3.22 ± 0.34 ^{*†}	1.23 ± 0.08 ^{*†}	5.49 ± 0.69 ^{*†}	168.98 ± 0.15 ^{*†}	37.18 ± 0.13 ^{*†}
VI	3.16 ± 0.24 ^{*†}	2.77 ± 0.02 ^{*†}	4.12 ± 0.32 ^{*†}	152.46 ± 0.23 ^{*†}	21.20 ± 0.14 ^{*†}
VII	5.76 ± 0.17 [*]	2.73 ± 0.03 ^{*†}	4.32 ± 0.34 ^{*†}	164.16 ± 0.22 ^{*†}	27.83 ± 0.02 ^{*†}
VIII	4.64 ± 0.41 ^{*†}	1.09 ± 0.06 ^{*†}	5.85 ± 0.85 ^{*†}	165.52 ± 0.11 ^{*†}	39.22 ± 0.18 [†]

^a Values represent mean ± SEM from three independent experiments; n = 5 rats per group; I—Negative control, 1 mL/kg bwt olive oil, i.p.; II—Positive control, 1 mL/kg bwt of CCl₄, 1:1 mixture in olive oil, i.p.; III—1 mg/kg bwt of YY EO + 1 mL/kg bwt of CCl₄, i.p.; IV—200 mg/kg bwt of YY EO + 1 mL/kg bwt of CCl₄, i.p.; V—400 mg/kg bwt of YY EO + 1 mL/kg bwt of CCl₄, i.p.; VI—1 mg/kg bwt of CCP EO + 1 mL/kg bwt of CCl₄, i.p.; VII—200 mg/kg bwt of CCP EO + 1 mL/kg bwt of CCl₄, i.p.; VIII—400 mg/kg bwt of CCP EO + 1 mL/kg bwt of CCl₄, i.p.; * *p* < 0.05 when compared with the negative control group; † *p* < 0.05 when compared with the positive control group.

The *r*CAT Catalytic Activities

An excess of *r*H₂O₂ in the kidneys, such as that caused by CCl₄, was confirmed by lowering the *r*CAT catalytic activity to about 30% of the basal value (compare group II with I in Table 6). Either YY or CCP EO was shown to be very effective in neutralizing this effect by avoiding any *r*CAT catalytic activity loss. Although the maximal protection was achieved at the highest tested concentration, a significant effect was also visible at the lowest concentration (Table 6); for the YY or CCP EO, more than 86% and 89% of the *r*CAT activity was retained, respectively. At higher concentrations, the catalytic activity was almost completely rescued.

The *r*GSH Concentration

An evaluation of EOs' impact on kidneys' *r*GSH revealed that they have been capable of restoring the marker's concentration downregulated by CCl₄ to about 50% of the basal concentration (compare group II with I in Table 6). The maximal dosage restored the *r*GSH's concentration almost entirely, to about 93 and 99% of the basal *r*GSH concentration (compare groups V and VIII with I in Table 6), i.e., 1.17- and 2.01-fold higher *r*GSH concentration than that caused by CCl₄ (compare groups V and VIII with II in Table 6), with CCP EO being slightly more potent than YY EO.

3.4.4. Chronic Kidney Disease Markers

Kidneys' homogenates were further examined, as oxidative stress in kidneys is a biochemical hallmark of chronic kidney disease that could influence the progression of renal function deterioration and the onset of major systemic co-morbidities involving cardiovascular diseases [127]. Hence, the administration impact of either CCl₄/YY EO or CCl₄/CCP EO on renal redox status was elaborated on the level of ROS inducers *r*XO and *r*NOX, as well as on the level of renal redox defensive mechanisms, like *r*NO and *r*GPx.

The *r*XO Catalytic Activities

Upon the rats' kidneys toxication with CCl₄, *r*XO likely employed the *r*O₂ to act as a secondary co-factor, alongside NAD⁺, to catalyze the oxidation of hypoxanthine to xanthine and then xanthine to uric acid (Scheme 2, brown path, bold arrows, 25, 26 and 27), ending in an additional generation of *r*O₂^{•−} [125]. The process was quantified by the significative 2.76-fold upregulation of *r*XO's catalytic activity (compare group II with I in Table 7). The *r*XO's catalytic activity augmentation was prevented by either YY or CCP EO at the highest tested concentrations (compare groups V and VIII with I in Table 7) by reducing to about 43% and 51% the CCl₄-increased *r*XO, respectively, which was about 18% and 40% higher

than the activity recorded in the presence of only olive oil, as YY EO is more potent than CCP EO in neutralizing the effect of CCl₄.

Table 7. The catalytic activities of enzymes, and the concentrations of antioxidant markers in rat kidneys exposed to different doses of YY EO, CCP EO, and CCl₄.

Group	rXO (U/L)	rNOX (U/mg Protein)	rNO (μmol/L)	rGPx (U/mg Protein)
I	18.14 ± 0.58 ^{a†}	1.40 ± 0.05 [†]	30.15 ± 0.10 [†]	0.25 ± 0.09 [†]
II	50.01 ± 0.64 [*]	5.14 ± 0.24 [*]	11.58 ± 0.11 [*]	0.12 ± 0.03 [*]
III	37.64 ± 0.31 ^{*†}	4.62 ± 0.15 ^{*†}	20.95 ± 0.31 ^{*†}	0.15 ± 0.04 [†]
IV	30.57 ± 0.14 ^{*†}	2.11 ± 0.31 ^{*†}	27.98 ± 0.22 ^{*†}	0.20 ± 0.03 ^{*†}
V	21.36 ± 0.95 ^{*†}	1.82 ± 0.03 ^{*†}	28.68 ± 0.20 ^{*†}	0.24 ± 0.02 [†]
VI	33.03 ± 0.60 ^{*†}	3.56 ± 0.17 ^{*†}	16.41 ± 0.09 ^{*†}	0.18 ± 0.01 ^{*†}
VII	29.16 ± 0.36 ^{*†}	1.99 ± 0.09 ^{*†}	21.16 ± 0.15 ^{*†}	0.21 ± 0.03 [†]
VIII	25.31 ± 0.22 ^{*†}	1.66 ± 0.26 ^{*†}	27.54 ± 0.30 ^{*†}	0.22 ± 0.06 [†]

^a Values represent mean ± SEM from three independent experiments; n=5 rats per group; I—Negative control, 1 mL/kg bwt olive oil, i.p.; II—Positive control, 1 mL/kg bwt of CCl₄, 1:1 mixture in olive oil, i.p.; III—1 mg/kg bwt of YY EO + 1 mL/kg bwt of CCl₄, i.p.; IV—200 mg/kg bwt of YY EO + 1 mL/kg bwt of CCl₄, i.p.; V—400 mg/kg bwt of YY EO + 1 mL/kg bwt of CCl₄, i.p.; VI—1 mg/kg bwt of CCP EO + 1 mL/kg bwt of CCl₄, i.p.; VII—200 mg/kg bwt of CCP EO + 1 mL/kg bwt of CCl₄, i.p.; VIII—400 mg/kg bwt of CCP EO + 1 mL/kg bwt of CCl₄, i.p.; * *p* < 0.05 when compared with the negative control group; [†] *p* < 0.05 when compared with the positive control group.

The rNOX Catalytic Activities

NADPH oxidase (NOX), usually considered as a marker for cardiovascular, hemorrhagic-shock-induced organ injury [162,163], hepatic ischemia/reperfusion (I/R) injury [161], and lipopolysaccharide-induced lung injury [164], catalyzes the conversion of O₂ into O₂^{•−} (Scheme 2, pink path, bold arrows, 5) within kidneys' endoplasmic reticulum and may lead to the progression of oxidative stress. Therefore, a significant upregulation of NOX (alongside the downregulation of SOD in CKD) represents an indicator of renal insufficiency [164]. In fact, rNOX did respond intensively to the oxidative damage caused by CCl₄, as the positive control sample was characterized by a 3.67-fold higher enzyme catalytic activity than the negative control (compare group II with I in Table 7).

Such a rNOX response agrees with the EOs' rescued catalytic activity of rCAT, which can decompose rH₂O₂ generated by rSOD from the rO₂^{•−} decomposition. In this scenario, rNOX then captures rO₂ and converts it into rO₂^{•−} (Table 7: II) and, in the presence of either YY or CCP EO (compare groups V and VIII in Table 7), the rNOX catalytic activity was not higher than 30% of the basal value, thus reducing to 35% and 32% the rNOX catalytic activity caused by CCl₄ administration, with a global damage recovery of more than 65%.

The rNO Concentrations

The CCl₄-generated rO₂^{•−} in kidneys was administered, formed by either rXO or rNOX and quantified by the decrease in rNO concentration to only 38% of the negative control value (compare group II with I in Table 7). Still, both YY and CCP EO as potential supplements managed to restore the rNO concentration efficiently, reaching full potential at the highest concentrations (compare groups V and VIII with I in Table 7), showing 95.12 and 91.34% of the basal rNO concentration, respectively, with a slightly higher potency of YY EO.

The GPx Catalytic Activities

Glutathione peroxidase (GPx, Scheme 2, orange pathway, bold arrows) shares its affinity with CAT to decompose an excess of produced H₂O₂; therefore, a decrease in its catalytic activity is associated with oxidative stress [127]. Therefore, rGPx was involved in protecting the kidneys from rH₂O₂ and was downregulated by CCl₄ to only 48% of the basal catalytic activity (compare group II with I in Table 7). Both YY and CCP EO managed to gradually recuperate rGPx's catalytic activity, whereas YY EO performed

slightly better (compare groups V and VIII with I in Table 7). The rescue of 96% and 88% of the basal *r*GPx reduced catalytic activity caused by CCl₄ was recorded for YY EO and CCP EO, respectively.

3.5. EOs Antigenotoxic Activity In Vivo

In parallel with the in vivo antioxidant evaluation, the Wistar rats' liver and kidney samples were used for determining the selected YY and CCP EOs' antigenotoxic activities by means of the comet assay (Tables 6–8) [128,165]. While, to the best of the authors' knowledge, no genotoxicity and/or antigenotoxicity study has been reported for YY EO, the CCP EO isolated from the bark of *Cinnamomum burmanii* was already assessed using doxorubicin-induced Chinese Hamster Ovary (CHO-K1) cells using micronucleus assay [166], Ames Salmonella reversion assay, *Bacillus subtilis* DNA-repair test (Rec-assay), *Escherichia coli* WP2uvrA reversion test [167], and *Drosophila melanogaster* Somatic Mutation and Recombination Test [168]. Herein, the antigenotoxicity of EOs was evaluated against the *r*CCl₃OO• that could cause the formation of *r*MDA and transform the DNA into the aberrant adducts, like M₁G, M₁A, and M₁C (Scheme 2, purple pathway, bold arrows, 28, 29 and 30), which root the transversions and transitions of bases and, upon the quantitative ring-opening, ultimately form *N*²-oxopropenyl-dG, *N*²-oxopropenyl-dA, and *N*²-oxopropenyl-dC adducts (Scheme 2, purple pathway, bold arrows, 31, 32 and 33), leading to the DNA–DNA inter-strand cross-links or DNA–protein inter-strand crosslinks [169] to which the comet assay is sensitive [128,165].

Table 8. The DNA-protective activity of different concentrations of YY and CCP EO against DNA damage induced by CCl₄ in the livers of albino Wistar rats.

Groups	Comet Types ^a					Total Comet Score (TCS)	%R ^b
	T ₀	T ₁	T ₂	T ₃	T ₄		
I	72.5 ± 0.37 ^c	27.5 ± 0.51	NO ^d	NO	NO	27.5 ± 0.41 [†]	NA ^e
II	NO	61.5 ± 0.32	26.2 ± 0.81	8.5 ± 0.12	3.8 ± 0.72	154.6 ± 0.53 [*]	NA
III	54.2 ± 0.82	21.5 ± 0.81	19.5 ± 0.23	4.8 ± 0.56	NO	74.9 ± 0.55 ^{*†}	62.7
IV	55.3 ± 0.61	31.6 ± 0.23	11.2 ± 0.32	1.9 ± 0.51	NO	59.7 ± 0.34 ^{*†}	74.7
V	67.8 ± 0.90	23.9 ± 0.41	8.3 ± 0.71	NO	NO	40.5 ± 0.84 ^{*†}	89.8
VI	49.4 ± 0.23	35.5 ± 0.92	11.9 ± 1.24	3.2 ± 0.12	NO	68.9 ± 0.51 ^{*†}	67.4
VII	66.1 ± 0.17	17.7 ± 0.13	14.1 ± 0.82	2.1 ± 0.85	NO	52.2 ± 0.72 ^{*†}	80.6
VIII	61.9 ± 0.11	27.9 ± 0.72	10.2 ± 0.84	NO	NO	48.3 ± 0.92 ^{*†}	83.6

^a Comet types defined as T₀, T₁, T₂, T₃, and T₄ (no or very low damage, low, medium, and long DNA migration, and the highest level of DNA damage, respectively); ^b %R, percentage reduction of DNA damage; ^c Values represent mean ± SEM from three independent experiments; n = 5 rats per group; ^d Not observed; ^e Not available; I—Negative control, 1 mL/kg bwt olive oil, i.p.; II—Positive control, 1 mL/kg bwt of CCl₄, 1:1 mixture in olive oil, i.p.; III—1 mg/kg bwt of YY EO + 1 mL/kg bwt of CCl₄, i.p.; IV—200 mg/kg bwt of YY EO + 1 mL/kg bwt of CCl₄, i.p.; V—400 mg/kg bwt of YY EO + 1 mL/kg bwt of CCl₄, i.p.; VI—1 mg/kg bwt of CCP EO + 1 mL/kg bwt of CCl₄, i.p.; VII—200 mg/kg bwt of CCP EO + 1 mL/kg bwt of CCl₄, i.p.; VIII—400 mg/kg bwt of CCP EO + 1 mL/kg bwt of CCl₄, i.p.; * *p* < 0.05 when compared with the negative control group; [†] *p* < 0.05 when compared with the positive control group.

3.5.1. Antigenotoxicity in Liver

As for the comet assay, both EOs have been compared with olive oil, characterized by a larger number of comets with no DNA damage (T₀) and a small number of comets associated with very low damage (T₁) (Table 8, I), or CCl₄, whose administration caused a significant increase in DNA damage (compare group II with I in Table 7), with a 5.62-fold higher total comet score (TCS) value. The co-administration of EOs with CCl₄ showed the YY EO as the more potent DNA protector; at the highest tested concentration, it provided TCS values that remained as low as 1.47-fold with respect to the negative control (compare group V with I in Table 8), corresponding to only 26.20% of the value associated with the administration of CCl₄, with a percentage reduction of DNA damage (%R) of 89.8% and an absence of comet types T₃ and T₄. Although the CCP EO delivered 1.8-fold higher TCS than in negative control group (Table 8), 31.24% of the TCS was associated with CCl₄ alone,

and there was a %R of 83.6% alongside the absence of comet types T₃ and T₄. The higher potency of YY EO to protect the DNA in vivo from the damage induced by *r*CCl₃OO• (i.e., the ROO•-type radical) compared to that observed for CCP EO could be, in part, associated with the higher percentage of caryophyllene (Table 3, 15.47 vs. 4.01%, respectively), which had the expressive affinity to neutralize the ROO• in vitro (Figure 3). Eugenol, which was 59.71-fold more abundant in CCP EO (Table 3), was a less significant feature against ROO• than caryophyllene. Yet, as previously noted, this speculation needs to be confirmed in further studies.

3.5.2. Antigenotoxicity in Kidneys

The potential protective features of selected EOs against the CCl₄-induced DNA damage were also assessed in the kidney cells of albino Wistar rats (Table 8) and compared to the negative control group, in which most of the comets showed no DNA damage (type T₀) and a few of them indicated very low damage (type T₁) (Table 9, I), or CCl₄ alone, which significantly increased TSC in kidney cells compared with the CCl₄-free group (Table 9, II vs. I) due to large-damage comets' presence (viz. types T₃ and T₄). Differently from what was observed in the case of the liver, CCP EO was more potent than YY EO at the highest tested concentration. Both YY and CCP EO showed lower DNA protection (compare data in Tables 8 and 9), dropping the TCSs to 1.69- and 1.31-fold higher values than the basal ones (compare groups V and VIII with I in Table 9), reducing to about 27% and 21% the TCSs induced by CCl₄, and causing the %Rs equal to 87.2 and 94.4%, respectively.

Table 9. The DNA-protective activity of different concentrations of YY and CCP EO against DNA damage induced by CCl₄ in kidneys of albino Wistar rats.

Groups	T ₀	Comet Types ^a				Total Comet Score (TCS)	%R ^b
		T ₁	T ₂	T ₃	T ₄		
I	78.2 ± 0.6 ^c	21.8 ± 0.54	NO ^d	NO	NO	21.8 ± 0.52 [†]	NA ^e
II	20.6 ± 0.72	38.3 ± 0.81	27.2 ± 0.11	9.6 ± 0.24	4.3 ± 0.83	138.7 ± 0.42 [*]	NA
III	54.5 ± 0.25	36.4 ± 0.54	9.1 ± 0.32	NO	NO	54.6 ± 0.6 ^{*†}	71.9
IV	64.1 ± 0.8	29.3 ± 0.68	6.6 ± 0.51	NO	NO	42.5 ± 0.21 ^{*†}	82.3
V	67.5 ± 1.24	28.2 ± 0.62	4.3 ± 0.21	NO	NO	36.8 ± 0.38 ^{*†}	87.2
VI	62.3 ± 0.25	31.5 ± 0.71	6.2 ± 0.34	NO	NO	43.9 ± 0.51 ^{*†}	81.1
VII	75.1 ± 0.12	18.3 ± 0.36	4.5 ± 0.50	2.1 ± 0.24	NO	33.6 ± 0.12 ^{*†}	89.9
VIII	71.5 ± 0.9	28.5 ± 0.40	NO	NO	NO	28.5 ± 0.31 [†]	94.4

^a Comet types defined as T₀, T₁, T₂, T₃, and T₄ (no or very low damage, low, medium, and long DNA migration, and the highest level of DNA damage, respectively); ^b %R, percentage reduction of DNA damage; ^c Values represented mean ± SEM from three independent experiments; n = 5 rats per group; ^d Not observed; ^e Not available; I—Negative control, 1 mL/kg bwt olive oil, i.p.; II—Positive control, 1 mL/kg bwt of CCl₄, 1:1 mixture in olive oil, i.p.; III—1 mg/kg bwt of YY EO + 1 mL/kg bwt of CCl₄, i.p.; IV—200 mg/kg bwt of YY EO + 1 mL/kg bwt of CCl₄, i.p.; V—400 mg/kg bwt of YY EO + 1 mL/kg bwt of CCl₄, i.p.; VI—1 mg/kg bwt of CCP EO + 1 mL/kg bwt of CCl₄, i.p.; VII—200 mg/kg bwt of CCP EO + 1 mL/kg bwt of CCl₄, i.p.; VIII—400 mg/kg bwt of CCP EO + 1 mL/kg bwt of CCl₄, i.p.; ^{*} *p* < 0.05 when compared with the negative control group; [†] *p* < 0.05 when compared with the positive control group.

4. Conclusions

Extensive in vitro assays on a list of 61 EOs were performed, leading to interesting and unique results. Many EO samples were shown to be able to modulate the TAC, to chelate the transition metal ions, and to neutralize the DPPH•, LOO•, ABTS•+, and OH•. The titled EOs also protected the DNA from damage induced by ROO• or OH•. Among the tested EOs, those obtained from YY and CCP showed the best antioxidant profile and were selected for in vivo investigations.

By correlating the chemical compositions of 61 commercial EOs with their in vitro experimentally determined abilities against Mⁿ⁺, DPPH•, LOO•, ABTS•+, OH• (either on the level of nucleotides or a DNA double-strand), or ROO• (protecting the DNA) by means of the machine learning (ML) classification algorithms, like SVM, RF, GB, DT, and KNN, various QCAR models were generated, yielding the most important features to be limonene,

linalool, carvacrol, eucalyptol, α -pinene, thymol, caryophyllene, *p*-cymene, eugenol, and chrysanthone, and characterizing their either positive or negative contributions through features importance plots as well as indicating the percentages of features within the EO mixtures required to either positively or negatively contribute to the listed antioxidant activities through the Partial Dependencies plots. The features' predicted contributions were in good agreement with their previously reported experimentally defined biological profiles while exerting antioxidant potential, thus validating the models' accuracies. As an added value of this research, all of the generated models can be freely used for the prediction of any untested EO for its antioxidant potencies, as a part of the AI4EssOil project (<https://www.ai4essoil.com/front/>, accessed on 20 September 2023).

The features' potential contributions in vivo were thereafter anticipated upon the administration of the most potent EOs (from YY and CCP) in adult Wistar rats against the redox and genotoxic damage caused by CCl₄. Experimental in vivo data strongly suggested that both YY and CCP EO represent potential new and effective antioxidant agents able to protect the cell from injuries caused by toxicants, such as CCl₄. Further studies are in due course to investigate the isolated components indicated by the ML models as possible new antioxidant compounds.

Supplementary Materials: The following Supplementary Materials can be downloaded at: <https://www.mdpi.com/article/10.3390/antiox12101815/s1>, Table S1. Essential oils previously investigated as antioxidant and their main chemical components. Table S2. Chemical composition of the tested essential oils chemical. Table S3. Total antioxidant capacity of examined EOs. Table S4. DNA-protective potential of selected 61 commercial essential oils on peroxy-radical-induced DNA damage. Table S5. DNA-protective potential of selected 61 commercial essential oils on hydroxyl-radical-induced DNA damage. Table S6. List of dataset pretreatment parameters settings randomly varied during ML hyperparameters optimization. Table S7. List of the initial thresholds used for the ML models for each antioxidant evaluation. Table S8. List of hyperparameters settings used for the ML models through random search optimization performed at 100 and 1000 iterations. Table S9. List of hyperparameters settings used for the ML models through random search optimization performed at 10,000 and 100,000 iterations. **Final ML Models Development.** 1. **Mⁿ⁺** 1.1. 100 random iterations. Table S10. Coarse best models obtained for each classifier. Table S11. Hyperparameters associated with models **MN1–MN5**. The list is reported as Python dictionaries. 1.2. 1000 random iterations. Table S12. Coarse best models obtained for each classifier. Table S13. Hyperparameters associated with models **MN6–MN9**. The list is reported as Python dictionaries. 1.3. 10,000 random iterations. Table S14. Refined best models obtained for each classifier. Table S15. Hyperparameters associated with models **MN10–MN13**. The list is reported as Python dictionaries. 1.4. 100,000 random iterations. Table S16. Refined best models obtained for each classifier. Table S17. Hyperparameters associated with models **MN14–MN16**. The list is reported as Python dictionaries. 2. **DPPH[•]** 2.1. 100 random iterations. Table S18. Coarse best models obtained for each classifier. Table S19. Hyperparameters associated with models **DPPH1–DPPH5**. The list is reported as Python dictionaries. 2.2. 1000 random iterations. Table S20. Coarse best models obtained for each classifier. Table S21. Hyperparameters associated with models **DPPH6–DPPH10**. The list is reported as Python dictionaries. 2.3. 10,000 random iterations. Table S22. Refined best models obtained for each classifier. Table S23. Hyperparameters associated with models **DPPH11–DPPH13**. The list is reported as Python dictionaries. 2.4. 100,000 random iterations. Table S24. Refined best models obtained for each classifier. Table S25. Hyperparameters associated with models **DPPH14–DPPH16**. The list is reported as Python dictionaries. 3. **LOO[•]** 3.1. 100 random iterations. Table S26. Coarse best models obtained for each classifier. Table S27. Hyperparameters associated with models **LOO1–LOO5**. The list is reported as Python dictionaries. 3.2. 1000 random iterations. Table S28. Coarse best models obtained for each classifier. Table S29. Hyperparameters associated with models **LOO6–LOO10**. The list is reported as Python dictionaries. 3.3. 10,000 random iterations. Table S30. Refined best models obtained for each classifier. Table S31. Hyperparameters associated with models **LOO10–LOO14**. The list is reported as Python dictionaries. 3.4. 100,000 random iterations. Table S32. Refined best models obtained for each classifier. Table S33. Hyperparameters associated with models **LOO15–LOO17**. The list is reported as Python dictionaries. 4. **ABTS^{•+}** 4.1. 100 random iterations. Table S34. Coarse best models obtained for each classifier. Table S35. Hyperparameters associated with models **ABTS1–ABTS5**. The list is

reported as Python dictionaries. 4.2. 1000 random iterations. Table S36. Coarse best models obtained for each classifier. Table S37. Hyperparameters associated with models **ABTS6–ABTS10**. The list is reported as Python dictionaries. 4.3. 10,000 random iterations. Table S38. Refined best models obtained for each classifier. Table S39. Hyperparameters associated with models **ABTS11–ABTS14**. The list is reported as Python dictionaries. 4.4. 100,000 random iterations. Table S40. Refined best models obtained for each classifier. Table S41. Hyperparameters associated with models **ABTS15–ABTS17**. The list is reported as Python dictionaries. 5. **OH•** 5.1. 100 random iterations. Table S42. Coarse best models obtained for each classifier. Table S43. Hyperparameters associated with models **OH1–OH5**. The list is reported as Python dictionaries. 5.2. 1000 random iterations. Table S44. Coarse best models obtained for each classifier. Table S45. Hyperparameters associated with models **OH6–OH10**. The list is reported as Python dictionaries. 5.3. 10,000 random iterations. Table S46. Refined best models obtained for each classifier. Table S47. Hyperparameters associated with models **OH11–OH14**. The list is reported as Python dictionaries. 5.4. 100,000 random iterations. Table S48. Refined best models obtained for each classifier. Table S49. Hyperparameters associated with models **OH15–OH16**. The list is reported as Python dictionaries. 6. **ROO-RBD₅₀s** 6.1. 100 random iterations. Table S50. Coarse best models obtained for each classifier. Table S51. Hyperparameters associated with models **ROO1–ROO5**. The list is reported as Python dictionaries. 6.2. 1000 random iterations. Table S52. Coarse best models obtained for each classifier. Table S53. Hyperparameters associated with models **ROO6–ROO9**. The list is reported as Python dictionaries. 6.3. 10,000 random iterations. Table S54. Refined best models obtained for each classifier. Table S55. Hyperparameters associated with models **ROO10–ROO13**. The list is reported as Python dictionaries. 6.4. 100,000 random iterations. Table S56. Refined best models obtained for each classifier. Table S57. Hyperparameters associated with models **ROO14–ROO16**. The list is reported as Python dictionaries. 7. **OH-RBD₅₀** 7.1. 100 random iterations. Table S58. Coarse best models obtained for each classifier. Table S59. Hyperparameters associated with models **OH-RBD1–OH-RBD5**. The list is reported as Python dictionaries. 7.2. 1000 random iterations. Table S60. Coarse best models obtained for each classifier. Table S61. Hyperparameters associated with models **OH-RBD6–OH-RBD10**. The list is reported as Python dictionaries. 7.3. 10,000 random iterations. Table S62. Refined best models obtained for each classifier. Table S63. Hyperparameters associated with models **OH-RBD11–OH-RBD13**. The list is reported as Python dictionaries. 7.4. 100,000 random iterations. Table S64. Refined best models obtained for each classifier. Table S65. Hyperparameters associated with models **OH-RBD14–OH-RBD16**. The list is reported as Python dictionaries. Figure S1. Protective effect of Chamomile Morocco EO against peroxy- (A) and hydroxyl- (B) radicals-induced DNA damage. DNA from salmon sperm (lane 1, negative control), DNA damage control (lane 2, positive control), quercetin (lane 3, 100 µg/mL, standard), essential oils in concentrations of 25, 50, 100, 200, and 400 µg/mL (lanes 4, 5, 6, 7, and 8). * $p < 0.05$ when compared with the negative control group; † $p < 0.05$ when compared with the positive control group. Figure S2. Protective effect of Clary sage EO against peroxy- (A) and hydroxyl- (B) radicals-induced DNA damage. DNA from salmon sperm (lane 1, negative control), DNA damage control (lane 2, positive control), quercetin (lane 3, 100 µg/mL, standard), essential oils in concentrations of 25, 50, 100, 200, and 400 µg/mL (lanes 4, 5, 6, 7, and 8). * $p < 0.05$ when compared with the negative control group; † $p < 0.05$ when compared with the positive control group. Figure S3. Protective effect of Sage EO against peroxy- (A) and hydroxyl- (B) radicals-induced DNA damage. DNA from salmon sperm (lane 1, negative control), DNA damage control (lane 2, positive control), quercetin (lane 3, 100 µg/mL, standard), essential oils in concentrations of 25, 50, 100, 200, and 400 µg/mL (lanes 4, 5, 6, 7, and 8). * $p < 0.05$ when compared with the negative control group; † $p < 0.05$ when compared with the positive control group. Figure S4. Protective effect of Red thyme EO against peroxy- (A) and hydroxyl- (B) radicals-induced DNA damage. DNA from salmon sperm (lane 1, negative control), DNA damage control (lane 2, positive control), quercetin (lane 3, 100 µg/mL, standard), essential oils in concentrations of 25, 50, 100, 200, and 400 µg/mL (lanes 4, 5, 6, 7, and 8). * $p < 0.05$ when compared with the negative control group; † $p < 0.05$ when compared with the positive control group. Figure S5. Protective effect Tea tree EO against peroxy- (A) and hydroxyl- (B) radicals-induced DNA damage. DNA from salmon sperm (lane 1, negative control), DNA damage control (lane 2, positive control), quercetin (lane 3, 100 µg/mL, standard), essential oils in concentrations of 25, 50, 100, 200, and 400 µg/mL (lanes 4, 5, 6, 7, and 8). * $p < 0.05$ when compared with the negative control group; † $p < 0.05$ when compared with the positive control group. Figure S6. Protective effect of Melissa EO against peroxy- (A) and hydroxyl- (B) radicals-induced DNA damage. DNA from salmon sperm (lane 1, negative control), DNA damage control (lane 2, positive control), quercetin (lane 3,

with the positive control group. Figure S55. Protective effect of Incense EO against peroxy- (A) and hydroxyl- (B) radicals-induced DNA damage. DNA from salmon sperm (lane 1, negative control), DNA damage control (lane 2, positive control), quercetin (lane 3, 100 µg/mL, standard), essential oils in concentrations of 25, 50, 100, 200, and 400 µg/mL (lanes 4, 5, 6, 7, and 8). * $p < 0.05$ when compared with the negative control group; † $p < 0.05$ when compared with the positive control group. Figure S56. Protective effect of *Mentha suaveolens* EO against peroxy- (A) and hydroxyl- (B) radicals-induced DNA damage. DNA from salmon sperm (lane 1, negative control), DNA damage control (lane 2, positive control), quercetin (lane 3, 100 µg/mL, standard), essential oils in concentrations of 25, 50, 100, 200, and 400 µg/mL (lanes 4, 5, 6, 7, and 8). * $p < 0.05$ when compared with the negative control group; † $p < 0.05$ when compared with the positive control group. Figure S57. Protective effect of *Coridodthymus capitatus* EO against peroxy- (A) and hydroxyl- (B) radicals-induced DNA damage. DNA from salmon sperm (lane 1, negative control), DNA damage control (lane 2, positive control), quercetin (lane 3, 100 µg/mL, standard), essential oils in concentrations of 25, 50, 100, 200, and 400 µg/mL (lanes 4, 5, 6, 7, and 8). * $p < 0.05$ when compared with the negative control group; † $p < 0.05$ when compared with the positive control group. Figure S58. Protective effect of *Thymus vulgaris* EO against peroxy- (A) and hydroxyl- (B) radicals-induced DNA damage. DNA from salmon sperm (lane 1, negative control), DNA damage control (lane 2, positive control), quercetin (lane 3, 100 µg/mL, standard), essential oils in concentrations of 25, 50, 100, 200, and 400 µg/mL (lanes 4, 5, 6, 7, and 8). * $p < 0.05$ when compared with the negative control group; † $p < 0.05$ when compared with the positive control group. Figure S59. Protective effect of *Origanum hirtum* EO against peroxy- (A) and hydroxyl- (B) radicals-induced DNA damage. DNA from salmon sperm (lane 1, negative control), DNA damage control (lane 2, positive control), quercetin (lane 3, 100 µg/mL, standard), essential oils in concentrations of 25, 50, 100, 200, and 400 µg/mL (lanes 4, 5, 6, 7, and 8). * $p < 0.05$ when compared with the negative control group; † $p < 0.05$ when compared with the positive control group. Figure S60. Partial dependence graphs of limonene in the model of M^{n+} (A), DPPH• (B), LOO• (C), ABTS•+ (D), OH• (E), ROO-RBD₅₀ (F), HO-RBD₅₀ (G). Figure S61. Partial dependence graphs of thymol in the model of M^{n+} (A), DPPH• (B), LOO• (C), ABTS•+ (D), OH• (E), ROO-RBD₅₀ (F), HO-RBD₅₀ (G). Figure S62. Partial dependence graphs of eugenol in the model of M^{n+} (A), DPPH• (B), LOO• (C), ABTS•+ (D), OH• (E), ROO-RBD₅₀ (F), HO-RBD₅₀ (G). Figure S63. Partial dependence graphs of chrysanthone in the model of M^{n+} (A), DPPH• (B), LOO• (C), ABTS•+ (D), OH• (E), ROO-RBD₅₀ (F), HO-RBD₅₀ (G). Figure S64. Partial dependence graphs of chrysanthone in the model of M^{n+} (A), DPPH• (B), LOO• (C), ABTS•+ (D), OH• (E), ROO-RBD₅₀ (F), HO-RBD₅₀ (G). Figure S65. Partial dependence graphs of α -pinene in the model of M^{n+} (A), DPPH• (B), LOO• (C), ABTS•+ (D), OH• (E), ROO-RBD₅₀ (F), HO-RBD₅₀ (G). Figure S66. Partial dependence graphs of caryophyllene in the model of M^{n+} (A), DPPH• (B), LOO• (C), ABTS•+ (D), OH• (E), ROO-RBD₅₀ (F), HO-RBD₅₀ (G). Figure S67. Partial dependence graphs of *p*-cymene in the model of M^{n+} (A), DPPH• (B), LOO• (C), ABTS•+ (D), OH• (E), ROO-RBD₅₀ (F), HO-RBD₅₀ (G). Results. ABTS cation-radical-neutralizing activity of EOs. Antigenotoxic activity in vitro. EOs with increasing dose-dependent potency to protect DNA from ROO• and OH•. EOs with decreasing dose-dependent potency to protect from ROO• and OH•. EOs with increasing and decreasing dose-dependent potency to protect DNA from ROO• and OH•, respectively. EOs with decreasing and increasing dose-dependent potency to protect DNA from ROO• and OH•, respectively. Liver redox status. 3.4.1.1. The rTBARS concentrations. 3.4.1.2. The rSOD catalytic activities. 3.4.1.3. The rCAT catalytic activities. The rGSH concentrations. The hepatocytes toxicity status. The rAST and rALT catalytic activities. The rALP and γ -GT catalytic activities. Kidneys' redox status. The rTBARS concentrations. The rSOD catalytic activities. The rCAT catalytic activities. The rGSH concentration. Chronic kidney disease markers. The rXO catalytic activities. The rXO catalytic activities. The rNO concentrations. The GPx catalytic activities. EOs antigenotoxic activity in vivo. Antigenotoxicity in liver. Antigenotoxicity in kidneys.

Author Contributions: Conceptualization, M.M. and R.R.; methodology, M.M., N.T., S.M., M.B., F.S., R.A. and R.R.; software, F.S., R.A. and R.R.; validation, M.M. and R.R.; formal analysis, M.M. and R.R.; investigation, M.M., N.T., S.M., M.B., F.S., R.A. and R.R.; resources, M.M., N.T., S.M., M.B., F.S., R.A. and R.R.; data curation, M.M., N.T., S.M., M.B., F.S., R.A. and R.R.; writing—original draft preparation, M.M., N.T., S.M., M.B., F.S., R.A. and R.R.; writing—review and editing, M.M. and R.R.; visualization, M.M., N.T., S.M., M.B., F.S., R.A. and R.R.; supervision, M.M. and R.R.; project administration, M.M. and R.R.; funding acquisition, M.M., S.M. and R.R. All authors have read and agreed to the published version of the manuscript.

Funding: This work was supported by the Serbian Ministry of Science, Technological Development, and Innovation (Agreement Nos. 451-03-47/2023-01/200122 and 451-03-47/2023-01/200378) and supported by two grants from Progetti di Ricerca di Università 2015, Sapienza Università di Roma (C26A15RT82 and C26A15J3BB).

Institutional Review Board Statement: The animal study was conducted in accordance with the Declaration of Helsinki and approved by the Institutional Review Board (or Ethics Committee) of the Faculty of Science, the University of Kragujevac (number of ethical approval 1-03/2023), which acts following the relevant Serbian guidelines, including the Guidelines for the Care and Use of Laboratory Animals and Law on Animal Welfare (“Official Gazette of Republic of Serbia,” No. 810 41/09) and the European Directive for the Welfare of Laboratory Animals Directive 2010/63/EU.

Informed Consent Statement: Not applicable.

Data Availability Statement: All of the experimental results in vitro and in vivo can be obtained upon request from Milan Mladenović. All of the Python notebooks considering the ML models can be obtained upon request from Rino Ragno.

Conflicts of Interest: The authors declare no conflict of interest.

References

1. Amorati, R.; Foti, M.C.; Valgimigli, L. Antioxidant activity of essential oils. *J. Agric. Food Chem.* **2013**, *61*, 10835–10847. [[CrossRef](#)]
2. Miguel, M.G. Antioxidant and anti-inflammatory activities of essential oils: A short review. *Molecules* **2010**, *15*, 9252–9287. [[CrossRef](#)] [[PubMed](#)]
3. Reichling, J.; Schnitzler, P.; Suschke, U.; Saller, R. Essential oils of aromatic plants with antibacterial, antifungal, antiviral, and cytotoxic properties—An overview. *Forsch. Komplementmed.* **2009**, *16*, 79–90. [[CrossRef](#)]
4. Edris, A.E. Pharmaceutical and therapeutic potentials of essential oils and their individual volatile constituents: A review. *Phytother. Res.* **2007**, *21*, 308–323. [[CrossRef](#)] [[PubMed](#)]
5. Torres-Martínez, R.; García-Rodríguez, Y.M.; Ríos-Chávez, P.; Saavedra-Molina, A.; López-Meza, J.E.; Ochoa-Zarzosa, A.; Garciglia, R.S. Antioxidant activity of the essential oil and its major terpenes of *Satureja macrostema* (Moc. and Sessé ex Benth.) Briq. *Pharmacogn. Mag.* **2018**, *13*, S875–S880. [[CrossRef](#)]
6. Lanigan, R.S.; Yamarik, T.A. Final report on the safety assessment of BHT(1). *Int. J. Toxicol.* **2002**, *21* (Suppl. S2), 19–94. [[CrossRef](#)] [[PubMed](#)]
7. Andrés, C.M.C.; Pérez de la Lastra, J.M.; Andrés Juan, C.; Plou, F.J.; Pérez-Lebeña, E. Superoxide anion chemistry—Its role at the core of the innate immunity. *Int. J. Mol. Sci.* **2023**, *24*, 1841. [[CrossRef](#)] [[PubMed](#)]
8. López-Alarcón, C.; Denicola, A. Evaluating the antioxidant capacity of natural products: A review on chemical and cellular-based assays. *Anal. Chim. Acta* **2013**, *763*, 1–10. [[CrossRef](#)] [[PubMed](#)]
9. Burg, A.; Meyerstein, D. Chapter 7—The chemistry of monovalent copper in aqueous solutions. In *Advances in Inorganic Chemistry*; Eldik, R.V., Ivanović-Burmazović, I., Eds.; Academic Press: Cambridge, MA, USA, 2012; Volume 64, pp. 219–261.
10. Kehler, J.P. The Haber-Weiss reaction and mechanisms of toxicity. *Toxicology* **2000**, *149*, 43–50. [[CrossRef](#)]
11. Prieto, P.; Pineda, M.; Aguilar, M. Spectrophotometric quantitation of antioxidant capacity through the formation of a phosphomolybdenum complex: Specific application to the determination of vitamin E. *Anal. Biochem.* **1999**, *269*, 337–341. [[CrossRef](#)]
12. Chew, Y.-L.; Goh, J.-K.; Lim, Y.-Y. Assessment of in vitro antioxidant capacity and polyphenolic composition of selected medicinal herbs from Leguminosae family in Peninsular Malaysia. *Food Chem.* **2009**, *116*, 13–18. [[CrossRef](#)]
13. Kumarasamy, Y.; Byres, M.; Cox, P.J.; Jaspars, M.; Nahar, L.; Sarker, S.D. Screening seeds of some Scottish plants for free radical scavenging activity. *Phytother. Res.* **2007**, *21*, 615–621. [[CrossRef](#)] [[PubMed](#)]
14. Hsu, C.K.; Chiang, B.H.; Chen, Y.S.; Yang, J.H.; Liu, C.L. Improving the antioxidant activity of buckwheat (*Fagopyrum tataricum* Gaertn) sprout with trace element water. *Food Chem.* **2008**, *108*, 633–641. [[CrossRef](#)]
15. Re, R.; Pellegrini, N.; Proteggente, A.; Pannala, A.; Yang, M.; Rice-Evans, C. Antioxidant activity applying an improved ABTS radical cation decolorization assay. *Free Radic. Biol. Med.* **1999**, *26*, 1231–1237. [[CrossRef](#)] [[PubMed](#)]
16. Kunchandy, E.; Rao, M.N.A. Oxygen radical scavenging activity of curcumin. *Int. J. Pharm.* **1990**, *58*, 237–240. [[CrossRef](#)]
17. Halliwell, B.; Gutteridge, J.M.; Aruoma, O.I. The deoxyribose method: A simple “test-tube” assay for determination of rate constants for reactions of hydroxyl radicals. *Anal. Biochem.* **1987**, *165*, 215–219. [[CrossRef](#)] [[PubMed](#)]
18. Lin, Y.W.; Wang, Y.T.; Chang, H.M.; Wu, J.S.B. DNA protection and antitumor effect of water extract from residue of jelly fig (*Ficus awkeotsang* Makino) achenes. *J. Food Drug Anal.* **2020**, *16*, 14. [[CrossRef](#)]
19. Poorna, C.A.; Resmi, M.S.; Soniya, E.V. In vitro antioxidant analysis and the dna damage protective activity of leaf extract of the *Excoecaria agallocha* Linn Mangrove Plant. In *Agricultural Chemistry*; Margarita, S., Roumen, Z., Eds.; IntechOpen: Rijeka, Croatia, 2013; p. Ch. 7.
20. Zhang, L.L.; Zhang, L.F.; Xu, J.G.; Hu, Q.P. Comparison study on antioxidant, DNA damage protective and antibacterial activities of eugenol and isoeugenol against several foodborne pathogens. *Food Nutr. Res.* **2017**, *61*, 1353356. [[CrossRef](#)]

21. Elouaddari, A.; Elamrani, A.; Moutia, M.; Oubrim, N.; Habti, N.; JamalEddine, J. Chemical composition and evaluation of antioxidant, antimicrobial and cytotoxic activities of Moroccan *Cladanthus mixtus* Essential Oil and Extracts. *J. Essent. Oil Bear. Plants* **2019**, *22*, 1450–1466. [[CrossRef](#)]
22. Ovidi, E.; Laghezza Masci, V.; Zambelli, M.; Tiezzi, A.; Vitalini, S.; Garzoli, S. *Laurus nobilis*, *Salvia sclarea* and *Salvia officinalis* essential oils and hydrolates: Evaluation of liquid and vapor phase chemical composition and biological activities. *Plants* **2021**, *10*, 707. [[CrossRef](#)] [[PubMed](#)]
23. Ilić, Z.S.; Kevrešan, Ž.; Šunić, L.; Stanojević, L.; Milenković, L.; Stanojević, J.; Milenković, A.; Cvetković, D. Chemical profiling and antioxidant activity of wild and cultivated sage (*Salvia officinalis* L.) essential oil. *Horticulturae* **2023**, *9*, 624. [[CrossRef](#)]
24. Noumi, E.; Snoussi, M.; Hajlaoui, H.; Trabelsi, N.; Ksouri, R.; Valentin, E.; Bakhrouf, A. Chemical composition, antioxidant and antifungal potential of *Melaleuca alternifolia* (tea tree) and *Eucalyptus globulus* essential oils against oral *Candida* species. *J. Med. Plants Res.* **2011**, *5*, 4147–4156.
25. Zhang, X.; Guo, Y.; Guo, L.; Jiang, H.; Ji, Q. In vitro Evaluation of Antioxidant and Antimicrobial Activities of *Melaleuca alternifolia* essential oil. *Biomed. Res. Int.* **2018**, *2018*, 2396109. [[CrossRef](#)] [[PubMed](#)]
26. Mapeka, T.M.; Sandasi, M.; Viljoen, A.M.; van Vuuren, S.F. Optimization of antioxidant synergy in a polyherbal combination by experimental design. *Molecules* **2022**, *27*, 4196. [[CrossRef](#)]
27. Mimica-Dukić, N.; Božin, B.; Soković, M.; Simin, N. Antimicrobial and antioxidant activities of *Melissa officinalis* L. (*Lamiaceae*) essential oil. *J. Agric. Food Chem.* **2004**, *52*, 2485–2489. [[CrossRef](#)] [[PubMed](#)]
28. Garzoli, S.; Masci, V.L.; Caradonna, V.; Tiezzi, A.; Giacomello, P.; Ovidi, E. Liquid and vapor phase of four conifer-derived essential oils: Comparison of chemical compositions and antimicrobial and antioxidant properties. *Pharmaceuticals* **2021**, *14*, 134. [[CrossRef](#)]
29. Karapandzova, M.; Stefkov, G.; Karanfilova, I.C.; Panovska, T.K.; Stanoeva, J.P.; Stefova, M.; Kulevanova, S. Chemical characterization and antioxidant activity of mountain pine (*Pinus mugo Turra*, *Pinaceae*) from Republic of Macedonia. *Rec. Nat. Prod.* **2018**, *13*, 50–63. [[CrossRef](#)]
30. Ramdan, B.; Amakran, A.; Mohamed, N. In vitro study of anti-glycation and radical scavenging activities of the essential oils of three plants from Morocco: *Origanum compactum*, *Rosmarinus officinalis* and *Pelargonium asperum*. *Pharmacogn. J.* **2015**, *7*, 124–135.
31. Ouedrhiri, W.; Balouiri, M.; Bouhdid, S.; Harki, E.H.; Moja, S.; Greche, H. Antioxidant and antibacterial activities of *Pelargonium asperum* and *Ormenis mixta* essential oils and their synergistic antibacterial effect. *Environ. Sci. Pollut. Res. Int.* **2018**, *25*, 29860–29867. [[CrossRef](#)]
32. Han, F.; Ma, G.Q.; Yang, M.; Yan, L.; Xiong, W.; Shu, J.C.; Zhao, Z.D.; Xu, H.L. Chemical composition and antioxidant activities of essential oils from different parts of the oregano. *J. Zhejiang Univ. Sci. B* **2017**, *18*, 79–84. [[CrossRef](#)]
33. Stanojević, L.P.; Stanojević, J.S.; Savić, V.L.; Cvetković, D.J.; Kolarević, A.; Marjanović-Balaban, Z.; Nikolić, L.B. Peppermint and basil essential oils: Chemical composition, in vitro antioxidant activity and in vivo estimation of skin irritation. *J. Essent. Oil Bear. Plants* **2019**, *22*, 979–993. [[CrossRef](#)]
34. Kačaniová, M.; Vukovic, N.L.; Hleba, L.; Bobková, A.; Pavelkova, A.; Rovná, K.; Arpášová, H. Antimicrobial and antiradicals activity of *Origanum vulgare* L. and *Thymus vulgaris* essential oils. *J. Microbiol. Biotechnol. Food Sci.* **2019**, *2019*, 263–271.
35. Martiniaková, S.; Ácsová, A.; Hojerová, J.; Krepsová, Z.; Kreps, F. Ceylon cinnamon and clove essential oils as promising free radical scavengers for skin care products. *Acta Chim. Slovaca* **2022**, *15*, 1–11. [[CrossRef](#)]
36. Handayani, W.; Yasman; Yunilawati, R.; Fauzia, V.; Imawan, C. *Coriandrum sativum* L. (*Apiaceae*) and *Elettaria cardamomum* (L.) maton (*Zingiberaceae*) for antioxidant and antimicrobial protection. *J. Phys. Conf. Ser.* **2019**, *1317*, 012092. [[CrossRef](#)]
37. Jafari, S.; Mori, Y. Chemical composition and antioxidant activity of essential oil of coriandrum sativum l. seeds cultivated in Afghanistan. *Eur. J. Med. Plants* **2021**, *32*, 82–92. [[CrossRef](#)]
38. Jeya, K.R.; Veerapagu, M.; Sangeetha, V. Antimicrobial and antioxidant properties of *Coriandrum sativum* L. seed essential oil. *Am. J. Essent. Oils Nat. Prod.* **2019**, *7*, 6–10.
39. Gharib, F.A.; Badr, S.E.A.; Al-Ghazali, B.A.S.; Zahran, M.K. Chemical composition, antioxidant and antibacterial activities of lavender and marjoram essential oils. *Egypt. J. Chem.* **2013**, *56*, 1–24. [[CrossRef](#)]
40. Hamad, K.J.; Al-Shaheen, S.J.A.; Kaskoos, R.A.; Ahamad, J.; Jameel, M.; Mir, S.R. Essential oil composition and antioxidant activity of *Lavandula angustifolia* from Iraq. *Int. Res. J. Pharm.* **2013**, *4*, 117–120. [[CrossRef](#)]
41. Salavati Hamedani, M.; Rezaeigoolestani, M.; Mohsenzadeh, M. Chemical composition, antimicrobial and antioxidant activities of *Lavandula angustifolia* essential oil. *J. Nutr. Fasting Health* **2020**, *8*, 273–279. [[CrossRef](#)]
42. Benhadid, R.; Hadeif, Y.; Djahoudi, A.; Hosni, K. Chemical characterization, evaluation of the antibacterial and antioxidant activities of the essential oil of Algerian (*Myrtus communis* L.). *Prog. Nutr.* **2022**, *24*, e2022029. [[CrossRef](#)]
43. Snoussi, A.; Chaabouni, M.M.; Bouzouita, N.; Kachouri, F. Chemical composition and antioxidant activity of *Myrtus communis* L. floral buds essential oil. *J. Essent. Oil Res.* **2011**, *23*, 10–14. [[CrossRef](#)]
44. Herrera-Calderon, O.; Chacaltana-Ramos, L.J.; Huayanca-Gutiérrez, I.C.; Algarni, M.A.; Alqarni, M.; Batiha, G.E.-S. Chemical Constituents, in vitro antioxidant activity and in silico study on NADPH oxidase of *Allium sativum* L. (Garlic) essential oil. *Antioxidants* **2021**, *10*, 1844. [[CrossRef](#)] [[PubMed](#)]
45. Chekki, R.Z.; Snoussi, A.; Hamrouni, I.; Bouzouita, N. Chemical composition, antibacterial and antioxidant activities of Tunisian garlic (*Allium sativum*) essential oil and ethanol extract. *Mediterr. J. Chem.* **2014**, *3*, 947–956. [[CrossRef](#)]

46. Fayed, S.A. Antioxidant and anticancer activities of *Citrus reticulata* (Petitgrain mandarin) and *Pelargonium graveolens* (Geranium) essential oils. *Res. J. Agric. Biol. Sci.* **2009**, *5*, 740–747.
47. Meryem, S.; Mohamed, D.; Nour-eddine, C.; Faouzi, E. Chemical composition, antibacterial and antioxidant properties of three Moroccan citrus peel essential oils. *Sci. Afr.* **2023**, *20*, e01592. [[CrossRef](#)]
48. Kizil, S.; HaşİMİ, N.; Tolan, V.; KilinÇ, E.; KarataŞ, H. Chemical composition, antimicrobial and antioxidant activities of Hyssop (*Hyssopus officinalis* L.) essential oil. *Not. Bot. Horti Agrobot. Cluj-Napoca* **2010**, *38*, 99–103. [[CrossRef](#)]
49. Moulodi, F.; Khezerlou, A.; Zolfaghari, H.; Mohamadzadeh, A.; Alimoradi, F. Chemical composition and antioxidant and antimicrobial properties of the essential oil of *Hyssopus officinalis* L. *J. Kermanshah Univ. Med. Sci.* **2019**, *in press*. [[CrossRef](#)]
50. Deng, W.; Liu, K.; Cao, S.; Sun, J.; Zhong, B.; Chun, J. Chemical composition, antimicrobial, antioxidant, and antiproliferative properties of grapefruit essential oil prepared by molecular distillation. *Molecules* **2020**, *25*, 217. [[CrossRef](#)]
51. Ling, Q.; Zhang, B.; Wang, Y.; Xiao, Z.; Hou, J.; Xiao, C.; Liu, Y.; Jin, Z. Chemical composition and antioxidant activity of the essential oils of citral-rich chemotype *Cinnamomum camphora* and *Cinnamomum bodinieri*. *Molecules* **2022**, *27*, 7356. [[CrossRef](#)]
52. El Hajjouji, H.; Rahhal, R.; Gmouh, S.; Hsaine, M.; Fougrach, H.; Badri, W. Chemical composition, antioxidant and antibacterial activities of the essential oils of *Juniperus phoenicea*, *Juniperus thurifera* and *Juniperus oxycedrus*. *Mediterr. J. Chem.* **2019**, *9*, 190–198. [[CrossRef](#)]
53. Ghalem, B.R.; Malika, O.; Fatiha, S. Antioxidant capacity of essential oils of two *Juniperus* species from northwest of Algeria. *Am. J. Appl. Ind. Chem.* **2016**, *2*, 33–36. [[CrossRef](#)]
54. Abbdellaoui, M.; Bouhlali, E.d.T.; Rhaffari, L.E. Chemical composition and antioxidant activities of the essential oils of Cumin (*Cuminum cyminum*) conducted under organic production conditions. *J. Essent. Oil Bear. Plants* **2019**, *22*, 1500–1508. [[CrossRef](#)]
55. Badalamenti, N.; Bruno, M.; Schicchi, R.; Geraci, A.; Leporini, M.; Gervasi, L.; Tundis, R.; Loizzo, M.R. Chemical compositions and antioxidant activities of essential oils, and their combinations, obtained from Flavedo by-product of seven cultivars of sicilian *Citrus aurantium* L. *Molecules* **2022**, *27*, 1580. [[CrossRef](#)]
56. Hariyanti, H.E.; Dayatri, D.Y. Phytochemical identification and antioxidant activity of essential oil of *Pogostemon cablin* Benth. cultivated in Java Island Indonesia. *Int. J. Phytopharm.* **2019**, *9*, e5297. [[CrossRef](#)]
57. Mohammad-Bagher, M. Chemical composition, cytotoxicity and antioxidant activities of the essential oil from the leaves of *Citrus aurantium* L. *Afr. J. Biotechnol.* **2011**, *11*, 498–503. [[CrossRef](#)]
58. Salem, N.; Kefi, S.; Tabben, O.; Ayed, A.; Jallouli, S.; Feres, N.; Hammami, M.; Khammassi, S.; Hrigua, I.; Nefisi, S.; et al. Variation in chemical composition of *Eucalyptus globulus* essential oil under phenological stages and evidence synergism with antimicrobial standards. *Ind. Crops Prod.* **2018**, *124*, 115–125. [[CrossRef](#)]
59. Noshad, M.; Alizadeh Behbahani, B. Investigation of phytochemical compounds, antioxidant potential and the antimicrobial effect of bergamot essential oil on some pathogenic strains causing infection in vitro. *J. Ilam Univ. Med. Sci.* **2019**, *26*, 122–132. [[CrossRef](#)]
60. Stoilova, I.; Wanner, J.; Trifonova, D.; Stoyanova, S.; Krastanov, I.; Schloss, H.A. Chemical composition and antioxidant properties of juniper berry (*Juniperus communis* L.) essential oil. *Bulg. J. Agric. Sci.* **2014**, *20*, 227–237.
61. Stoilova, I.; Bail, S.; Buchbauer, G.; Krastanov, A.; Stoyanova, A.; Schmidt, E.; Jirovets, L. Chemical composition, olfactory evaluation and antioxidant effects of the essential oil of *Satureja montana* L. *Nat. Prod. Commun.* **2008**, *3*, 1035–1042. [[CrossRef](#)]
62. Sabzi Nojadeh, M.; Poursmaeil, M.; Younessi-Hamzekhanlu, M.; Venditti, A. Phytochemical profile of fennel essential oils and possible applications for natural antioxidant and controlling *Convolvulus arvensis* L. *Nat. Prod. Res.* **2021**, *35*, 4164–4168. [[CrossRef](#)]
63. Šunić, L.; Ilić, Z.S.; Stanojević, L.; Milenković, L.; Stanojević, J.; Kovač, R.; Milenković, A.; Cvetković, D. Comparison of the essential oil content, constituents and antioxidant activity from different plant parts during development stages of Wild Fennel (*Foeniculum vulgare* Mill.). *Horticulturae* **2023**, *9*, 364. [[CrossRef](#)]
64. Vahidi, R.; Pourahmad, R.; Mahmoudi, R. Chemical compounds and antibacterial and antioxidant properties of citron (*Citrus medica* L.) peel essential oil. *J. Food Bioprocess Eng.* **2019**, *2*, 71–76.
65. Ben Hsouna, A.; Ben Halima, N.; Smaoui, S.; Hamdi, N. Citrus lemon essential oil: Chemical composition, antioxidant and antimicrobial activities with its preservative effect against *Listeria monocytogenes* inoculated in minced beef meat. *Lipids Health Dis.* **2017**, *16*, 146. [[CrossRef](#)] [[PubMed](#)]
66. El Aboubi, M.; Ben Hdech, D.; Bikri, S.; Benayad, A.; El Magri, A.; Aboussaleh, Y.; Aouane, E.M. Chemical composition of essential oils of Citrus limon peel from three Moroccan regions and their antioxidant, anti-inflammatory, antidiabetic and dermatoprotective properties. *J. Herbmed. Pharmacol.* **2023**, *12*, 118–127. [[CrossRef](#)]
67. Himed, L.; Merniz, S.; Monteagudo-Olivan, R.; Barkat, M.; Coronas, J. Antioxidant activity of the essential oil of citrus limon before and after its encapsulation in amorphous SiO₂. *Sci. Afr.* **2019**, *6*, e00181. [[CrossRef](#)]
68. Farhoudi, R.; Lee, D.-J. P 021—Chemical constituents and antioxidant properties of *Matricaria recutita* and *Chamaemelum nobile* essential oil growing in south west of Iran. *Free. Radic. Biol. Med.* **2017**, *108*, S24. [[CrossRef](#)]
69. Miladi, H.; Ben Slama, R.; Mili, D.; Zouari, S.; Bakhrouf, A.; Ammar, E. Chemical composition and cytotoxic and antioxidant activities of *Satureja montana* L. essential oil and its antibacterial potential against *Salmonella* Spp. Strains. *J. Chem.* **2013**, *2013*, 275698. [[CrossRef](#)]
70. Hashemi, S.M.B.; Gholamhosseinpour, A.; Barba, F.J. *Rosmarinus officinalis* L. essential oils impact on the microbiological and oxidative stability of Sarshir (Kaymak). *Molecules* **2023**, *28*, 4206. [[CrossRef](#)]

71. Beniaich, G.; Zouirech, O.; Allali, A.; Bouslamti, M.; Maliki, I.; El Moussaoui, A.; Chebaibi, M.; Nafidi, H.-A.; Bin Jardan, Y.A.; Bourhia, M.; et al. Chemical characterization, antioxidant, insecticidal and anti-cholinesterase activity of essential oils extracted from *Cinnamomum verum* L. *Separations* **2023**, *10*, 348. [[CrossRef](#)]
72. Kamaly, O.A.; Numan, O.; Almradi, O.M.A.; Alanazi, A.S.; Conte, R. Separation and evaluation of potential antioxidant, analgesic, and anti-inflammatory activities of limonene-rich essential oils from *Citrus sinensis* (L.). *Open Chem.* **2022**, *20*, 1517–1530. [[CrossRef](#)]
73. Siddique, S.; Mazhar, S.; Firdaus-e-Bareen; Parveen, Z. Chemical characterization, antioxidant and antimicrobial activities of essential oil from *Melaleuca quinquenervia* leaves. *Indian J. Exp. Biol.* **2018**, *56*, 686–693.
74. Sbai El Otmani, I.; El Jaziz, H.; Zarayby, L.; Ousaid, A.; Elbakri, W.; Montassif, S.; Ait Haj Said, A. Chemical composition and antioxidant activity of the essential oil of *Artemisia vulgaris* from Morocco. *Res. J. Pharm. Biol. Chem. Sci.* **2018**, *9*, 1524.
75. Pino, J.A.; Regalado, E.L.; Rodríguez, J.L.; Fernández, M.D. Phytochemical analysis and in vitro free-radical-scavenging activities of the essential oils from leaf and fruit of *Melaleuca leucadendra* L. *Chem. Biodivers.* **2010**, *7*, 2281–2288. [[CrossRef](#)]
76. Bagheri, H.; Abdul Manap, M.Y.; Solati, Z. Antioxidant activity of *Piper nigrum* L. essential oil extracted by supercritical CO₂ extraction and hydro-distillation. *Talanta* **2014**, *121*, 220–228. [[CrossRef](#)]
77. Ballester-Costa, C.; Sendra, E.; Fernández-López, J.; Pérez-Álvarez, J.A.; Viuda-Martos, M. Assessment of antioxidant and antibacterial properties on meat homogenates of essential oils obtained from four *Thymus* species achieved from organic growth. *Foods* **2017**, *6*, 59. [[CrossRef](#)]
78. Sabah, E.; Omayma, B.; Elidrissi, M.; Bouymajane, A.; Choukrad, M. *Comparative Study of Chemical -Composition and Physico-Chemical Characteristics of Thymus vulgaris's Essential Oil Harvested from Deraa-Tafilelet's Region (Morocco) with Previous Studies*; SSRN: Rochester, NY, USA, 2020. [[CrossRef](#)]
79. Paudel, P.N.; Satyal, P.; Satyal, R.; Setzer, W.N.; Gyawali, R. Chemical Composition, enantiomeric distribution, antimicrobial and antioxidant activities of *Origanum majorana* L. essential oil from Nepal. *Molecules* **2022**, *27*, 6136. [[CrossRef](#)] [[PubMed](#)]
80. Ben Nouri, A.; Dhifi, W.; Bellili, S.; Ghazghazi, H.; Aouadhi, C.; Chérif, A.; Hammami, M.; Mnif, W. Chemical composition, antioxidant potential, and antibacterial activity of essential oil cones of Tunisian *Cupressus sempervirens*. *J. Chem.* **2015**, *2015*, 538929. [[CrossRef](#)]
81. Fayed, S.A. Chemical Composition, Antioxidant, anticancer properties and toxicity evaluation of leaf essential oil of *Cupressus sempervirens*. *Not. Bot. Horti Agrobot. Cluj-Napoca* **2015**, *43*, 320–326. [[CrossRef](#)]
82. Nikolić, V.; Nikolić, L.; Dinić, A.; Gajić, I.; Urosević, M.; Stanojević, L.; Stanojević, J.; Danilović, B. Chemical composition, antioxidant and antimicrobial activity of Nutmeg (*Myristica fragrans* Houtt.) seed essential oil. *J. Essent. Oil Bear. Plants* **2021**, *24*, 218–227. [[CrossRef](#)]
83. Wu, Z.; Tan, B.; Liu, Y.; Dunn, J.; Martorell Guerola, P.; Tortajada, M.; Cao, Z.; Ji, P. Chemical composition and antioxidant properties of essential oils from Peppermint, Native Spearmint and Scotch Spearmint. *Molecules* **2019**, *24*, 2825. [[CrossRef](#)] [[PubMed](#)]
84. Fitsiou, E.; Mitropoulou, G.; Spyridopoulou, K.; Vamvakias, M.; Bardouki, H.; Galanis, A.; Chlichlia, K.; Kourkoutas, Y.; Panayiotidis, M.; Pappa, A. Chemical composition and evaluation of the biological properties of the essential oil of the dietary phytochemical *Lippia citriodora*. *Molecules* **2018**, *23*, 123. [[CrossRef](#)]
85. Sprea, R.M.; Fernandes, L.H.M.; Pires, T.C.S.P.; Calhelha, R.C.; Rodrigues, P.J.; Amaral, J.S. Volatile compounds and biological activity of the essential oil of *Aloysia citrodora* Paláu: Comparison of hydrodistillation and microwave-assisted hydrodistillation. *Molecules* **2023**, *28*, 4528. [[CrossRef](#)] [[PubMed](#)]
86. Farouk, A.; Fikry, R.; Mohsen, M. Chemical composition and antioxidant activity of *Ocimum basilicum* L. essential oil cultivated in Madinah Monawara, Saudi Arabia and its comparison to the Egyptian chemotype. *J. Essent. Oil Bear. Plants* **2016**, *19*, 1119–1128. [[CrossRef](#)]
87. Lawrence, K.; Lawrence, R.; Parihar, D.; Srivastava, R.; Charan, A. Antioxidant activity of Palmarosa essential oil (*Cymbopogon martini*) grown in north Indian plains. *Asian Pac. J. Trop. Biomed.* **2012**, *2*, S888–S891. [[CrossRef](#)]
88. Bettaieb Rebey, I.; Bourgou, S.; Ben Kaab, S.; Aidi Wannes, W.; Ksouri, R.; Saidani Tounsi, M.; Fauconnier, M.-L. On the effect of initial drying techniques on essential oil composition, phenolic compound and antioxidant properties of anise (*Pimpinella anisum* L.) seeds. *J. Food Meas. Charact.* **2020**, *14*, 220–228. [[CrossRef](#)]
89. Ouis, N.; Hariri, A. Chemical analysis, antioxidant and antibacterial activities of Aniseeds essential oil. *Agric. Conspec. Sci.* **2021**, *86*, 337–348.
90. Salamatullah, A.M. Identification of volatile compounds and antioxidant, antibacterial, and antifungal properties against drug-resistant microbes of essential oils from the leaves of *Mentha rotundifolia* var. *apodysa* Briq. (Lamiaceae). *Open Chem.* **2022**, *20*, 484–493. [[CrossRef](#)]
91. Zekri, N.; Elazzouzi, H.; Ailli, A.; Gouruch, A.A.; Radi, F.Z.; El Belghiti, M.A.; Zair, T.; Nieto, G.; Centeno, J.A.; Lorenzo, J.M. Physicochemical characterization and antioxidant properties of essential oils of *M. pulegium* (L.), *M. suaveolens* (Ehrh.) and *M. spicata* (L.) from Moroccan Middle-Atlas. *Foods* **2023**, *12*, 760. [[CrossRef](#)] [[PubMed](#)]
92. Ouariachi, E.M.E.; Paolini, J.; Bouyanzer, A.; Tomi, P.; Hammouti, B.; Salghi, R.; Majidi, L.; Costa, J. Chemical composition and antioxidant activity of essential oils and solvent extracts of *Thymus capitatus* (L.) Hoffmanns and link from Morocco. *J. Med. Plants Res.* **2011**, *5*, 5773–5778.

93. Assaggaf, H.M.; Naceiri Mrabti, H.; Rajab, B.S.; Attar, A.A.; Alyamani, R.A.; Hamed, M.; El Omari, N.; El Menyiy, N.; Hazzoumi, Z.; Benali, T.; et al. Chemical analysis and investigation of biological effects of *Salvia officinalis* essential oils at three phenological stages. *Molecules* **2022**, *27*, 5157. [[CrossRef](#)]
94. Aazza, S.; Lyoussi, B.; Miguel, M.G. Antioxidant and antiacetylcholinesterase activities of some commercial essential oils and their major compounds. *Molecules* **2011**, *16*, 7672–7690. [[CrossRef](#)]
95. Wang, B.; Ma, L.; Yin, L.; Chen, J.; Zhang, Y.; Dong, L.; Zhang, X.; Fu, X. Report: Regional variation in the chemical composition and antioxidant activity of *Rosmarinus officinalis* L. from China and the Mediterranean region. *Pak. J. Pharm. Sci.* **2018**, *31*, 221–229. [[PubMed](#)]
96. Patsilinos, A.; Artini, M.; Papa, R.; Sabatino, M.; Božović, M.; Garzoli, S.; Vrenna, G.; Buzzi, R.; Manfredini, S.; Selan, L.; et al. Machine learning analyses on data including essential oil chemical composition and in vitro experimental antibiofilm activities against *Staphylococcus* species. *Molecules* **2019**, *24*, 890. [[CrossRef](#)] [[PubMed](#)]
97. Papa, R.; Garzoli, S.; Vrenna, G.; Sabatino, M.; Sapienza, F.; Relucanti, M.; Donfrancesco, O.; Fiscarelli, E.V.; Artini, M.; Selan, L.; et al. Essential oils biofilm modulation activity, chemical and machine learning analysis. application on *Staphylococcus aureus* isolates from cystic fibrosis patients. *Int. J. Mol. Sci.* **2020**, *21*, 9258. [[CrossRef](#)] [[PubMed](#)]
98. Artini, M.; Patsilinos, A.; Papa, R.; Božović, M.; Sabatino, M.; Garzoli, S.; Vrenna, G.; Tilotta, M.; Pepi, F.; Ragno, R.; et al. Antimicrobial and antibiofilm activity and machine learning classification analysis of essential oils from different mediterranean plants against *Pseudomonas aeruginosa*. *Molecules* **2018**, *23*, 482. [[CrossRef](#)] [[PubMed](#)]
99. Ragno, A.; Baldisserotto, A.; Antonini, L.; Sabatino, M.; Sapienza, F.; Baldini, E.; Buzzi, R.; Vertuani, S.; Manfredini, S. Machine learning data augmentation as a tool to enhance quantitative composition–activity relationships of complex mixtures. A new application to dissect the role of main chemical components in bioactive essential oils. *Molecules* **2021**, *26*, 6279. [[CrossRef](#)]
100. Sabatino, M.; Fabiani, M.; Božović, M.; Garzoli, S.; Antonini, L.; Marcocci, M.E.; Palamara, A.T.; De Chiara, G.; Ragno, R. Experimental data based machine learning classification models with predictive ability to select in vitro active antiviral and non-toxic essential oils. *Molecules* **2020**, *25*, 2452. [[CrossRef](#)]
101. Di Martile, M.; Garzoli, S.; Sabatino, M.; Valentini, E.; D’Aguanno, S.; Ragno, R.; Del Bufalo, D. Antitumor effect of *Melaleuca alternifolia* essential oil and its main component terpinen-4-ol in combination with target therapy in melanoma models. *Cell Death Discov.* **2021**, *7*, 127. [[CrossRef](#)]
102. Thalappil, M.A.; Butturini, E.; Carcereri de Prati, A.; Bettin, I.; Antonini, L.; Sapienza, F.U.; Garzoli, S.; Ragno, R.; Mariotto, S. Pinus mugo essential oil impairs STAT3 activation through oxidative stress and induces apoptosis in prostate cancer cells. *Molecules* **2022**, *27*, 4834. [[CrossRef](#)] [[PubMed](#)]
103. Vukić, M.D.; Vuković, N.L.; Mladenović, M.; Tomašević, N.; Matić, S.; Stanić, S.; Sapienza, F.; Ragno, R.; Božović, M.; Kačaniová, M. chemical composition of various *Nepeta cataria* plant organs’ methanol extracts associated with in vivo hepatoprotective and antigenotoxic features as well as molecular modeling investigations. *Plants* **2022**, *11*, 2114. [[CrossRef](#)]
104. McKinney, W. *Python for Data Analysis*; O’Reilly: Beijing, China, 2013; p. xiii, 447p.
105. Perkel, J.M. Programming: Pick up Python. *Nature* **2015**, *518*, 125–126. [[CrossRef](#)]
106. Ragno, R.; Papa, R.; Patsilinos, A.; Vrenna, G.; Garzoli, S.; Tuccio, V.; Fiscarelli, E.; Selan, L.; Artini, M. Essential oils against bacterial isolates from cystic fibrosis patients by means of antimicrobial and unsupervised machine learning approaches. *Sci. Rep.* **2020**, *10*, 2653. [[CrossRef](#)] [[PubMed](#)]
107. Pedregosa, F.; Varoquaux, G.; Gramfort, A.; Michel, V.; Thirion, B.; Grisel, O.; Blondel, M.; Prettenhofer, P.; Weiss, R.; Dubourg, V.; et al. Scikit-learn: Machine Learning in Python. *J. Mach. Learn. Res.* **2011**, *12*, 2825–2830.
108. McKinney, W. *Pandas: Powerful Python Data Analysis Toolkit*; O’Reilly Media, Inc.: Sebastopol, CA, USA, 2011.
109. McKinney, W. *Python for Data Analysis: Data Wrangling with Pandas, NumPy, and IPython*, 2nd ed.; O’Reilly Media, Inc.: Sebastopol, CA, USA, 2018; p. xvi, 524p.
110. Tipping, M.E.; Bishop, C.M. Probabilistic principal component analysis. *J. R. Stat. Soc. Ser. B* **1999**, *61*, 611–622. [[CrossRef](#)]
111. Bergstra, J.; Bardenet, R.; Bengio, Y.; Kégl, B. Algorithms for hyper-parameter optimization. In Proceedings of the 24th International Conference on Neural Information Processing Systems, Granada, Spain, 12–14 December 2011; pp. 2546–2554.
112. Friedman, J.H. Greedy function approximation: A gradient boosting machine. *Ann. Stat.* **2001**, *29*, 1189–1232. [[CrossRef](#)]
113. Wei, P.; Lu, Z.; Song, J. Variable importance analysis: A comprehensive review. *Reliab. Eng. Syst. Saf.* **2015**, *142*, 399–432. [[CrossRef](#)]
114. Baldi, P.; Brunak, S.; Chauvin, Y.; Andersen, C.A.F.; Nielsen, H. Assessing the accuracy of prediction algorithms for classification: An overview. *Bioinformatics* **2000**, *16*, 412–424. [[CrossRef](#)] [[PubMed](#)]
115. Szende, B.; Timár, F.; Hargitai, B. Olive oil decreases liver damage in rats caused by carbon tetrachloride (CCl₄). *Exp. Toxicol. Pathol.* **1994**, *46*, 355–359. [[CrossRef](#)] [[PubMed](#)]
116. Misra, H.P.; Fridovich, I. The role of superoxide anion in the autoxidation of epinephrine and a simple assay for superoxide dismutase. *J. Biol. Chem.* **1972**, *247*, 3170–3175. [[CrossRef](#)]
117. Ohkawa, H.; Ohishi, N.; Yagi, K. Assay for lipid peroxides in animal tissues by thiobarbituric acid reaction. *Anal. Biochem.* **1979**, *95*, 351–358. [[CrossRef](#)]
118. Góth, L. A simple method for determination of serum catalase activity and revision of reference range. *Clin. Chim. Acta* **1991**, *196*, 143–151. [[CrossRef](#)]
119. Ellman, G.L. Tissue sulfhydryl groups. *Arch. Biochem. Biophys.* **1959**, *82*, 70–77. [[CrossRef](#)]

120. Lowry, O.H.; Rosebrough, N.J.; Farr, A.L.; Randall, R.J. Protein measurement with the Folin phenol reagent. *J. Biol. Chem.* **1951**, *193*, 265–275. [[CrossRef](#)] [[PubMed](#)]
121. Quick, A.J.; Stanley-Brown, M.; Bancroft, F.W. A Study of the Coagulation Defect in Hemophilia and in Jaundice. *Thromb. Haemost.* **1980**, *44*, 002–005. [[CrossRef](#)]
122. Bergmeyer, H.U.; Bowers, G.N., Jr.; Horder, M.; Moss, D.W. Provisional recommendations on IFCC methods for the measurement of catalytic concentrations of enzymes. Part 2. IFCC method for aspartate aminotransferase. *Clin. Chim. Acta* **1976**, *70*, F19–F29. [[CrossRef](#)] [[PubMed](#)]
123. Bergmeyer, H.U. IFCC methods for the measurement of catalytic concentrations of enzymes. part 3, IFCC. Method for alanine aminotransferase (L-alanine 2 -oxoglutarate aminotransferase, ec 2.6.1.2). *Clin. Chim. Acta* **1980**, *105*, 145f–172f.
124. Tietz, N.W.; Rinker, A.D.; Shaw, L.M. IFCC methods for the measurement of catalytic concentration of enzymes Part 5. IFCC method for alkaline phosphatase (orthophosphoric-monoester phosphohydrolase, alkaline optimum, EC 3.1.3.1). *J. Clin. Chem. Clin. Biochem.* **1983**, *21*, 731–748.
125. Schumann, G.; Bonora, R.; Ceriotti, F.; Férard, G.; Ferrero, C.A.; Franck, P.F.; Gella, F.J.; Hoelzel, W.; Jørgensen, P.J.; Kanno, T.; et al. IFCC primary reference procedures for the measurement of catalytic activity concentrations of enzymes at 37 degrees C. International Federation of Clinical Chemistry and Laboratory Medicine. Part 6. Reference procedure for the measurement of catalytic concentration of gamma-glutamyltransferase. *Clin. Chem. Lab. Med.* **2002**, *40*, 734–738. [[CrossRef](#)]
126. Shibuya, S.; Watanabe, K.; Ozawa, Y.; Shimizu, T. Xanthine oxidoreductase-mediated superoxide production is not involved in the age-related pathologies in Sod1-deficient mice. *Int. J. Mol. Sci.* **2021**, *22*, 3542. [[CrossRef](#)]
127. El-Sawalhi, M.M.; Ahmed, L.A. Exploring the protective role of apocynin, a specific NADPH oxidase inhibitor, in cisplatin-induced cardiotoxicity in rats. *Chem. Biol. Interact.* **2014**, *207*, 58–66. [[CrossRef](#)]
128. Daenen, K.; Andries, A.; Mekahli, D.; Van Schepdael, A.; Jouret, F.; Bammens, B. Oxidative stress in chronic kidney disease. *Pediatr. Nephrol.* **2019**, *34*, 975–991. [[CrossRef](#)]
129. Singh, N.P.; McCoy, M.T.; Tice, R.R.; Schneider, E.L. A simple technique for quantitation of low levels of DNA damage in individual cells. *Exp. Cell Res.* **1988**, *175*, 184–191. [[CrossRef](#)] [[PubMed](#)]
130. Collins, A.R. The comet assay for DNA damage and repair. *Mol. Biotechnol.* **2004**, *26*, 249–261. [[CrossRef](#)] [[PubMed](#)]
131. Manoharan, K.; Banerjee, M.R. β -Carotene reduces sister chromatid exchanges induced by chemical carcinogens in mouse mammary cells in organ culture. *Cell Biol. Int. Rep.* **1985**, *9*, 783–789. [[CrossRef](#)]
132. Napolitano, G.; Fasciolo, G.; Venditti, P. The ambiguous aspects of oxygen. *Oxygen* **2022**, *2*, 382–409. [[CrossRef](#)]
133. Huie, R.E.; Padmaja, S. The reaction of NO with superoxide. *Free Radic. Res. Commun.* **1993**, *18*, 195–199. [[CrossRef](#)] [[PubMed](#)]
134. Ayala, A.; Muñoz, M.F.; Argüelles, S. Lipid peroxidation: Production, metabolism, and signaling mechanisms of malondialdehyde and 4-hydroxy-2-nonenal. *Oxid. Med. Cell Longev.* **2014**, *2014*, 360438. [[CrossRef](#)]
135. Bielski, B.H.; Arudi, R.L.; Sutherland, M.W. A study of the reactivity of HO_2/O_2^- with unsaturated fatty acids. *J. Biol. Chem.* **1983**, *258*, 4759–4761. [[CrossRef](#)]
136. Zielinski, Z.A.M.; Pratt, D.A. Lipid peroxidation: Kinetics, mechanisms, and products. *J. Org. Chem.* **2017**, *82*, 2817–2825. [[CrossRef](#)]
137. Foti, M.C. Use and abuse of the DPPH \cdot radical. *J. Agric. Food Chem.* **2015**, *63*, 8765–8776. [[CrossRef](#)] [[PubMed](#)]
138. Nguyen, T.T.K.; Laosinwattana, C.; Teerarak, M.; Pilasombut, K. Potential antioxidant and lipid peroxidation inhibition of *Phyllanthus acidus* leaf extract in minced pork. *Asian-Australas. J. Anim. Sci.* **2017**, *30*, 1323–1331. [[CrossRef](#)]
139. Munteanu, I.G.; Apetrei, C. Analytical methods used in determining antioxidant activity: A review. *Int. J. Mol. Sci.* **2021**, *22*, 3380. [[CrossRef](#)] [[PubMed](#)]
140. Ilyasov, I.R.; Beloborodov, V.L.; Selivanova, I.A.; Terekhov, R.P. ABTS/PP decolorization assay of antioxidant capacity reaction pathways. *Int. J. Mol. Sci.* **2020**, *21*, 1131. [[CrossRef](#)] [[PubMed](#)]
141. Lim, P.; Wuenschell, G.E.; Holland, V.; Lee, D.H.; Pfeifer, G.P.; Rodriguez, H.; Termini, J. Peroxyl radical mediated oxidative DNA base damage: Implications for lipid peroxidation induced mutagenesis. *Biochemistry* **2004**, *43*, 15339–15348. [[CrossRef](#)]
142. Higuchi, H.; Gores, G.J. Mechanisms of liver injury: An overview. *Curr. Mol. Med.* **2003**, *3*, 483–490. [[CrossRef](#)]
143. Jabir, M.S.; Taha, A.; Sahib, U. Antioxidant activity of linalool. *Eng. Technol. J.* **2018**, *36*, 64–67. [[CrossRef](#)]
144. Baschieri, A.; Ajvazi, M.D.; Tonfack, J.L.F.; Valgimigli, L.; Amorati, R. Explaining the antioxidant activity of some common non-phenolic components of essential oils. *Food Chem.* **2017**, *232*, 656–663. [[CrossRef](#)]
145. Bounatirou, S.; Smiti, S.; Miguel, M.G.; Faleiro, L.; Rejeb, M.N.; Neffati, M.; Costa, M.M.; Figueiredo, A.C.; Barroso, J.G.; Pedro, L.G. Chemical composition, antioxidant and antibacterial activities of the essential oils isolated from Tunisian *Thymus capitatus* Hoff. et Link. *Food Chem.* **2007**, *105*, 146–155. [[CrossRef](#)]
146. Gulcin, I.; Alwasel, S.H. Metal Ions, metal chelators and metal chelating assay as antioxidant method. *Processes* **2022**, *10*, 132. [[CrossRef](#)]
147. Horvathova, E.; Navarova, J.; Galova, E.; Sevcovicova, A.; Chodakova, L.; Snahnicanova, Z.; Melusova, M.; Kozics, K.; Slamenova, D. Assessment of antioxidative, chelating, and DNA-protective effects of selected essential oil components (eugenol, carvacrol, thymol, borneol, eucalyptol) of plants and intact *Rosmarinus officinalis* oil. *J. Agric. Food Chem.* **2014**, *62*, 6632–6639. [[CrossRef](#)] [[PubMed](#)]

148. Ferreira, V.R.F.; Militani, I.A.; de Almeida, K.J.; Lunguinho, A.d.S.; Saczk, A.A.; Ionta, M.; da Silva, G.Á.F.; Felix, F.S.; Nelson, D.L.; Cardoso, M.D.G. Antioxidant and cytotoxic activity of essential oils and their principal components: Spectrophotometric, voltammetric, and theoretical investigation of the chelating effect of eugenol and carvacrol. *ACS Food Sci. Technol.* **2023**, *3*, 350–360. [[CrossRef](#)]
149. Liu, S.; Zhao, C.; Cao, Y.; Li, Y.; Zhang, Z.; Nie, D.; Tang, W.; Li, Y. Comparison of chemical compositions and antioxidant activity of essential oils from *Litsea Cubeba*, Cinnamon, Anise, and Eucalyptus. *Molecules* **2023**, *28*, 5051. [[CrossRef](#)] [[PubMed](#)]
150. Rolletter, M.; Kaminski, M.; Acir, I.H.; Bohn, B.; Dorn, H.P.; Li, X.; Lutz, A.; Nehr, S.; Rohrer, F.; Tillmann, R.; et al. Investigation of the α -pinene photooxidation by OH in the atmospheric simulation chamber SAPHIR. *Atmos. Chem. Phys.* **2019**, *19*, 11635–11649. [[CrossRef](#)]
151. Xanthis, V.; Fitsiou, E.; Voulgaridou, G.-P.; Bogadakis, A.; Chlichlia, K.; Galanis, A.; Pappa, A. Antioxidant and cytoprotective potential of the essential oil *Pistacia lentiscus* var. chia and its major components myrcene and α -pinene. *Antioxidants* **2021**, *10*, 127. [[CrossRef](#)] [[PubMed](#)]
152. Francomano, F.; Caruso, A.; Barbarossa, A.; Fazio, A.; La Torre, C.; Ceramella, J.; Mallamaci, R.; Saturnino, C.; Iacopetta, D.; Sinicropi, M.S. β -caryophyllene: A sesquiterpene with countless biological properties. *Appl. Sci.* **2019**, *9*, 5420. [[CrossRef](#)]
153. Fouqueau, A.; Cirtog, M.; Cazaunau, M.; Pangui, E.; Doussin, J.F.; Picquet-Varrault, B. An experimental study of the reactivity of terpinolene and β -caryophyllene with the nitrate radical. *Atmos. Chem. Phys.* **2022**, *22*, 6411–6434. [[CrossRef](#)]
154. Sharopov, F.S.; Wink, M.; Setzer, W.N. Radical scavenging and antioxidant activities of essential oil components—An experimental and computational investigation. *Nat. Prod. Commun.* **2015**, *10*, 153–156. [[CrossRef](#)]
155. Milani, L.; Galindo, C.M.; Turin de Oliveira, N.M.; Corso, C.R.; Adami, E.R.; Stipp, M.C.; Beltrame, O.C.; Acco, A. The GLP-1 analog liraglutide attenuates acute liver injury in mice. *Ann. Hepatol.* **2019**, *18*, 918–928. [[CrossRef](#)]
156. Majnooni, M.B.; Mohammadi-Farani, A.; Gholivand, M.B.; Nikbakht, M.R.; Bahrami, G.R. Chemical composition and anxiolytic evaluation of *Achillea wilhelmsii* C. Koch essential oil in rat. *Res. Pharm. Sci.* **2013**, *8*, 269–275.
157. Abdel-Wahhab, K.G.; El-Shamy, K.A.; El-Beih, N.A.E.-Z.; Morcy, F.A.; Mannaa, F.A. Protective effect of a natural herb (*Rosmarinus officinalis*) against hepatotoxicity in male albino rats. *Commun. Sci.* **2011**, *2*, 9–17. [[CrossRef](#)]
158. Carini, R.; Chiarpotto, E.; Biasi, F.; Leonarduzzi, G.; Comoglio, A.; Carpi, C.; Poli, G. Relation between liver necrosis and intrahepatic cholestasis in rats poisoned with CCl_4 . *Boll. Soc. Ital. Biol. Sper.* **1987**, *63*, 273–280.
159. Yang, S.Y.; Hong, C.O.; Lee, G.P.; Kim, C.T.; Lee, K.W. The hepatoprotection of caffeic acid and rosmarinic acid, major compounds of *Perilla frutescens*, against t-BHP-induced oxidative liver damage. *Food Chem. Toxicol.* **2013**, *55*, 92–99. [[CrossRef](#)]
160. Giannini, E.G.; Testa, R.; Savarino, V. Liver enzyme alteration: A guide for clinicians. *Cmaj* **2005**, *172*, 367–379. [[CrossRef](#)]
161. Abdelrahman, M.; Mazzon, E.; Bauer, M.; Bauer, I.; Delbosc, S.; Cristol, J.-P.; Patel, N.S.A.; Cuzzocrea, S.; Thiemermann, C. Inhibitors of NADPH oxidase reduce the organ injury in hemorrhagic shock. *Shock* **2005**, *23*, 107–114. [[CrossRef](#)] [[PubMed](#)]
162. Hasegawa, T.; Malle, E.; Farhood, A.; Jaeschke, H. Generation of hypochlorite-modified proteins by neutrophils during ischemia-reperfusion injury in rat liver: Attenuation by ischemic preconditioning. *Am. J. Physiol.-Gastrointest. Liver Physiol.* **2005**, *289*, G760–G767. [[CrossRef](#)]
163. Chian, C.F.; Chiang, C.H.; Yuan-Jung, C.; Chuang, C.H.; Liu, S.L.; Yi-Han, J.; Zhang, H.; Ryu, J.H. Apocynin attenuates lipopolysaccharide-induced lung injury in an isolated and perfused rat lung model. *Shock* **2012**, *38*, 196–202. [[CrossRef](#)]
164. Ratliff, B.B.; Abdulmahdi, W.; Pawar, R.; Wolin, M.S. Oxidant mechanisms in renal injury and disease. *Antioxid. Redox Signal.* **2016**, *25*, 119–146. [[CrossRef](#)]
165. Hartmann, A.; Speit, G. The contribution of cytotoxicity to DNA-effects in the single cell gel test (comet assay). *Toxicol. Lett.* **1997**, *90*, 183–188. [[CrossRef](#)] [[PubMed](#)]
166. Wikanthi, L.; Wulandari, N.; Esti, Y.; Sari, N.; Susidarti, R. Cinnamomum essential oil prevents DNA damage-induced by doxorubicin on CHO-K1 Cells. *Indones. J. Cancer Chemoprev.* **2017**, *8*, 27. [[CrossRef](#)]
167. Sekizawa, J.; Shibamoto, T. Genotoxicity of safrole-related chemicals in microbial test systems. *Mutat. Res.* **1982**, *101*, 127–140. [[CrossRef](#)]
168. Mezzoug, N.; Idaomar, M.; Baudoux, D.; Debauche, P.; Liemans, V.; Zhiri, A. Genotoxicity of some essential oils frequently used in aromatherapy. *Adv. Biosci. Biotechnol.* **2016**, *07*, 63–73. [[CrossRef](#)]
169. Marnett, L.J. Oxyradicals and DNA damage. *Carcinogenesis* **2000**, *21*, 361–370. [[CrossRef](#)] [[PubMed](#)]

Disclaimer/Publisher’s Note: The statements, opinions and data contained in all publications are solely those of the individual author(s) and contributor(s) and not of MDPI and/or the editor(s). MDPI and/or the editor(s) disclaim responsibility for any injury to people or property resulting from any ideas, methods, instructions or products referred to in the content.